Distribution Agreement

In presenting this thesis or dissertation as a partial fulfillment of the requirements for an advanced degree from Emory University, I hereby grant to Emory University and its agents the non-exclusive license to archive, make accessible, and display my thesis or dissertation in whole or in part in all forms of media, now or hereafter known, including display on the world wide web. I understand that I may select some access restrictions as part of the online submission of this thesis or dissertation. I retain all ownership rights to the copyright of the thesis or dissertation. I also retain the right to use in future works (such as articles or books) all or part of this thesis or dissertation.

Signature:

_____ _____

Mallika Halder Date

MODULATING SYMPATHETIC OUTPUT: FACTORS INFLUENCING CONDUCTION IN THORACIC PREGANGLIONIC AXONS

By

Mallika Halder

Doctor of Philosophy

Neuroscience

_____

Shawn Hochman, PhD

Advisor

_____

Francisco Alvarez, PhD

Committee Member

_____

Astrid Prinz, PhD

Committee Member

_____

Nicholas Au Yong, MD, PhD

Committee Member

_____

Peter Wenner PhD

Committee Member

Accepted:

_____

Kimberly Jacob Amiola, Ph.D.

Dean of the James T. Laney School of Graduate Studies

_____

Date

MODULATING SYMPATHETIC OUTPUT: FACTORS INFLUENCING CONDUCTION IN THORACIC PREGANGLIONIC AXONS

By

Mallika Halder

B.S., B.A, Emory University, 2013

Advisor: Shawn Hochman, PhD

An abstract of

A dissertation submitted to the Faculty of the James T. Laney School of Graduate Studies of Emory University in partial fulfillment of the requirements for the degree of Doctor of Philosophy in Neuroscience

2024

Abstract

MODULATING SYMPATHETIC OUTPUT: FACTORS INFLUENCING CONDUCTION IN THORACIC PREGANGLIONIC AXONS

By

Mallika Halder

Spinal cord sympathetic preganglionic neurons (SPNs) are crucial for transmitting signals from the CNS to the peripheral postganglionic neurons that control organ function. It has been assumed that SPN peripheral axonal spike propagation along its projections is reliable. To assess this, I developed an *ex vivo* approach having intact thoracic paravertebral sympathetic chain ganglia and ventral roots maintained *in situ*. Suprathreshold stimulation of SPN axons in thoracic ventral roots was achieved through optical and electrical methods in ChAT-CHR2 adult mice, allowing capture of evoked population compound action potential responses across multiple ganglia. Variability in axonal recruitment was overt and found to be particularly significant in the slow-conducting unmyelinated axons. That SPN peripheral axon projections have a low safety-factor with demonstrable conduction failures challenges the traditional assumption that SPN spike propagation across its broad distribution occurs without failure.

Focusing on mechanisms affecting spike propagation, slow-conducting SPN axons were found to be particularly susceptible to conduction failures via temperature increases and frequency-dependent conditioning stimuli. Pharmacological block of $GABA_A$ receptors and activation of serotonin receptors, acetylcholine receptors, and K_2P leak channels depressed conduction in these axons. Conversely, the convulsant 4-aminopyridine greatly facilitated conduction - presumably via block of voltage-gated K_A channels.

Overall, this work identified variability of spike conduction in SPN axons as fundamental features of its operation. As autonomic neural drive to organ systems commonly involve continuous activity with slow temporal dynamics, we hypothesize that population-encoded responses utilize small-diameter unmyelinated axons with low safety factor as a metabolically efficient method for population control of peripheral autonomic circuitry. That axonal conduction failures are history dependent and under neuromodulatory controls, suggests that alterations in conduction reliability provide a mechanism of output gain control beyond those encoded by centrally-driven SPN spike recruitment.

MODULATING SYMPATHETIC OUTPUT: FACTORS INFLUENCING CONDUCTION IN THORACIC PREGANGLIONIC AXONS

By

Mallika Halder

B.S., B.A, Emory University, 2013

Advisor: Shawn Hochman, PhD

A dissertation submitted to the Faculty of the James T. Laney School of Graduate Studies of Emory University in partial fulfillment of the requirements for the degree of Doctor of Philosophy in Neuroscience

2024

Table of Contents

List of Figures

List of Tables

List of Abbreviations

ACh	acetylcholine
ACSF	artificial cerebrospinal fluid
ANS	autonomic nervous system
CART	cocaine and amphetamine-regulated transcript
CAP	compound action potential
CGRP	calcitonin gene-related peptide
CRF	corticotropin-releasing factor
ENS	enteric nervous system
EPSP	excitatory postsynaptic potential
IGN	interganglionic nerve
IML	intermediolateral nucleus
IPSP	inhibitory postsynaptic potential
nAChR	nicotinic acetylcholine receptor
nNOS	neuronal nitric oxide synthase
PNS	parasympathetic nervous system
SND	sympathetic nerve discharge
SNS	sympathetic nervous system
SPN	sympathetic preganglionic neuron
tPostN	thoracic postganglionic neuron
TEA	tetraethylammonium
VR	ventral root
4-AP	4-aminopyradine

Acknowledgements

The ancient wisdom that 'Better than a thousand days of diligent study is one day with a great teacher' perfectly captures the essence of my experience under the guidance of my advisor, Shawn. His mentorship transcended conventional learning, always going deeper into the depths of physiology, creative experimental design, and the thrill of scientific discovery. In a world increasingly dominated by algorithms, Shawn's dedication to teaching us to see beyond the data crunching, to truly understand and interpret the living, dynamic systems before us, has been my favorite lesson. For his unwavering support, trust, and off-topic discussions about the goings-on in the world, I am eternally grateful.

Of course under the leadership of such an advisor, is a team comprised of the very best people. Mike has been a cornerstone of both my research support and some of my most cherished lab memories. Bill's engineering genius shaped so much of my research, while Alan's histology work and guidance on each of my presentations have been immensely appreciated. I extend my heartfelt gratitude to all the post-docs, graduate students, and research specialists whose paths have intersected with mine in the Hochman lab. Their roles as both sounding boards and friends have enriched my journey immeasurably: Don, Celia, Michael, Matt, Jacob, Shaquia, Heidi, Maka, and Brittney, thank you for your friendship!

Thank you to my committee members and rotation advisors, Paco, Astrid, Pete, Nick and Marie-Claude for your mentorship and patience. Working under your guidance at different phases of my graduate journey has been an honor and has provided a masterclass in what it means to conduct elegant science.

To my cherished friends, Maite and Camille, who have been my personal role models since our sophomore year of college, and to my remarkable cohort-mates, whose motivation and camaraderie have infused my graduate journey with joy and levity—I am forever grateful.

In closing, I've come to recognize that beyond data and researched paragraphs, a dissertation requires a unique blend of sustenance and support. A constant supply of love, peace, sage advice, caffeine and chicken nuggets all generously provided by my remarkable parents and sister, have been pivotal to this work. My adventure in science started with playful explorations, from projecting images on walls with binoculars alongside my dad, a precursor to lessons in optics I'd encounter in Physics years later, to observing my mom's inventive seed germination strategies that hinted at a deeper understanding of experimental design. My grandfather, Manoranjan Das, Ph.D. (London), a pioneer in filaria research in India, was our family's original scientist. His blend of science and art fostered a legacy of creative experimentation that endures in our family. To them, I extend profound thanks for their steadfast support and for being the foundations of my scientific spirit.

1 Introduction

To thrive in ever-changing environments, animals must adeptly adjust the function of the various organ systems. As a major component of the Autonomic Nervous System (**ANS**), the Sympathetic Nervous System (**SNS**) is an instrumental component in facilitating these adjustments, ensuring animals are attuned and reactive to their surroundings—essential for behavioral tasks like sourcing food, evading predators, and addressing various environmental demands. A prime example of the role of the SNS is its ability to tap into energy reserves, enhancing glucose release from the liver to sufficiently fuel muscles during emergencies. It reroutes blood flow from less urgent systems, such as digestion, to prioritize essential organ systems like the musculoskeletal system for urgent action. This strategic reallocation of resources is paramount to survival, priming organisms for adaptive reactions to imminent threats. Beyond moments of crisis, the SNS persistently surveys and tweaks physiological operations, maintaining a stable internal milieu; a state known as homeostasis. This ensures that the animal can seamlessly function and acclimatize to external shifts. Among its homeostatic functions, the SNS regulates body temperature, blood pressure, and even fine-tunes immune responses. Yet, despite its significance, a comprehensive understanding of the output dynamics of the SNS from the central nervous system to peripheral target organs remains elusive. The focus of this dissertation is to illustrate how the SNS can modulate its output with particular attention paid to a population of spinal cord neurons known as the Sympathetic Preganglionic Neurons (**SPN**s). SPNs are the final arbiters of sympathetic output from the central nervous system. A major population of SPNs project to the paravertebral sympathetic chain ganglia where they branch extensively and issue divergent, multisegmental projections onto postganglionic neurons. These postganglionic neurons in turn innervate target tissues and organs. It has always been assumed

that “preganglionic signals are distributed widely through paravertebral ganglia with little modification” [3], a notion which will be challenged in this thesis.

This introductory chapter first provides an overview on the organization of the ANS, then focuses on SNS central circuitry with emphasis on the anatomical and physiological properties of SPNs as the final common output of the CNS. Final focus will be on SPN axons as potential sites for output modification.

1.1 Overview of the autonomic nervous system

The ANS provides neural control for all parts of the body through the visceral motor system and plays a pivotal role in regulating involuntary bodily functions to achieve homeostasis. Homeostasis refers to the organized process of maintaining a stable internal environment within an organism, regardless of external changes, through carefully orchestrated control mechanisms and feedback loops [4]. This balance is crucial for sustaining essential physiological parameters. The three divisions of the ANS are: the Sympathetic (**SNS**), Parasympathetic (**PNS**) and Enteric Nervous Systems (**ENS**). Autonomic nerve pathways of the PNS and SNS typically consist of two nerve cells[5]. The first cell resides in the brainstem or spinal cord and connects via nerve fibers to the second cell, the postganglionic neuron located in an autonomic ganglion[6]. Postganglionic neurons in turn innervate and control vasculature in muscle, skin and visceral organs, as well as piloerector muscles, sweat glands, and brown adipose tissue[6-8]. Many effector organs receive innervation from both ANS systems (for example, the iris muscle of the eyes and sexual organs receive PNS and SNS innervation); but others receive innervation from either the SNS or PNS (**Figure 1.1**)[4]. It is notable that the location of the ganglia which constitute postganglionic neurons differs between the PNS and SNS. Specifically, in the PNS, the ganglia are situated close to or inside the target organ, whereas, in the SNS, they are typically positioned

nearer to the spinal cord. The remainder of this chapter and the focus of this dissertation will be on circuitry of the SNS.

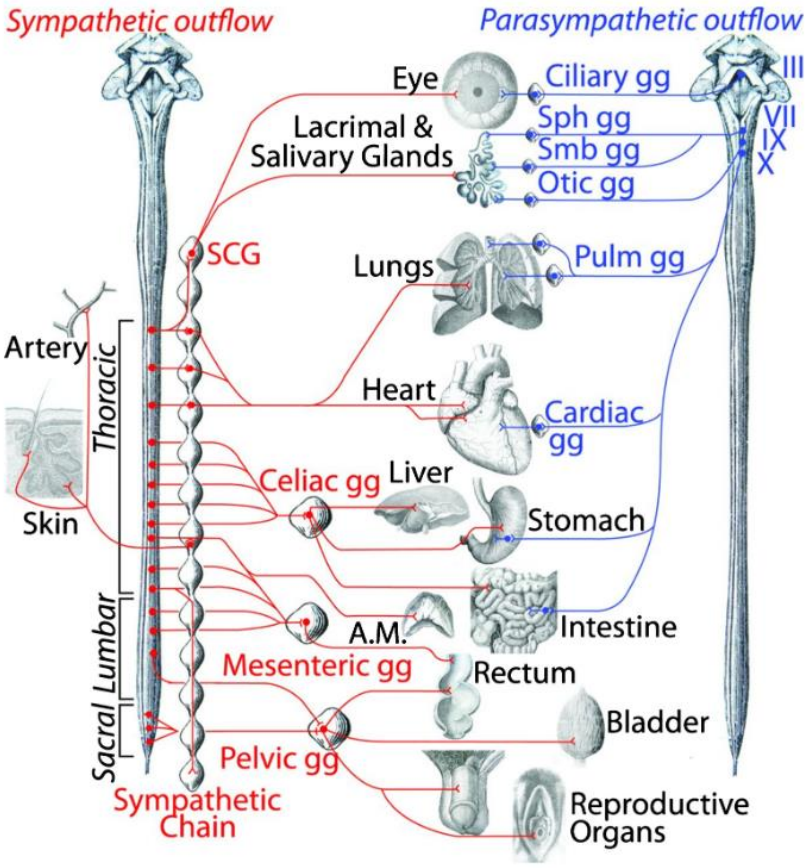

Figure 1.1. Structural organization and target organ innervation of the sympathetic and parasympathetic nervous systems.

Many organs are controlled primarily by either the sympathetic or the parasympathetic division. Sometimes the two divisions have opposite effects on the same organ. For example, the sympathetic division increases blood pressure, and the parasympathetic division decreases it. Overall, the two divisions work together to ensure that the body responds appropriately to different situations. Image taken from [9]. (SCG: superior cervical ganglion, gg: ganglion, sph: sphenopalatine, smb: submandibular, pulm: pulmonary)

1.2 Overview of the sympathetic nervous system

1.2.1 Circuitry

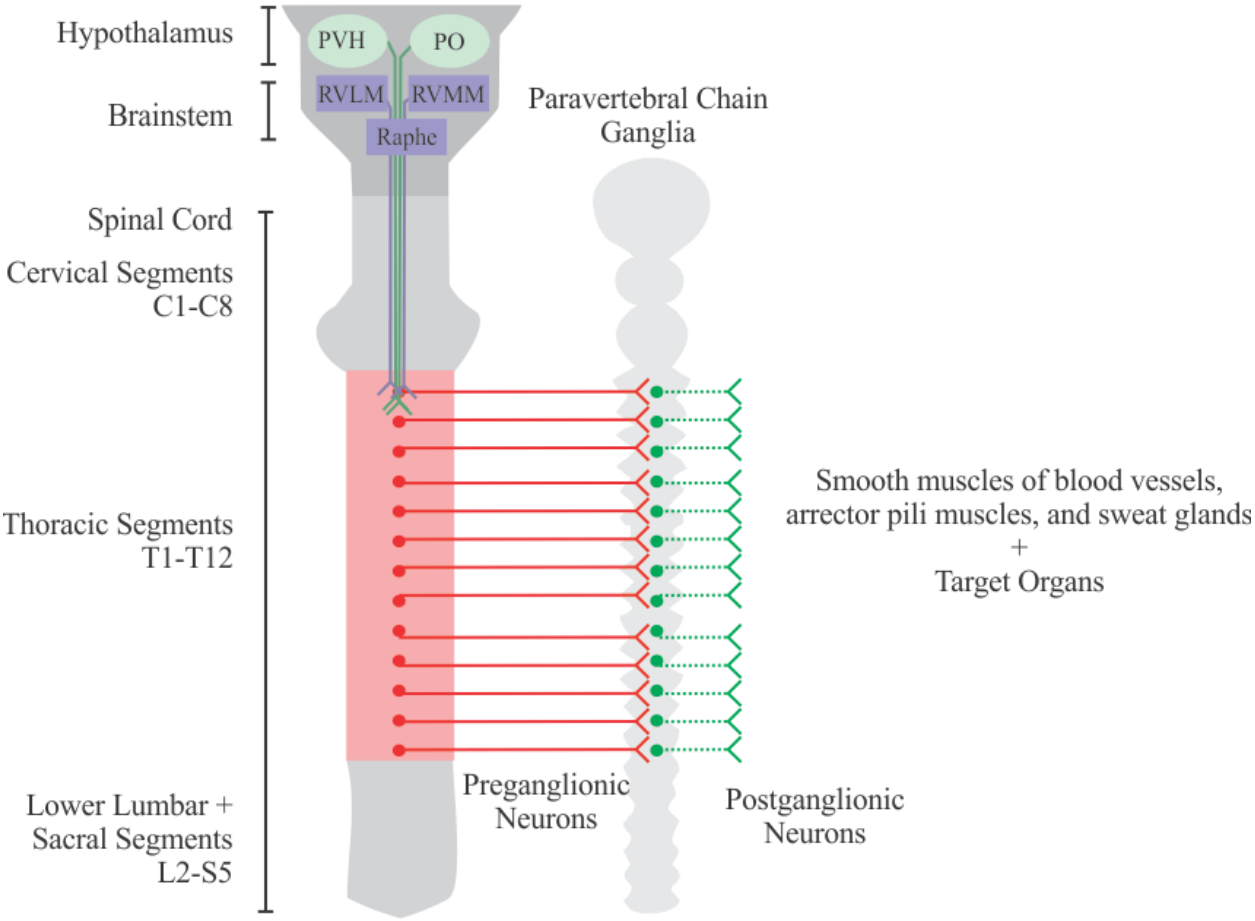

Figure 1.2. General organization of sympathetic nervous system circuitry

Schematics show an overview of the interconnections within the SNS. (compiled and modified from previous studies[10 11 12]) (PVH: paraventricular nucleus of the hypothalamus, PO: preoptic area, RVLM: rostral ventrolateral medulla, RVMM: rostral ventromedial medulla)

The SNS is anatomically organized in a manner that facilitates widespread control and adaptive responses to environmental changes. SPNs are located in the spinal cord and represent the final central elements of this system [13]. SPNs integrate information from two major "Pre-sympathetic" centers in the brainstem and hypothalamus. These regions integrate physiological signals from relevant peripheral receptors before setting the level of sympathetic activity and initiating

outflow to SPNs [14](**Figure 1.2**). In the brainstem, the rostral ventrolateral medulla (**RVLM)** plays a significant role in blood pressure regulation by maintaining outflow to the heart and blood vessels [10] while the rostral ventromedial medulla **(RVMM)** and raphe control cutaneous circulation [15]. Associated with these regions of the medulla are descending adrenergic and serotonergic systems, respectively, that project throughout the spinal autonomic regions housing SPNs, particularly the intermediolateral nucleus (**IML**) [16]. In the hypothalamus, the paraventricular nucleus of the hypothalamus (**PVH**) is involved in the stress response, fluid balance and energy homeostasis [17] while central control of thermoregulation begins in the preoptic area of the hypothalamus (**PO**) [12].

Sensory input from somatic and visceral receptors influence sympathetic efferent activity through spinal reflexes or through supraspinal neural systems [18]. With respect to spinal cord, information from somatic and visceral primary afferents act on SPNs via interneurons in laminae 5, 7, and 10 [18-20]. Information from chemoreceptors of the carotid glomus and aortic bodies, which sense oxygen, carbon dioxide and hydrogen ion concentration of arterial blood, transmit to the nucleus tractus solitarius [21] which act on medullary circuits that project to SPNs.

1.2.2 Anatomical organization of sympathetic preganglionic neurons

SPNs are responsible for transmitting signals from the CNS to various effector organs. Their cell bodies are primarily situated in the lateral horn of the spinal cord, predominantly within the thoracic and upper lumbar regions (though a few are located at the cervical level 8) in four topographically distinct populations: pars funicularis (**ILf**), pars principalis (**ILp**), intercalatus spinalis (**IC**) and, intercalatus spinalis pars paraependymalis (**ICpe**). The ILp (also known as the intermediolateral column, or **IML**) has the largest number and density of SPNs (75% in rat). [22] [23](**Figure 1.3**).

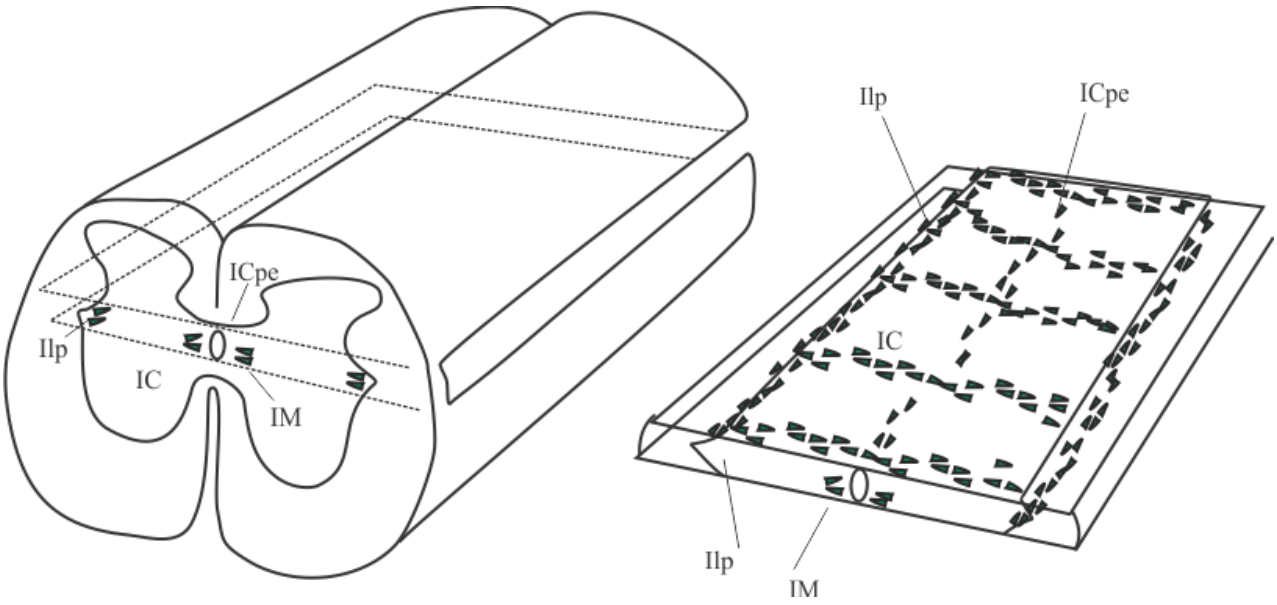

Figure 1.3. Anatomical organization of sympathetic preganglionic neurons in the spinal cord.

Schematic drawings of the spinal cord showing the locations of SPN cells: of zona intermedia: nucleus intermediolateralis thoracolumbalis pars principalis (IML); nucleus intercalatus spinalis (IC); nucleus interealatus pars paraependymalis (ICpe) ; and nucleus intermediomedialis (IM). Note that SPN somas in more caudal segments are arranged in a ladder-like distribution around the central canal [22].

SPNs are topographically organized and exhibit segmental localization in the spinal cord which roughly corresponds to end-organ projections (**Figure 1.1**) [24]. For example, SPNs contributing to the eyes and, myocardium and pineal gland are in high thoracic spinal segments (T1-T3) while the bladder and colon-targeting SPNs are located in T13-L2 [20 25] (**Figure 1.1**).

Electrophysiological studies in mammals have revealed a distinct pattern of innervation in the paravertebral ganglia: the more rostrally positioned ganglia receive innervation from higher, or rostral, spinal cord levels, while the ganglia situated more caudally are connected to the lower, or caudal, spinal cord segments. [26,27].

SPN somas can be found in clusters corresponding to each spinal segment (**Figure 1.3**) [28]. Their dendrites are mainly oriented rostro-caudally within the lateral funiculus and to a lesser extent

medially within the gray matter toward the central autonomic area in lamina X, thus forming a ladder-like distribution symmetric around the central canal [28,29] (**Figure 1.3**). Cell bodies of SPNs are quite variable in shape; most are triangular, oval or fusiform and range from 10-40um in diameter [4].

1.2.1 Sympathetic preganglionic projections and actions on postganglionic neurons

SPN actions on peripheral organs are indirect and occur via synaptic actions on the postganglionic neurons that innervate effector organs. SPNs project ipsilaterally through the adjacent segmental ventral root and connect to a sympathetic ganglion of that segment via the white ramus (**Figure 1.4**). These ganglia are part of a network known as the paravertebral sympathetic chain, which runs parallel to the spinal cord. Whereas prevertebral sympathetic ganglia are typically associated with one or more visceral organs in a discrete location, chain ganglia can be thought of as a distribution system for sympathetic activity that must span the body such as vasculature [6]. Thoracic ganglia contain sympathetic postganglionic neurons which control vasomotor function in the trunk and upper extremity [6].

Ganglia in the paravertebral chain are connected to one another via interganglionic nerves (**Figure 1.4**) (**IGN**). Connections between these neurons and the sympathetic ganglia vary in length: some are short, connecting to an adjacent ganglion; others are long, bypassing several ganglia to link with a distant one. Additionally, there are instances where connections are non-existent, meaning the neurons bypass the sympathetic chain entirely and form direct connections with prevertebral ganglia, such as the mesenteric and celiac ganglia[26]. The splanchnic nerve is an example of the latter. The left splanchnic nerve comprises SPN axons originating from a range of thoracic segments, specifically T3 to T13, with the highest contribution of axons emanating from the T8-T10 segments[29]. It's important to note that the axons from these segments contributing to

the splanchnic nerve represent just a fraction of the total SPNs exiting at that segment[29]. SPN axons mainly connect with postganglionic neurons, though some directly interact with the modified postganglionic neurons called chromaffin cells in the adrenal medulla for rapid endocrine release of adrenaline and noradrenaline [6].

SPN axons emerge from the spinal cord through the ventral roots of the segments containing their cell bodies [30]. SPNs axons can project in both directions: up or down the chain for various segments before making connections onto postganglionic neurons. For the most part, an SPN axon projects into the paravertebral chain ganglia via the white ramus and continues either rostral or caudal to neighboring ganglia [31]. Only 3% of SPNs bifurcate upon exiting the white ramus to travel bidirectionally [31].

SPNs communicate with postganglionic neurons located in the sympathetic ganglia through synaptic connections. The primary neurotransmitter of SPNs is acetylcholine (**ACh**)[32]. When released, ACh elicits rapid excitatory postsynaptic potentials (**EPSPs**) [33] via actions on nicotinic acetylcholine receptors (**nAChRs**). The most common nicotinic receptor is the $\alpha_3\beta_4$ subtype [34,35], though other receptor subunits (α_4, α_5, α_7, β_3) are present in autonomic ganglia [34]. Nicotinic nAChR-mediated EPSPs last up to 150 ms, depending on the resting conductance of the membrane [36,37]. SPN neurotransmitter release can elicit four additional actions: (i) slow, muscarinic EPSP; (ii) slow, muscarinic inhibitory postsynaptic potential (**IPSP**); (iii) slow, noncholinergic EPSP; (iv) slow, noncholinergic IPSP [38].

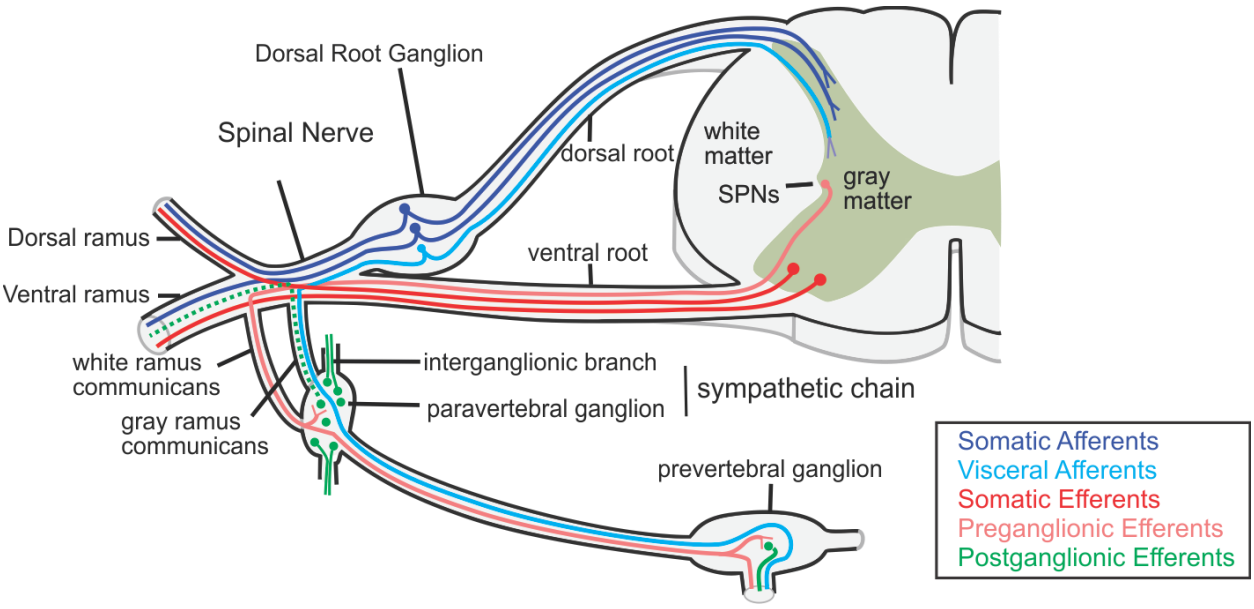

Figure 1.4. Anatomical organization of sympathetic preganglionic projections to sympathetic ganglia.

The organization of the SPNs and its innervation of postganglionic neurons in paravertebral and prevertebral ganglia are shown for one segment. SPN axons exit the spinal cord via the ventral root and enter the sympathetic chain via the white ramus communicans. From here, SPN axons can extend rostrally or caudally along the interganglionic nerve (IGN) to neighboring paravertebral ganglia to contact postganglionic efferents. Dotted line represents postganglionic axons which innervate end-organs.

1.2.1.1 SPN populations distinguished by neurochemical markers

It is assumed that observed SPN non-cholinergic actions are via co-transmitters. Indeed, many SPNs contain various neuropeptides that could support non-cholinergic actions on postganglionic neurons. Somatostatin is present in 33% of SPN somas with the highest concentrations in the T4-T7 and T12-L1 segments [38]. Leucine-enkephalin, an endogenous opioid peptide neurotransmitter, is found in 25% of all SPNs. Substance P is present in 16% of T12-L1 SPNs [38]. Other neuropeptides include: neurotensin, corticotropin-releasing factor (**CRF**), vasoactive intestinal peptide [39], peptide histidine isoleucine amide [40], calcitonin gene-related peptide

(**CGRP**) [41], calretinin, nociceptin [42], secretoneurin [42], cocaine and amphetamine-regulated transcript (**CART**) [43], and luteinizing hormone-releasing hormone [20]. Neuropeptide markers like CRF and CART have been shown to preferentially identify sudomotor and vasoconstrictor SPNs, respectively [11,44]. In addition, many SPNs express nitric oxide synthase and may have actions on postganglionic neurons via nitrergic transmission [45].

Recent work involving single-cell and single-nucleus transcriptomics have found the sympathetic visceral motor system consists of 16 transcriptionally diverse preganglionic clusters, some of which are distributed in unique spinal levels (cervical, thoracic, lumbar) [46,47]. Cluster markers include transcription factors (*Rorb, Nfib, Sox5, Etv1, Dach2*), neuropeptides (*Ccbe1, Sst, Penk*), genes involved in neuropeptide production (*Pcsk2*), secreted molecules (*Fam19a1, Fam 19a2*) and extracellular matrix proteins (*Postn, Fras1, Reln, Mamdc2*) [47]. Further study is needed to identify functional populations of SPNs, including their specific innervation targets and associate them with unique biomarkers.

1.3 Impulse Conduction Through Autonomic Ganglia

1.3.1 Principles of Convergence

The autonomic nervous system differs fundamentally from the somatic motor system in that a single autonomic motor preganglionic neuron (SPN) innervates multiple postganglionic neurons. With respect to sympathetic innervation of paravertebral ganglia, this relationship is characterized by both convergent actions of multiple SPNs on individual postganglionic neurons and divergent projections from individual SPNs onto multiple postganglionic neurons. The expected functional role of convergence would be to spatially and temporally integrate information arising from SPNs across multiple segments to increase probability of recruitment and firing frequency [28 37] (**Figure 1.5**). The expected functional role of divergence is to allow

individual SPNs to influence a multitude of postganglionic neurons, possibly extending their effects across several spinal segments (**Figure 1.5**). In this manner the CNS output response can be amplified.

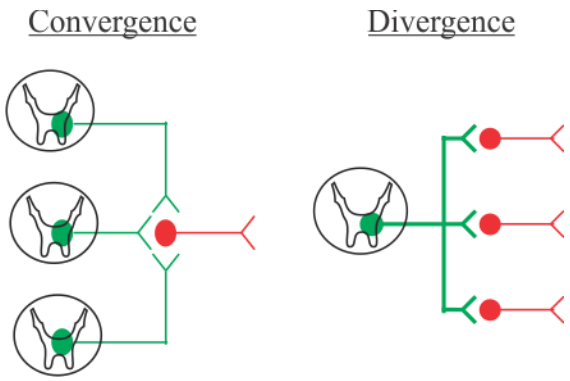

Figure 1.5 Schematic representation of convergence and divergence of SPN axons. Convergence is a mechanism for providing input to a single postganglionic neuron from multiple SPNs. Divergence is a mechanism for spreading stimulation from a single SPN to multiple postganglionic neurons. (green = SPNs, red = postganglionic neurons)

Convergence in the SNS is a mechanism that enables the synaptic drive from multiple SPNs to influence activity in individual postganglionic neurons (**Figure 1.5**). Typically, postganglionic neurons are thought to receive 1-2 primary or strong synapses with the rest being secondary or weaker synapses.

1.3.1.1 The N+1 rule.

The presumed organization of pre-to-postganglionic synaptic connections, initially demonstrated in the superior cervical ganglia of bullfrogs, is known as the "N+1" rule. This organizational rule suggests that a postganglionic neuron gets several subthreshold minor (or weak) synapses (the 'N') plus one suprathreshold primary or strong synapse (the '+1') [48-50]. Nicotinic synaptic events in individual SPNs are categorized as primary when they elicit excitatory postsynaptic potentials

(**EPSPs**) that consistently exceed the threshold strength. Conversely, they are termed secondary when they generate significantly smaller and subthreshold EPSPs during low-frequency stimulation [51]. Karila and Horn (2000) proposed that the n+1 pattern of synaptic convergence is important for managing various peripheral targets with largely invariant amplification levels for crucial operations like blood pressure regulation that required precise timing and responses, in comparison to less critical activities such as piloerection [51].

1.3.1.2 Evidence supporting the N+1 rule.

The recruitment of postganglionic neurons can be achieved through two primary strategies. The first strategy involves a scenario where the EPSP generated by the discharge of a single SPN is sufficiently large to consistently trigger an action potential in the postganglionic neuron [6]. The second strategy relies on spatial summation, where multiple weak SPN inputs converge on a single target neuron [52]. The combined effect of these weak inputs can cumulatively exceed the activation threshold of the postganglionic neuron, leading to the generation of an action potential. In a study using intracellular recordings from postganglionic neurons in the lumbar sympathetic chain, only <5% of action potentials were observed to be triggered by summation of otherwise subthreshold EPSPs [53].

Furthermore, there are two additional mechanisms by which weak synapses might still effectively trigger action potentials in postganglionic neurons. These include fluctuations in the amplitude of EPSPs, a phenomenon known as two-pulse facilitation, and the coactivation of the neuron alongside a slow peptidergic EPSP [51].

1.3.1.3 Evidence challenging the N+1 rule

The thoracic paravertebral ganglia have not shown evidence of operating predominantly by N+1. A variety of EPSPs have been observed, but there is no clear evidence of distinct suprathreshold EPSPs [54]. This finding contributes to the understanding that the thoracic paravertebral ganglia do not predominantly operate through an N+1 mechanism. Furthermore, studies on the thoracic chain revealed that neurons free from impalement injury exhibit significantly higher resistance and membrane time constants. This is an important observation, as when whole-cell recordings are made, the EPSPs appear larger and have a longer duration[36]. This characteristic of EPSPs facilitates the summation of smaller EPSPs, which is crucial for triggering spiking in neurons.

1.3.1.4 Anatomical studies give insight to the degree of SPN convergence.

The exact number of synapses made by each SPN axon, especially those classified as strong or weak, and their specific locations on the soma and dendrites, remains unclear. However, insights can be made from anatomical studies. Only 1 to 2% of the postganglionic neuron surface area is covered by synapses, with the majority being covered by Schwann cells [55]. This observation, derived from detailed electron microscopy studies in guinea pigs, is believed to be consistent across different species [37].

Moreover, the number of SPN fibers innervating a postganglionic neuron, and the total number of synaptic boutons, is related to the surface area of the postganglionic neuron's soma and dendrites [56]. For example, postganglionic neurons in the lateral celiac ganglion, primarily functioning as vasoconstrictors, have a smaller dendritic surface area (about 1300 μm^2) and receive roughly 80 synaptic boutons [57-59]. In contrast, postganglionic neurons in the medial celiac

ganglion, which mostly control intestinal motility or secretion, have a larger surface area (about 3500 μm^2) and receive 300 to 400 synaptic boutons from SPN axons and intestinofugal neurons.

1.3.1.5 Physiological studies on degree of SPN convergence.

Intracellular recordings of postganglionic rat SCG neurons with intact SPN innervation reveal that these neurons typically receive strong inputs from only 1-2, and occasionally 3, sympathetic SPNs [60] [61]. Intracellular recordings conducted *in vivo* on rat lumbar ganglia cells, specifically vasoconstrictor cells, also indicate that, on average, 2-3 SPN axons are estimated to contribute to the generation of each ganglion cell's action potential [53]. In both studies, weaker excitatory SPN inputs were seen that could evoke postsynaptic action potentials, but only when stimulated together.

Currently, the number of synapses that arise from an individual SPN axon has not been definitively determined but estimates on paravertebral neurons suggest that between 2 and 6 SPNs (estimated from electrophysiology) act on postganglionic neurons having ~40-80 putative synapses (having both pre- and post-synaptic markers)[59]. Thus, either individual SPNs generate as many as 13-40 synapses, or electrophysiological studies were unable to recruit and/or generate synaptic actions from all synaptically-connected SPNs.

Physiological findings in studies of SPN convergence could be underestimated due to factors that limit spike conduction of SPNs throughout their projection territories. First, conduction failures are seen in unmyelinated axons and at axonal branch points [62]. Paravertebral SPNs may be prone to such failures as they branch extensively and are predominantly unmyelinated. *In vivo* experiments are undertaken in the presence of anesthesia. Thus, factors that alter autonomic neural excitability may be involved in changes in SPN excitability. Moreover, the experiments

described above were conducted at core body temperature where temperature-dependent conduction failures, particularly of branching axons are more likely [63].

Using an *ex vivo* approach at room temperature, **Table 1.1** estimates the degree of convergence of SPN axons onto individual superior cervical ganglion (**SCG**) neurons in multiple mammalian species by recording discrete evoked synaptic responses following stimulation of T1-9 ventral roots at increasing stimulus intensities. Convergence estimates show that the ratio of SPN inputs to postganglionic neurons varies significantly among different species.

Table 1.1 Average innervation ratios of SPNs onto postganglionic neurons in superior cervical ganglia across mammalian species.

Shown are the differences across these species in two key aspects: animal size and the number of axons innervating each ganglion cell (convergence). The number of axons innervating each ganglion cell was determined by counting the excitatory postsynaptic potentials that could be recruited by gradually increasing the stimulus strength to each of the ventral roots that supplies innervation to the ganglion. [64]

Animal	Weight	Convergence: Mean # SPNs innervating a SCG postganglionic
Mouse	20-32g	4.5
Hamster	90-120g	7.2
Rat	150-170g	8.7
Guinea Pig	360-400g	12.3
Rabbit	1.6-1.7kg	15.5

1.3.2 Principles of divergence.

An SPN axon can pass through multiple paravertebral ganglia before establishing its primary synaptic connections. Typically, each preganglionic axon will diverge to form synapses with postganglionic neurons across various paravertebral ganglia [6]. In bullfrog, estimates show that SPN axons can diverge to form synapses with 50 ganglionic neurons, the majority of which are weak synapses [51]. In cat experiments studying piloerection, SPN axons in the thoracic region ascended four segments, making synapses onto postganglionic neurons in each ganglion [65].

Estimates of divergence ratios made by comparing labelled SCG cell bodies to retrogradely labelled SPNs in spinal cord show that the number of SPNs do not increase in proportion to animal size but rather the degree of SPN to postganglionic neuron divergence increases with the size of the animal and the target organ [20] (**Table 1.2**). Overall, divergence serves to amplify CNS output responses.

Table 1.2. Estimates of divergence based on anatomical labelling in superior cervical ganglion.

Highlighted are the differences across these species in the number of ganglion cells each axon innervates (divergence). Counts of SPNs were conducted following a process of retrograde labeling of the SPNs, coupled with the labeling of postganglionic neurons. This table was adapted from SCG [66 3,20].

Animal	Weight	Divergence: Ratio of SPNs to SCG Cells
Mouse	20-32g	1:14
Hamster	90-120g	1:25
Rat	150-170g	1:27
Guinea Pig	360-400g	1:26, 1:15
Rabbit	1.6-1.7kg	1:27
Human	60-80kg	1:200

1.3.1 Sympathetic gain control.

The limits of sympathetic signal amplification from the central nervous system remain largely uncharted. SPNs can form either strong, primary nicotinic synapses or weak, subthreshold secondary synapses. It is unclear whether diverging SPN axons form both strong and weak nicotinic synapses. Karila and Horn (2000) proposed the maximum amplification gain is determined by the combined effect of both primary and secondary synapses (1°+2°), while the minimum gain is governed by the primary synapse alone [51].

1.4 Axonal action potential propagation in SPNs.

The traditional perspective of axonal spike conduction, grounded in cable theory, posits that spikes begin at the axon initial segment and propagate faithfully down the axon. Thus, axons function as fail-safe conduits for neural signals to act specifically on their synaptically connected cellular targets [67-69]. SPN axons are believed to reliably transmit information from the CNS to postganglionic neurons with little to no modification [3] However, most SPNs are unmyelinated with very small diameters which are expected to be prone to activity-dependent changes in conduction including conduction failures [70,71]. Moreover, SPNs branch to innervate multiple targets, forming axonal branch points which are also prone to conduction failure [67,72]. The consistency and dependability of SPN axonal conduction are yet to be thoroughly investigated. Considering their extensive multisegmental and divergent actions, the variability in spike conduction could represent a significant and adjustable aspect of sympathetic output regulation.

1.4.1 Anatomical features of the preganglionic axon that affect spike propagation.

The percentage of SPNs that are unmyelinated varies between species: 43% in cats, 99% in mice and rats [73]. In humans, reports of myelination vary with ranges between 20-94% [74,75]. SPN fiber types can be classified by conduction velocity using the Erlanger-Gasser system ranging from Aδ , B- to C-fibers[76]. Thinly myelinated, smaller diameter Aδ or B- fibers have conduction speeds ranging from 1.8-17 m/s while unmyelinated, small diameter C fiber primary afferents range between 0.3-1.3 m/s [77]. Variance in myelination results in a broad range of conduction velocities in thoraco-lumbar SPN axons, with cats exhibiting velocities between 0.6-15 m/s, rats between 0.2-15 m/s, and guinea pig between 0.1-10m/s [20,54,78-81]. Conduction velocity in mouse splanchnic nerve was ~1 m/s [82]. In rats, 92% of SPNs recorded in the cervical sympathetic trunk have conduction velocities in the C-fiber range [81]. It is unknown whether conduction velocity of axons (which is proportional to diameter) can predict whether observed variation is related to

differences in function. Spontaneously active rat SPNs with discharge rates linked to the cardiac cycle had similar distribution of conduction velocities of axons to the total SPN population suggesting conduction velocity may not be a predictor of a particular SPN's function [81].

Small-diameter unmyelinated axons, like SPNs, face greater variability in action potential conduction propagation than thicker myelinated axons because of their very high axial electrical resistance, large surface-to-volume ratio, variations in diameter along the axon and extensive branching patterns [83]. Large axon calibers (axon diameters) conduct action potentials faster than smaller ones in part because the flow of ionic current meets less internal resistance. While larger axons can transmit signals faster, they also require more energy to maintain. Mitochondrial volume per unit of axonal length rises linearly with axon diameter for small profiles ($d<0.7um$) and quadratically for larger axons [84]. The standard explanation for requiring thick axons is that higher conduction velocities are needed to reduce conduction times and information transfer [85]. While useful for the skeletal muscle system, if higher velocity information transfer is not critical to system performance, it is metabolically efficient to sacrifice speedy conduction to lower energy demands [86]. A principle forwarded called 'the law of diminishing returns' describes that for an axon to double its information rate, it must more than quadruple its volume and energy use [86]. As the SNS has many SPNs that require continuous activity at low frequency and with slow temporal dynamics (e.g. cardiovascular and respiratory encoding neurons), a metabolically more cost-effective strategy is to encode information via small-diameter axons [86]. Given how small the SNS axons diameters are, it is likely that they have been evolutionarily tuned to operate by the law of diminishing returns. In human SPNs, the number of unmyelinated axons has not been determined, but the dominant SPN myelinated fiber type is the small-myelinated fiber (**SMF**) which makes up 90% of all preganglionic myelinated fibers and has a diameter range of 1.7-2.5

μm[87]. Limited data is available regarding SPN axons of mice but what is known is that mean diameters are ~0.4 μm with smallest fibers seen at 0.1 μm [73]. In cats, the diameter of myelinated axons ranges from 1-5 μm [88].

SPN axons come out of the spinal cord via the ventral roots located in the same segments as their cell bodies. At the level of the ventral root, each segment has an equal number of SPN axons as somas [89]. However, after projecting from the communicating white ramus into the sympathetic chain, SPN axons exhibit extensive collateral branches that are multisegmented and innervate multiple ganglia [89,90]. Thus, in branching axons, geometrical features of the primary axon and its branching collaterals can dictate the success of spike propagation. For example, if the combined cross-sectional area of daughter branches is greater than the cross-sectional area of the parent axon, the lower input impedance creates a current sink ahead of a propagating spike that can reduce spike amplitude and cause conduction failure [91,92].

Currently only a few studies describe distinct SPN populations that project to postganglionic neurons of the same effector organs. For example, cocaine and amphetamine-regulated transcript peptide (**CART**) is prevalent in sympathetic preganglionic neurons in rats, predominantly targeting vasoconstrictor neurons and cardiac-projecting postganglionic neurons, but not non-vasoconstrictor neuron [44]. In the parasympathetic network, research has demonstrated that vagal preganglionic axonal arbors create connections both internally and amongst ganglia with neuronal nitric oxide synthase (**nNOS**) immunopositive (**nNOS$^+$**) enteric postganglionic neurons, while other SPNs with arborizing axons selectively connect with nNOS$^-$ enteric postganglionic neurons [93]. This suggests the possibility that SPN branching axons may operate in a comparable manner, exerting multisegmental influences on a uniform population of postganglionic neurons.

1.4.2 Firing Properties of SPNs.

Surprisingly, *in vivo* studies observed that 40-70% of neurons projecting to major sympathetic nerves in cats remain inactive and do not exhibit reflex activity under experimental conditions [56]. Notably, studies were undertaken in the presence of anesthetics expected to reduce excitability. Moreover, observations specifically pertain to neurons projecting to the cervical sympathetic trunk, lumbar sympathetic trunk, or lumbar splanchnic nerve. To my knowledge there are currently no *in vivo* studies on the excitability of SPNs projecting to the middle-lower thoracic paravertebral chain ganglia, but their unique distribution to truncal vascular systems may lead to higher levels of population excitability. It is generally agreed that postganglionic activity that contributes to effector organ 'tone' is driven by tonic discharge of SPNs [94]. SPN tonic activity is irregular, though many SPNs may have cardiac, respiratory rhythm or other frequencies superimposed [95 94,96-102]. One of the characteristic features of the firing of SPNs, is its extremely low rate of <1Hz and peak at 10Hz [3 103-105]. Functional populations of SPNs can broadly be divided based on their tonic and phasic firing patterns. Skin, muscle and gut vasoconstriction, gut motility and secretion, and relaxation of the detrusor muscle involve tonically firing SPNs. Phasically firing SPNs are sudomotor (sweating), pilomotor (piloerection), or involved in saliva production, pupil dilation, increased cardiac output and sexual activity [14]. Mannard and Polosa (1973) identified four distinct firing patterns in cat sympathetic preganglionic neurons (SPNs)[95]. The first is irregular background firing with rates varying from 0.4 to 1.9 spikes/sec, with the shortest interspike intervals ranging from 330 to 960ms, influenced by the state of the preparation. The second pattern, slow-rhythm, often linked to a hypotensive state, shows a frequency of 0.15Hz and an average spike rate of 1.6 spikes/sec. The third, respiratory-rhythm, is characterized by a frequency of 0.62 Hz and a mean spike rate of 1.5 spikes/sec, with SPNs discharging triplets per respiratory cycle. Finally, the pulse-rhythm pattern exhibits a frequency

of 2.1 Hz and an average spike rate of 4.0 spikes/sec, with SPN activity often entraining to the cardiac rhythm, marked by couplets of irregular firing synchronized with each heartbeat. Impulses in individual SPNs combine to generate overall sympathetic nerve discharge (**SND**). Thus, SND can be described as quasiperiodic; it has some degree of regularity but can also show variations in timing or frequency [106].

Whether or not an SPN fires tonically depends on the composition of subthreshold excitatory EPSPs received by the SPN membrane. Voltage clamp studies in rat estimate that the firing rate of input to sympathetic preganglionic neuron, capable of eliciting a spike discharge, is approximately 20 Hz [107]. In cat, background synaptic input to SPNs occur between 0.9-8.5 Hz [108]. This higher frequency input is then translated into a final spike discharge rate of around 2 Hz in the SPNs [107].

However, roughly half of SPNs exhibit very low levels of ongoing synaptic activity consisting of a few small amplitude EPSPs (1-3mV) which are not enough to generate tonic firing [109]. In fact, a significant proportion of SPNs are silent under basal conditions depending on species and SPN location: high thoracic (T1-T3) SPNs *in vivo* in cat [110,111], 53% in rat [110] , 29% in cat [112] or in rat thoracolumbar spinal cord slices *in vitro* (51%-92% depending on study) [28,113] [114].

Other factors which may play a role in determining whether an SPN will fire tonically include their intrinsic excitability (passive and active membrane properties) and the occurrence of slow synaptic potentials[28]. SPN intrinsic membrane properties have been studied in the mouse rat and cat[28,38,81,112,115-119] [120]. Differences in mean and peak firing across species are listed in Table 1.4. In somas of SPNs that combine to form the splanchnic nerve, active SPNs have an individual firing rate of ~0.7Hz but together SND (at a population level) is ~1Hz in the splanchnic nerve[106].

Table 1.3 Mean and Peak SPN Firing Rates Across Species

Animal	Mean ± SD or Range Firing Rates (Hz)	Peak evoked rate
Neonate mouse[121]	0.196 ± 0.11	28Hz
Neonate Rat[53,122,123]	2.08 ± 1.15	20Hz
Adult Rat[81,115]	2.1+/- 0.5	10Hz
Guinea Pig[116,124,125]	0.5- 4	20Hz
Cat[108]	0.06-4.6 (Type B) 0.8-6.5 (Type C)	?
Human[126]	0.22 Hz (Based on modeling data)	?

Higher than average firing rates are seen under certain physiological conditions. For instance, SPNs with a respiratory-modulated firing pattern have been observed to burst at frequencies of 10-20Hz during short inspiration phases [127]. Additionally, activation of somatic or visceral afferents can significantly elevate SPN firing rates above average [128], while hypoxic conditions prompt SPN somas to fire at rates surpassing 5-10Hz [129]. While not generated physiologically, intracellular somatic current injections provide insight into the range of evocable tonic firing frequencies. In the neonatal mouse, Zimmerman and Hochman (2010) demonstrated that SPNs can achieve peak firing frequencies of up to 28Hz before encountering depolarization block. In rat, injection of depolarizing current pulses incrementally increased their firing rate up to a maximum of 10Hz before block [107].

Descending neuromodulatory transmitters are well known to project to SPNs and alter their excitability. For example, SPNs receive dense innervation of 5-HT terminals from the caudal raphe nuclei and the rostroventrolateral medulla [130], and 5-HT application can generate sympathetic rhythmic discharge in SPNs. Activation of 5-HT2A receptors on SPNs has been shown to evoke rhythmic membrane oscillations resulting in discharged action potentials in bursts [130]. In addition, 5-HT application can generate the T-rhythm, a sympathetic motor rhythm

regulating the thermoregulatory circulation of the rat tail. It arises from SPNs of T11-L2 segments and can be elicited at 0.40–1.20 Hz [131].

A single action potential can lead to long lasting facilitation in postganglionic neurons that last several seconds [132,133] but attenuates the release of both cholinergic and non-cholinergic transmitters via muscarinic receptors of the SPN axon terminal [134]. Successive SPN impulses lead to increased number of quanta, more ACh release and facilitation [135]. A 2Hz repetitive stimulation of SPN releases ACh at a steady state in guinea pig [135]. For frequencies higher than 5Hz, ACh release peaks and then settles to a steady state within 15 seconds [135]. If left for 3.5 hours, 5Hz stimulation depletes non-cholinergic transmitter stores [136].

Prolonged high frequency SPN activation can attenuate ACh output, so to maintain effector organ activity, non-cholinergic transmission may play a role [38]. In both the superior cervical and stellate ganglion of the cat, prolonged stimulation of SPN axons has been reported to severely attenuate the evoked, nicotinic response at a time when non-cholinergic transmission should have been maximally activated [137,138]. Prolonged repetitive stimulation at higher rates (20 Hz, 20 sec-2 min) can release enough non-cholinergic transmitter(s) to initiate action potentials in SGN [136,137,139].

1.4.3 Factors controlling action potential propagation in SPNs.

The impact of repetitive activity on modifying conduction velocities and transforming spike patterns, resulting in potential conduction failures or ectopic spiking, has been recognized for quite some time [69,140-143]. Especially susceptible are thin unmyelinated axons, characterized by their high axial electrical resistance, significant surface-to-volume ratio, complex branching, and inconsistent diameters, all of which complicate the conduction of action potentials [83]. Understanding the activity-induced shifts in excitability along the proper axonal length is crucial

for decoding the overarching scheme of neuronal communication, particularly among the predominantly unmyelinated SPN neurons.

In many varieties of axons, repetitive stimulation at medium to high frequency (10– 50 Hz) has been shown to result in conduction failures occurring specifically at branch points [68]. Variations in diameter and branching reduce conduction reliability by creating regions of "impedance mismatch" [69]. Conduction block after high frequency stimulation appears first in the thicker daughter branch followed later by the thin branch [144]. Demonstrated first in spiny lobster, high frequency stimulation (30Hz or greater) administered to branching axons results in a 10-15 % reduction in amplitude of the action potential in the parent axon, a decrease in the rising slope of the action potential, a 25-30% decrease in conduction velocity, an increase in threshold and a prolongation of the refractory period [144]. Despite seeing a reduction in spike amplitude across the axon, conduction block was only seen in the bifurcation region [144].

Thin, unmyelinated fibers are especially prone to a reduction in conduction velocity in response to repetitive firing. When subjected to stimulation at frequencies of 1Hz or higher, the slowest-conducting unmyelinated axons, including those in rat SPNs, exhibit increased antidromic latency, a phenomenon also observed in various other systems [81,145,146]. However, a significant knowledge gap exists regarding the activity-dependent alterations in SPN conduction at higher frequencies. Predictive insights may be gleaned from studies on unmyelinated C-fibers and postganglionic axons. For instance, after being stimulated at 20Hz for 20 seconds (at twice the electrical threshold), C-fibers in the rat saphenous nerve demonstrated substantial conduction slowing: polymodal and heat nociception fibers showed a 29% reduction, mechanical nociceptors a 28% reduction, cold thermoreceptors a 11% reduction, mechanoreceptors a 15% reduction, and a 15% reduction in spontaneously active sympathetic postganglionic efferents [147].

Increasing stimulation duration for longer than 20 seconds resulted in conduction failure in polymodal nociceptors [147]. In a study comparing humans and pigs, 2 Hz – 3 minute stimulation slowed conduction velocity of mechano-insensitive C-fibers by 30%, and mechano-insensitive cold afferents by <10% [148]. Mechano-sensitive afferents showed conduction slowing at 14% and 23% for pig and human, respectively [148]. Sympathetic postganglionic efferent fibers in pig and human slowed only minimally (5% and 9%, respectively) [148]. Activity-dependent slow inactivation of voltage-gated sodium channels has been proposed as mechanism for conduction velocity slowing [149].

1.4.3.1 Ion channels on SPN axons.

The somatic SPN action potential waveform consists of a TTX-sensitive Na^+ and kinetically slower Ca^{2+} sensitive-TTX insensitive component. The latter results in a long afterhyperpolarization which involves Ca^{2+}-activated K^+ channels [20]. There are two parts to the afterhyperpolarization: a fast and slow component. The fast component can be blocked with cesium or high concentrations of TEA [20]. The slower component can be partially blocked with low-Ca^{2+} calcium concentrations or cobalt [20]. The currents found in SPN somas are listed in Table 1.4.

Table 1.4 Membrane currents found on SPN somas

Current Class	Current Type
Voltage-dependent K^+ currents [28,119,150-153]	Delayed rectifier (I_K)
	Ca^{2+} dependent transient current (I_C)
	Ca^{2+} dependent sustained current (I_{AHP})
	A-Current (I_A)
	M-current (I_M)
	Inward Rectifying (I_{ir})
	Quinine-sensitive outward rectifier
Low-voltage-activated calcium conductance (LVA) T-type [119]	

Calcium activated K+ currents [28,127]	AHP currents (gKCal, and gKCa2)
Sodium Currents	Transient (I_{NaT})[154]

More relevant to the current thesis is the identification of the voltage-dependent channels found in axons responsible for spike propagation. Voltage-gated Na^+ channels, activated by membrane depolarization, conduct an influx of Na^+ ions that generate the action potential. $Na_v1.1$, 1.2 and 1.6 are found in the nodes of Ranvier of myelinated PNS and CNS axons and are the most commonly found Na^+ channel isoforms [72,155]. $Na_v1.2$ is predominantly expressed in unmyelinated axons [155]. In myelinated axons, voltage-gated K^+ channels identified as involved in spike repolarization are $K_v3.1b$ and $K_v7.2/K_v7.3$, expressed between the nodes of Ranvier, and $K_v1.1$ and 1.2 which are expressed juxtaparanodally [72]. Unmyelinated axons express $K_v1.2$, 1.3, 3.3, 3.4, and 7 along the axon proper. Potassium channels seen at the axon terminals include: $K_v1.1/1.2$, 1.4, 3.1, 3.2, 3.4, 7.2/7.3, 7.5 [155]. The M current, a non-inactivating K^+ current mediated by the voltage-gated K_v7/KCNQ family, plays a pivotal role in increasing the action potential firing threshold and is responsible for the slow, prolonged afterhyperpolarization [156] through its Ca^{2+}-activated mechanism [155].

Table 1.6 categorizes ion channels based on their established expression in various axon types (myelinated and unmyelinated). Column 4 of Table 1.5 highlights channel RNA expression in sympathetic postganglionic neurons by mining data from single-nuclear RNA-sequencing of spinal 'visceral' cholinergic neurons provided in the study by Alkaslasi, Piccus, and colleagues [157].

Table 1.5 Ion channels on axons

Channel	Axon type	Action	RNAseq of SPNs
Sodium			

$Na_v1.2$[155]	Unmyelinated	Axon propagation	**SCN2A (high)**
$Na_v1.6$[155]	Myelinated	Axon propagation, maintenance of high-frequency firing	SCN8A (high)
Potassium			
$K_v1.1$[155,158,159]	Myelinated & unmyelinated	Repolarization	KCNA1 (low)
$K_v1.2$[155] [72,158,160]	Myelinated & unmyelinated	Repolarization	KCNA2 (low)
$K_v1.3$ [72,155]	Myelinated & unmyelinated		KCNA3 (none)
$K_v1.4$[155,161,162]	Myelinated & unmyelinated	Rapid inactivation	**KCNA4 (med)**
$K_v3.1$[155,163,164]	Myelinated	Fast nodal delayed rectifier	KCNA4 (low)
$K_v3.2$[155]	Myelinated & unmyelinated	Rapid repolarization in neurons with fast-spiking properties	KCNC2 (high)
$K_v3.4$[72,155,163,165,166]	Unmyelinated &myelinated	Outward current	KCNC4 (low)
$K_v4.3$[167]	Unmyelinated	Rapidly inactivating	**KCND3 (high)**
K_v7[155] [72,167-169]	Myelinated & unmyelinated	Slowly activating (Ks)	**KCNQ1 (high)** **KCNQ2 (high)** **KCNQ3 (high)** **KCNQ4 (high)** **KCNQ5 (high)**
$K_v\beta1$ & $K_v\beta2$[155]	Unmyelinated	Subunit influencing amplitude and duration	**KCNAB1 (high)** KCNAB2 (low)
GIRK[155]	Presynaptic terminal	Controls action potential duration	KCNJ3 (medium) KCNJ6 (low) KCNJ9 (low) KCNJ5 (none)
Slo1[170-172]	Myelinated & unmyelinated	Large conductance Ca^{2+}-activated potassium channels	**KCNMA1 (high)**
Slo2.2[20]	Myelinated & unmyelinated	Limit excitability of nerve terminal	KCNT2 (high)
HCN [173]	Myelinated & unmyelinated	Conducts a mixed Na^+/K^+ current in response to hyperpolarization, contributing to the spontaneous rhythmic activity and the control of neuronal excitability	**HCN1 (high)** **HCN2 (high)** HCN3 (low) HCN4 (low)
Calcium			
$Ca_v1.2$[155]	Myelinated & unmyelinated	L-type voltage-gated Ca^{2+} channel	CACNA1C (high)
$Ca_v2.1$[155,163]	Myelinated & unmyelinated	P/Q-type voltage-gated Ca^{2+} channels prevalent at presynaptic terminals	CACNA1A (high)

$Ca_v2.2$[155,174]	Myelinated & unmyelinated	N-type voltage-gated Ca^{2+} channel	CACNA1B (high)

As the present thesis concerns studies on SPNs in adult mouse which are predominantly unmyelinated and given the expression levels reported in the RNAseq study, the most relevant channels expressed associated with axonal conduction are expected to be the following: $Na_v1.2$ (SCN2A), $K_v1.4$ (KCNA4), $K_v4.3$ (KCND3), K_v7 (KCNQ1-5), Kvβ1 (KCNAB1), slo (KCNMA1), and HCN (HCN1,2).

While not specifically studied in relation to axon conduction, most neurons including SPNs have both Na^+ and K^+ leak conductances whose activity may be expected to alter resting membrane potential and conductance. Moreover, RNA sequencing studies identified channels with temperature sensitivity[47,175]. Overall, there are clearly both voltage-dependent and independent channels that may be involved in spike conduction. Details specific to the thesis will be provided in Chapters 3 and 4 in relation to the studies undertaken on control of conduction in SPNs.

1.5 Summary

In this introductory chapter, we present a comprehensive overview of the autonomic nervous system, emphasizing the sympathetic nervous system. Special attention is given to the SPNs, particularly examining factors that influence SPN convergence, divergence, excitability, and the control of conduction along axonal projections. This thesis delves into the factors affecting conduction in SPNs originating from the lower thoracic spinal cord, focusing on elements that contribute to variability in spike conduction.

Chapter 2 introduces a novel *ex vivo* methodology tailored for adult mice, enabling the investigation of SPNs and their influence on postganglionic neurons in thoracic paravertebral

ganglia. In Chapter 3, we characterize the specific features of thoracic sympathetic preganglionic axons, such as axon diameters, myelination, conduction velocity, and branching patterns, and how these attributes contribute to increased variability in axonal conduction. Chapter 4 conducts experimental investigations into preganglionic axon propagation failure, focusing on the effects of altering bath temperature and stimulation frequency. Chapter 5 explores the neuromodulatory actions on spike propagation along the axon, providing insights into the complex dynamics of sympathetic neural transmission. Finally, chapter 6 summarizes major conclusions.

2 Isolation and Electrophysiology of Murine Sympathetic Postganglionic Neurons in the Thoracic Paravertebral Ganglia

2.1 Abstract

Results and methodologies in this chapter have been published[176]. The thoracic paravertebral sympathetic chain postganglionic neurons (**tPostNs**) represent the predominant sympathetic control of vascular function in the trunk and upper extremities. tPostNs cluster to form ganglia linked by an interganglionic nerve and receive multisegmental convergent and divergent synaptic input from cholinergic sympathetic preganglionic neurons of the spinal cord [25,54]. Studies in the past have focused on cervical and lumbar chain ganglia in multiple species, but few have examined the thoracic chain ganglia, whose location and diminutive size make them less conducive to experimentation. Seminal studies on the integrative properties of preganglionic axonal projections onto tPostNs were performed in guinea pig [25,54], but as mice have become the accepted mammalian genetic model organism, there is need to reproduce and expand on these studies in this smaller model. We describe an *ex vivo* approach that enables electrophysiological, calcium imaging, and optogenetic assessment of convergence, divergence, and studies on pre- to postganglionic synaptic transmission, as well as whole-cell recordings from individual tPostNs. Preganglionic axonal connections from intact ventral roots and interganglionic nerves across multiple segments can be stimulated to evoke compound action potential responses in individual thoracic ganglia as recorded with suction electrodes. Chemical block of synaptic transmission differentiates spiking of preganglionic axons from synaptically recruited tPostNs. Further dissection, including removal of the sympathetic chain, enables whole-cell patch clamp recordings from individual tPostNs for characterization of cellular and synaptic properties.

2.2 Background

Thoracic sympathetic postganglionic neurons (**tPostNs**) are housed in bilateral paravertebral chain ganglia. Comprising a significant component of the final motor output of the sympathetic nervous system, paravertebral tPostNs contribute to autonomic homeostatic mechanisms by directly innervating effector tissues, including vasculature, adipose tissue, sweat glands, and piloerector muscles [6,7]. Thoracic sympathetic ganglia contain a distinct composition of genetically separable postganglionic neuron groups as compared to more rostral cervical and lower thoracic segments [177]. Their morphological and electrophysiological properties may also differ from tPostNs elsewhere [82]. Our understanding of the electrophysiological properties of paravertebral sympathetic chain postganglionic neurons has been largely derived from studies in cervical and lumbar ganglia [27,53,178-182] with intracellular recordings undertaken using sharp microelectrode approaches [25,54,82] [183] with an impalement injury conductance that alters basic membrane properties [183-185].

2.3 Materials and Reagents

1. 2 mm glass probes made from stringer (Bullseye Glass, catalog number: 000147-0272-F-Tube)
2. ½ ml Monoject Insulin Syringe, 29 G × ½” (Covidien, catalog number: 8881600350)
3. Needle 25 G (BD PrecisionGlide, catalog no: 14-826G)
4. 1.5 ml MCT Graduated Mixed Tubes (Fisherbrand, catalog number: 05-408-137)
5. 0.20 mm Stainless Steel Insect pins (Fine Science Tools, catalog number: 26002-20)
6. 0.22 μm Syringe Filter (Fisherbrand, catalog number: 09-719C)
7. 100 mm × 15 mm Petri Dish (VWR, catalog number: 25384-070)
8. Square plastic weighing dish (Dyn-A-Med, catalog number: 80055)

9. Electrode Storage (World Precision Instruments, catalog number: E215)
10. VWR micro cover glass 24 × 50 mm (VWR, catalog number: 48393081)
11. Adult C57Blk/6 mice (6+ weeks old, alternative animal strains can be used)
12. Collagenase Type III (Worthington Biochemical Corporation, catalog number: LS004180)
13. Isoflurane, USP (Piramal Critical Care, catalog number: 400648037)
14. Urethane (Sigma-Aldrich, catalog number: U2500)
15. Ketamine (Henry Schein, catalog number: 056344)
16. Xylazine (Sigma-Aldrich, catalog number: X1251)
17. Custom-built Sylgard-coated dissecting dish (see Procedure D)
18. SYLGARD^{TM} 170 Silicone Elastomer Kit (DOW Inc., catalog number: 4026157)
19. High vacuum grease (DOW Corning, catalog number: H051J89018)
20. Sodium chloride (Fisher Scientific, catalog number: S642-500)
21. Potassium chloride (Sigma-Aldrich, catalog number: P9541-1KG)
22. Magnesium sulfate Heptahydrate (Fisher Scientific, catalog number: BP213-1)
23. Calcium chloride dihydrate (Fisher Scientific, catalog number: C69-500)
24. Potassium phosphate monobasic (Sigma-Aldrich, catalog number: P5655-500G)
25. D-(+)-Glucose (Sigma-Aldrich, catalog number: G7528-1KG)
26. Sodium bicarbonate (Sigma-Aldrich, catalog number: S6297-1KG)
27. 95% O_2, 5% CO_2 gas (Nexair, catalog number: UN3156)
28. Potassium D-gluconate, 99% (Alfa Aesar, catalog number: B25135)
29. EGTA (Sigma-Aldrich, catalog number: E-3889)
30. HEPES (Sigma-Aldrich, catalog number: H3375-250G)
31. ATP (Sigma-Aldrich, catalog number: A9187)

32. GTP (Sigma-Aldrich, catalog number: G9002)

33. Artificial Cerebrospinal Solution (aCSF) for Electrophysiological Recordings (see Recipes)

34. High Magnesium Low Calcium Microdissection Solution (see Recipes)

35. Patch Electrode Solution (see Recipes)

2.4 Equipment

2.4.1 Surgical tools

1. 2.5 mm Vannas spring scissors (Fine Science Tools, catalog number: 15002-08)
2. Wagner scissors (Fine Science Tools, catalog number: 14068-12)
3. 9 mm Castroviejo microdissecting spring scissors (Roboz, catalog number: Rs-5658)
4. Dumont #5 Forceps (Fine Science Tools, catalog number: 11251-20)
5. pH meter (Denver Instruments, model: UB-10)
6. Osmometer (Vapro, model: Model 5600)
7. Magnetic stir plate (IKA Works USA, model: CERAMAG Midi)
8. Magnetic stir bar (VWR, catalog number: 76006-400)
9. 600 ml beaker (Pyrex, catalog number: CLS1000600)

2.4.2 Recording equipment for whole-cell recordings

Generally, there are multiple commercially available components that can be used to undertake visually guided whole-cell recordings from microdissected nervous tissue. We used an upright microscope containing 40× liquid immersion objectives with differential interference contrast and infrared imaging for image enhancement. Conventional electrophysiology recording methods were employed, including an experimental chamber with oxygenated aCSF, air table, micromanipulator with attached electrode holder, high impedance low noise patch clamp amplifier, A/D converter, and associated specialty software for data capture. Details are provided

in various reviews. Those used by our lab are described in a recent publication (McKinnon *et al.*, 2019) as listed below.

1. Upright DIC fluorescence microscope (Olympus, model: BX51WI) affixed with a low-light camera (Olympus, model: OLY-150)
2. Vertical Electrode Puller (Narishige, model: PP-83)
3. Micro-forge (Narshige, model: MF-9)
4. MultiClamp 700[a] and Digidata 1322[a] [186]
5. Custom Sylgard-coated recording chamber and perfusion system
6. Controllable blue light laser (custom built but are also commercially available; *e.g.*, Thorlabs S1FC473MM Multimode Fiber-Coupled Laser)
7. Electrical stimulation can be provided by commercially available stimulators (*e.g.*, A-M Systems, model: 2200 Analog Stimulus Isolator)
8. Gravity fed superfusion with Masterflex pump for recirculation (Cole Palmer, model: 77200-50)
9. Tubing for perfusion (Masterflex, catalog number: 96412-16)
10. 1.5-mm outer diameter filamented, borosilicate glass capillaries (World Precision Instruments, catalog number: TW150F-4)
11. Coated silver wire (A-M Systems, catalog number: 787000)
12. Connector Socket 20-24AWG gold crimp (Digi-Key, catalog number: 205090-1)
13. Connector D-Sub Pin 20-24 AWG AU (Digi-key, catalog number: 205089-1)
14. Silicone tubing for electrode (Masterflex, catalog number: 96410-10)
15. Cotton Swab with plastic shaft (Just The Basics, catalog number: PINSB0300DLJB01)
16. Quick-Setting Epoxy Syringe (J-B Weld, catalog number: 50112)

17. 4-Indent D-Sub Crimper 26-20 AWG (Paladin Tools, model: PA1440)
18. Multipurpose wire stripper and cutter (Klein Tools Inc., model: 1010)
19. Three-Way, Stopcock with Male Luer Lock, Non-Sterile (Cole-Palmer, catalog number: UX-30600-02)
20. 5 ml disposable syringe with Luer Lock (BD, catalog number: 309646)
21. Electrical tape (VWR, catalog number: 470020-186)
22. Insulated shielded Copper Wire 20AWG 300V BLK 25' (CNC Tech, catalog number: 1430-20-1-0500-001-1-TS)
23. Ground electrode probe (WPI, model: Ep2)
24. Communication Cable (Belden, catalog number: 8441)
25. Double banana plug Connectors for amplifier (Pomona Electronics, catalog number: 1330)
26. Single banana Plug (Pomona Electronics, catalog number: 1325)
27. Precision screwdriver (Westward, model: 401L69)
28. Clorox bleach (VWR, catalog number: 89501-620)

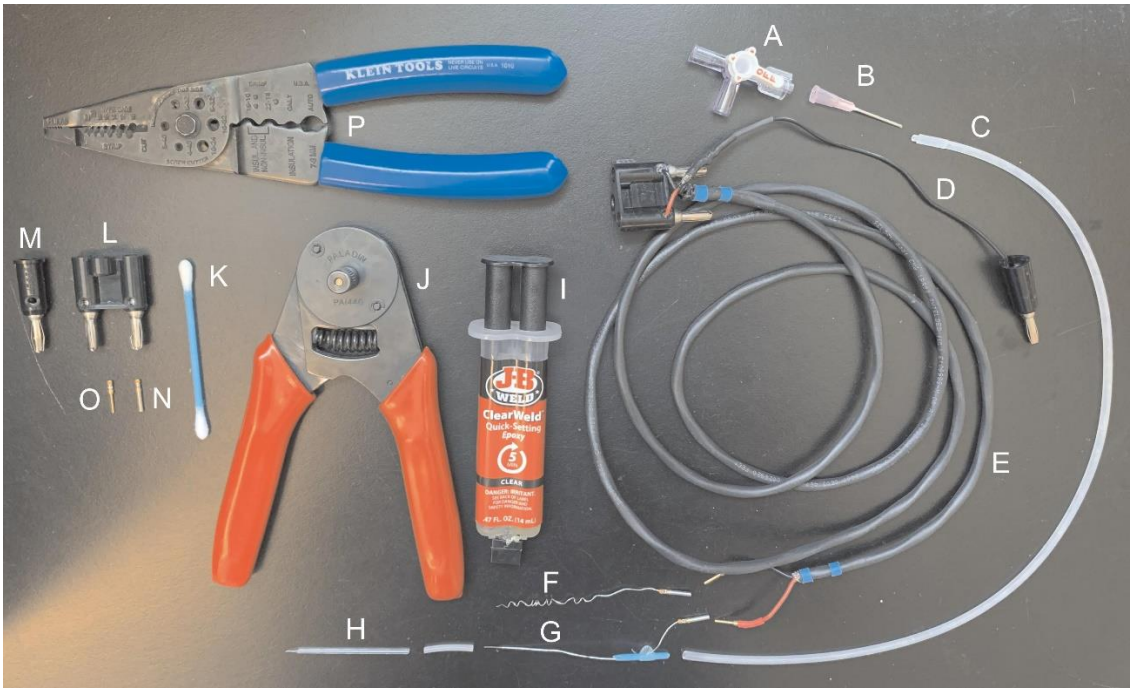

Figure 2.1 **Materials for manufacturing suction electrodes.**

[A] Three-way stopcock with Luer lock. **[B]** Blunt 25 G needle. **[C]** Silicone tubing. **[D]** Insulated copper wire. **[E]** Communication cable. Coated silver wire. **[H]** Glass electrode. **[I]** Quick-setting epoxy syringe. **[J]** D-sub crimper. **[K]** Cotton swab with plastic shaft**. [L**] Double banana plug. **[M]** Single banana plug. **[N]** Connector socket. **[O]** Connector D-Sub pin. **[P]** Wire stripper and cutter.

2.4.3 Recording equipment for studies involving multisegmental preganglionic and postganglionic compound action potentials

1. Stereo dissecting microscope with 0.8-5.6× zoom range and DFPL 0.5× objective (Olympus, model: SZX7)
2. Multichannel differential amplifier (custom-built but are also commercially available (*e.g.*, A-M Systems, model: 1700 Differential AC Amplifier)
3. Constant current stimulator (custom built but are also commercially available; *e.g.*, A-M Systems, model: 2200 Analog Stimulus Isolator)
4. Controllable blue light laser (custom built but are also commercially available; *e.g.*, Thorlabs, S1FC473MM Multimode Fiber-Coupled Laser)

5. Magnetic stand with 3-axis manual micromanipulator control (Kanetec, model: MB-PSL)
6. Gravity fed superfusion with Masterflex pump for recirculation (Cole Palmer, catalog number: 77200-50)
7. Tubing for perfusion (Masterflex, catalog number: 96412-16)
8. Digidata 1322A [186]
9. 1.5-mm outer diameter filamented, borosilicate glass capillaries (World Precision Instruments, catalog number: TW150F-4)
10. Coated silver wire (A-M Systems, catalog number: 787000).
11. Connector Socket 20-24AWG gold crimp (Digi-Key, catalog number: 205090-1).
12. Connector D-Sub Pin 20-24 AWG AU (Digi-key, catalog number: 205089-1).
13. Ground electrode probe (WPI, model: Ep2)
14. Communication Cable (Belden, catalog number: 8441)
15. Double banana plug Connectors for amplifier (Pomona Electronics, catalog number: 1330)
16. Single banana Plug (Pomona Electronics, catalog number: 1325)

2.4.4 Image Capture Equipment for Calcium Imaging

1. AC/DC differential amplifier (A-M Systems, model: 51249)
2. Master 8 system and an ISO-Flex stimulus isolator (A.M.P.I, model: 1955)
3. Inverted microscope (Olympus, model: IX70)
4. Xenon lamp housing (Olympus, model: U-ULS75XE)
5. Power supply (Olympus, model: AH2-RX-T)
6. Neutral density filter (Olympus, catalog number: Chroma ND-50)
7. Uniblitz shutter (Vincent Associates, model : VCM-D1)
8. 400 nm dichroic mirror (Olympus, model: Chroma NC474265)

9. 490-520nm Emission filter (Olympus, model: Chroma U-MF2)
10. CCD camera (Stanford Photonics, model: XR/ABF with XR/M camera)
11. Trinitron color video monitor (Sony, model: PVM-135MD)

2.4.5 Software

1. Clampex software (Molecular Devices, RRID: SCR_011323). Signals were amplified using a MultiClamp 700A and digitized at 10 kHz using a Digidata 1322A and Clampex software (Molecular Devices, RRID: SCR_011323).
2. PCI software (Hamamatsu, Sunayama-cho, Naka-ku, Hamamatsu City, Shizuoka, Japan)
3. Fiji (ImageJ from NIH)

2.5 Procedure

We describe the methodology developed for an *ex vivo* mouse model for physiologic characterization of their properties. Procedures and all experiments presented were undertaken in adult (8+ weeks) C57Bl/6 mice, but the approach has been used in mice as young as postnatal day 7. Thoracic chain ganglia in continuity with communicating rami, spinal nerves, and ventral roots are not dissected from surrounding tissue. Rather, they are left adherent to the ribcage to prevent nerve injury. Access to communicating rami in mice is difficult, so recruitment of preganglionic axons is instead achieved by stimulating ventral roots. Specialty fabrication of tight-fitting glass suction electrodes enables stable extracellular recordings of compound action potentials.

The anatomical organization of SPN projections to tPostNs is shown and described in Figure 2. To access the sympathetic ganglia and connections to the ventral root for recording, the following series of procedures is important: (1) the peritoneum must be removed; (2) to facilitate

recordings, the chain should be carefully separated from embedded brown adipose tissue, and care is required as separation can easily sever the interganglionic nerve or rami; (3) as the ganglia themselves are shrouded in a collagen sheath, with individual tPostNs further encased in a glial covering, preparations that require access to individual neurons for whole-cell recordings require both preincubation in collagenase and mechanical disruption of the glial casing using patch electrode shaped capillary tubes attached to a micromanipulator or glass probes.

Preparation for experimental studies first involves dissecting the vertebral column by making lateral incisions through the ribcage. Using a combination of iridectomy microdissection scissors, forceps, and fine-tipped glass probes, the peritoneum is peeled away. While collagenase is required for whole-cell recordings, we have undertaken population studies without it (Blum *et al.*, 2020). Nonetheless, seal quality and signal resolution of population suction electrode recordings are superior following collagenase treatment. If collagenase is used, the vertebral column is allowed to incubate in a heated chamber filled with continuously oxygenated artificial cerebrospinal fluid (aCSF) and collagenase solution (Blum *et al.*, 2020). The chain is cleaned of remaining fat and connective tissue. A ventral vertebrectomy exposes the spinal cord and ventral roots.

An *ex vivo* approach offers the ability to superfuse pharmacological agents to assess actions at known doses without concern for drug access (Blackman and Purves, 1969; Lichtman *et al.*, 1980; Thorne and Horn, 1997; Ireland *et al.*, 1998). This is shown in Figure 3 with blocked recruitment of tPostNs following application of hexamethonium, a ganglionic nicotinic receptor antagonist [4,182]. For studies on recruitment of segmental preganglionic axons, the spinal cord and dorsal roots are removed, leaving behind only intact ventral root connections.

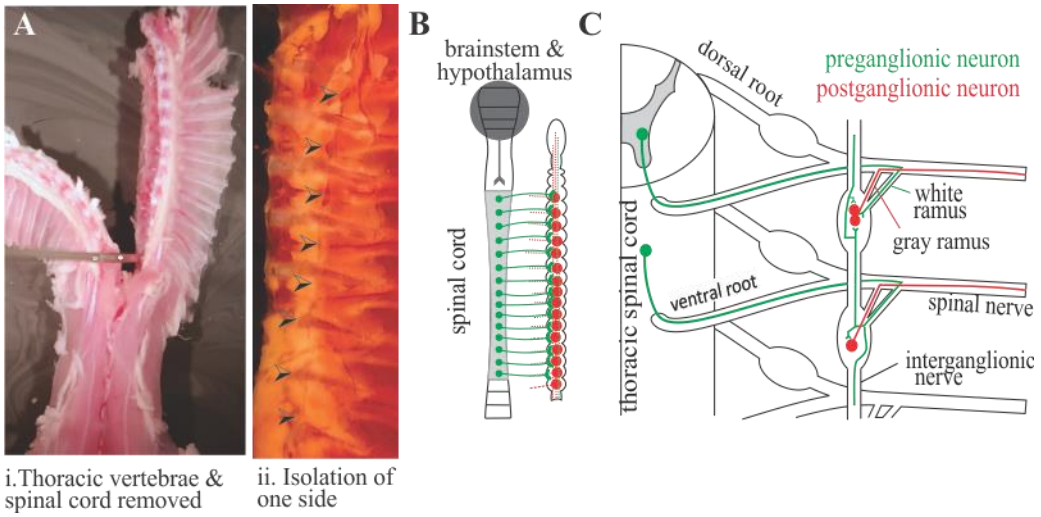

Figure 2.2 *Ex vivo* dissection enables the study of multisegmental preganglionic actions.

[A] *Ex vivo* dissection and identification of chain ganglia. Transparent chain ganglia are shown in the right panel (arrows). [29] **[B-C]** Overview of anatomical organization of connectivity between SPN and tPostNs. SPN axons exit the ventral root and enter the sympathetic chain via the white ramus. Those innervating paravertebral postganglionic neurons (tPostNs) do so within several chain ganglia via rostrocaudally projecting collaterals in the interganglionic nerve. Other SPN axons do not innervate tPostNs within chain ganglia but may travel along the interganglionic nerve before exiting to innervate prevertebral ganglia (not shown).

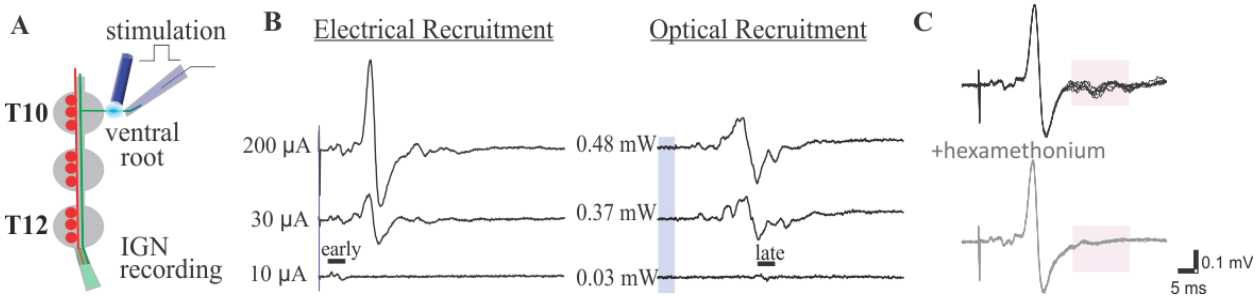

Figure 2.3. SPN axons are recruited using electrical and optical stimulation of ventral roots

[A] Experimental configuration. Trumpet-shaped glass electrodes placed on the ventral root (green arrow) and IGN (red arrow) enable stable extracellular recordings (left). Ganglia between sites of stimulation and recording are indicated by black arrows. Scheme of the experimental configuration for panels B and C shown on the right. **[B]** Recruitment of preganglionic axons and evoked synaptic tPostN responses following ventral root stimulation. Examples of electrical (left) and optogenetic (blue laser light; right) intensity-dependent recruitment of preganglionic axons from the T10 ventral root in ChAT-CHR2 transgenic mice. Here, the recording suction

electrode captured direct and synaptically-evoked population responses from the cut interganglionic nerve immediately caudal to the T12 chain ganglion. Stimulation intensity differences in recruitment are shown with duration kept constant (200 ms for electrical; 5 ms for optical). Blue vertical line and bar represent respective stimulus timing. Waveforms are averages of three episodes at labeled intensities. Shown is preferential intensity-dependent recruitment of the fastest conducting axons with electrical (early) and slowest conducting (late) axons with optogenetic stimulation, respectively. Recruitment profiles were undertaken in collagenase-treated tissue from a ChAT::ChR2 mouse. **[C]** Use of ganglionic blockers to discriminate preganglionic from postganglionic activity. Block of synaptically-recruited postganglionic (tPostN) activity following application of the nicotinic receptor antagonist hexamethonium (100 µM) is shown in the lower panel. The shaded area in both panels highlights this loss**.** See Video 1 for instructions on tissue preparation[176]. Video time stamps of individual steps are provided in the text.

2.5.1 Ex vivo mouse dissection for experiments recording multisegmental pre and postganglionic compound action potentials.

2.5.1.1 ***Tissue Preparation***

1. Anesthetize mice with inhaled isoflurane. Maintain with urethane (intraperitoneal injection, at 2 g/kg for *in vitro* electrophysiology). Confirm anesthetic depth via lack of pinch-evoked foot withdrawal reflex and eye blink reflex.
2. Use 25 G needles to pin animal down with dorsal side facing up in a dissection dish.
3. Pinch the skin near the tail and use scissors to cut up midline to remove dorsal skin and expose underlying dorsal surface of the vertebral column. The visible dorsal surface includes muscle overlying the vertebral column and dorsal spinal processes. Use forceps to remove excess or loose hair (Video 1. Sympathetic Chain Dissection 0:00-1:18).
4. To remove thoracic vertebral column and attached chain, begin lateral incisions 5 mm away from the midline near the L3 vertebrae. Cut through muscle and ribcage rostrally to the T1 vertebrae ensuring the scissors run parallel to the midline. Repeat incision on the opposite side. Pinch the column and make a transverse cut below T3. Lift vertebral column to separate and cut viscera. Make a transverse cut above T1 to remove thoracic vertebral column (Video 1. Sympathetic Chain Dissection 1:20-2:40).

5. Quickly rinse isolated tissue in oxygenated high-Mg^{2+} (6.5 mM)/low-Ca^{2+} (1.2 mM) aCSF (see Recipe 1) to remove excess blood and fat.
6. Perform collagenase treatment (if desired). Place tissue in a 1.5 ml tube or dish filled with a continuously oxygenated solution of 20 mg-Type III Collagenase per 1-ml aCSF (see Recipe 2), maintained at 36°C for 1 h. If necessary, trim tissue to fit collagenase treatment tube (Video 1. Sympathetic Chain Dissection 3:13-3:24).

*2.5.1.2 **Tissue Stabilization and Electrode Placement for Compound Action Potential Recordings***

1. If collagenase treatment was used, remove tissue from 1.5 ml tube and quickly rinse in oxygenated aCSF (see Recipe 2) to remove digested tissue.
2. Pin vertebral column dorsal up in perfusion dissection dish filled with oxygenated high magnesium low calcium microdissection fluid at room temperature. Using scissors, remove excess fat and muscle to expose midline (Video 1. Sympathetic Chain Dissection 3:26-3:46).
3. Using scissors, cut the vertebral column along midline from rostral to caudal end (Video 1. Sympathetic Chain Dissection 4:08-5:08).
4. Flip tissue and pin such that dorsal side is facing down. Using microdissecting spring scissors, cut vertebral column along midline to expose the spinal cord (Video 1. Sympathetic Chain Dissection 5:09-7:30).
5. Carefully separate two halves of the tissue to expose spinal roots. Using Vannas microscissors, cut ventral roots close to the spinal cord. Cut dorsal roots close to the vertebral column. Once all roots have been cut, remove spinal cord with attached dorsal roots and discard (Video 1. Sympathetic Chain Dissection 7:59-11:23).

6. Before electrode placement, ensure the tissue is securely pinned. Using glass probes or forceps, carefully peel away any remaining peritoneum and allow the tissue to rest for 30 min. The time required to set up and position electrodes is the ideal time to allow the tissue to rest (Video 1. Sympathetic Chain Dissection 11:24-12:12).
7. At this point, individual ganglia of the paravertebral chain should be visible. Glass suction electrodes can be placed on ventral roots and ganglia of interest. To place electrodes, move the electrode manipulator close to the recording dish. Use the manipulator's dials to move the electrode close to the intended nerve or ventral root such that the tip of the electrode is touching the cut end of the nerve or ventral root. Apply mild suction to stabilize initially. Once all electrodes are similarly placed, apply more suction to stabilize.
8. The sample can provide stable recordings for at least 12 h if the bath is continuously oxygenated and the bath temperature is maintained at 22°C. Viability at elevated temperatures has not been explored systematically.
9. The electrophysiology rig and perfusion system are detailed in Figure 4.

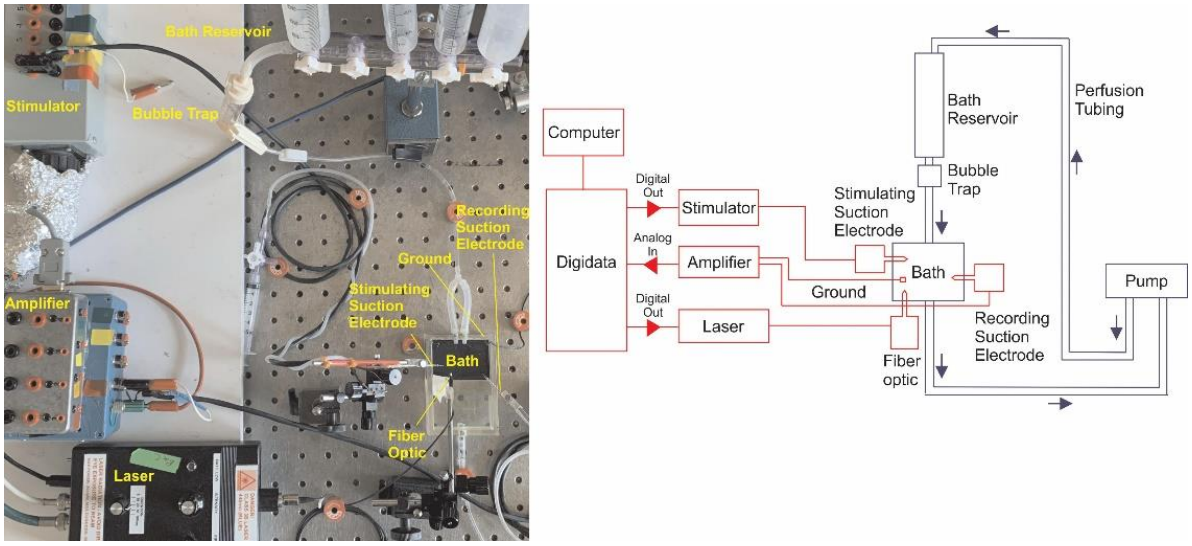

Figure 2.4. Overall set-up for experiments recording extracellular population potentials in paravertebral sympathetic chain ganglia.

Left: Picture of the electrophysiology rig. Right: Schematic of electrophysiology rig shown in photograph. The wiring diagram is shown in red. The bath perfusion system is shown in blue.

2.5.2 *Ex vivo* mouse dissection for whole-cell patch clamp recordings or calcium imaging

2.5.2.1 ***Tissue Preparation and Collagenase Treatment***

1. Anesthetize mice as described in Procedure A1.1.
2. Pin animal down with dorsal-side facing up in a dissection dish.
3. Use scissors to remove dorsal skin and expose underlying vertebral column.
4. To remove thoracic vertebral column and attached chain, begin lateral incisions 5 mm away from the midline near the L3 vertebrae. Cut through muscle and ribcage rostrally to the T1 vertebrae ensuring the scissors run parallel to the midline. Repeat incision on the opposite side. Make transverse cuts above T1 and L3 to remove thoracic vertebral column.
5. Halve the spinal column by cutting along midline of vertebral column on dorsal and ventral sides. Remove the spinal cord and reserve both halves of the vertebral column for the next step.

6. Quickly rinse isolated vertebral columns in oxygenated high magnesium low calcium microdissection fluid (see Recipe 1) to remove excess blood and fat.
7. Place tissue in a 1.5 ml tube or dish filled with a continuously oxygenated solution of 20 mg-Type III Collagenase per 1-ml aCSF (see Recipe 2) maintained at 36°C for 1 h.

2.5.2.2 ***Preparation for Whole-Cell Patch Clamp Recordings or Calcium Imaging***

1. Remove tissue from 1.5 ml tube and quickly rinse in oxygenated aCSF (see Recipe 2) to remove digested tissue and residual collagenase.
2. Pin vertebral column ventral up in perfusion dissection dish filled with oxygenated high magnesium low calcium microdissection solution (see Recipe 1) at room temperature.
3. Using glass probes or forceps, carefully peel away any remaining peritoneum.
4. Remove the chain by using microscissors to sever rami (Video 1. Sympathetic Chain Dissection 12:36-15:20).
5. Using forceps and insect pins, pin the chain down onto a clear Sylgaard recording dish through which recirculating, oxygenated aCSF (see Recipe 2) is continuously perfused. If the tissue is being used for calcium imaging place, the chain in a recording chamber fitted with a glass cover slip on the bottom. Take some high vacuum grease on a cotton swab and apply it to the bottom surface of the recording chamber. Press the glass cover slip onto the grease to secure the glass to the recording chamber and create a waterproof seal.
6. Before any electrode placement, allow the tissue to rest for 30 min. The time required to set up and position electrodes is the ideal time to allow the tissue to rest.
7. For calcium imaging, cells are imaged from below using an inverted Olympus scope. For whole-cell patch clamp, cells can be identified using an upright microscope affixed with a

low-light camera. Differential interference contrast (DIC) microscopy can be used to visualize tPostNs, while appropriate epifluorescent illumination can be used to identify fluorescently labeled tPostNs (*e.g.*, Cre-dependent reporter mice). See Figure 5 for representative examples of the field of view for whole-cell patch clamp (Figure 5B) and calcium imaging (Figure 5C) experiments.

8. After identifying a tPostN, gently clean the membrane by using an electrode filled with aCSF flushing the area lightly. Then replace the electrode with one filled with intracellular solution and gradually approach the tPostN with 0.2cc positive pressure, subsequently reduced to 0.05-0.1cc when the electrode is close to contacting the cell membrane.
9. Once the electrode contacts the membrane, release the positive pressure and apply a 0.1cc negative pressure and hold the electrode at -80mV. This allows the membrane to form a GohM seal around the electrode tip. After the resistance is stable at Gohm range with ~-10 nA injected current, quickly apply 1cc syringe suction or a mouth suction pulse to break through the membrane.
10. The sample can provide stable recordings for at least 12 h if the bath is continuously oxygenated and temperature is maintained at 22°C.

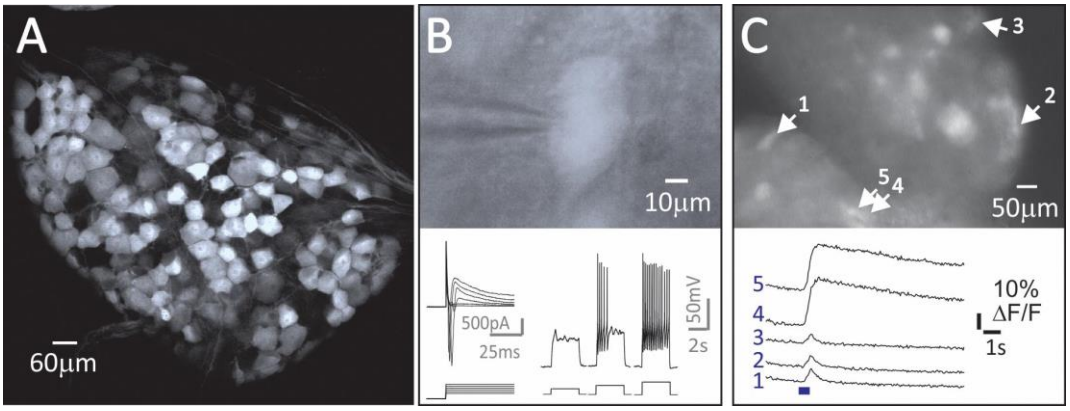

Figure 2.5. Genetic approaches enable the study of molecularly distinct tPostN subpopulations.

[A] A large fraction of tPostNs express Neuropeptide Y (NPY), as shown in NPY::tdTomato mice (T8 sympathetic ganglion in 6 wk old mouse). [29] Studies on activity in NPY+ tPostNs. **[B]**. Whole-cell recording from a fluorescently-identified NPY+ tPostN in a NYP::tdTomato mouse shows neuronal response properties to a series of depolarizing voltage or current steps.**[C]** Ca^{2+} signals in NPY::GcaMP6f tPostNs in T7-T8 whole thoracic ganglia evoked by stimulation of the interganglionic nerve. Shown are changes in activity following electrical stimulation with a 10Hz, 5-pulse train.

2.5.3 Manufacture of Trumpet-Shaped Tips of Glass Suction Electrodes and Patch Electrodes

1. Position glass capillary tubes on a vertical puller (Narishige, PP-83). Heat center and allow for two ends of capillary tube to be drawn apart 1-2 mm without breaking (Figure 2.5).
2. Allow the stretched capillary tube to come to room temperature. Without adjusting heating coil, heat capillary tube until two halves separate. Keep half with the bulbous tip.
3. Score electrode underneath the bulbous tip using the edge of a glass slide. Tap electrode tip against glass slide to remove section above the score mark.
4. Place electrode in a microforge (*e.g.*, Narishige MF-9 Microforge) fitted with a curved filament. The electrode should be placed such that the neck of the electrode tip is equidistant from the curved edges of the filament.

5. Heat filament using the medium heat setting to trumpet the neck of the electrode. The trumpet shape promotes tight-fitting, stable recordings. The large-diameter mouth of the electrode allows the whole nerve (and sometimes ganglion) to enter the electrode, while the small-diameter neck locks the nerve in place.
6. Pull patch electrodes from borosilicate glass capillaries (1.5-mm outer diameter, 1.2-mm inside diameter, filamented, borosilicate glass capillaries on the vertical puller) for a target resistance of 4-7 MΩ. Fill electrodes with patch electrode solution (see Recipe 3).

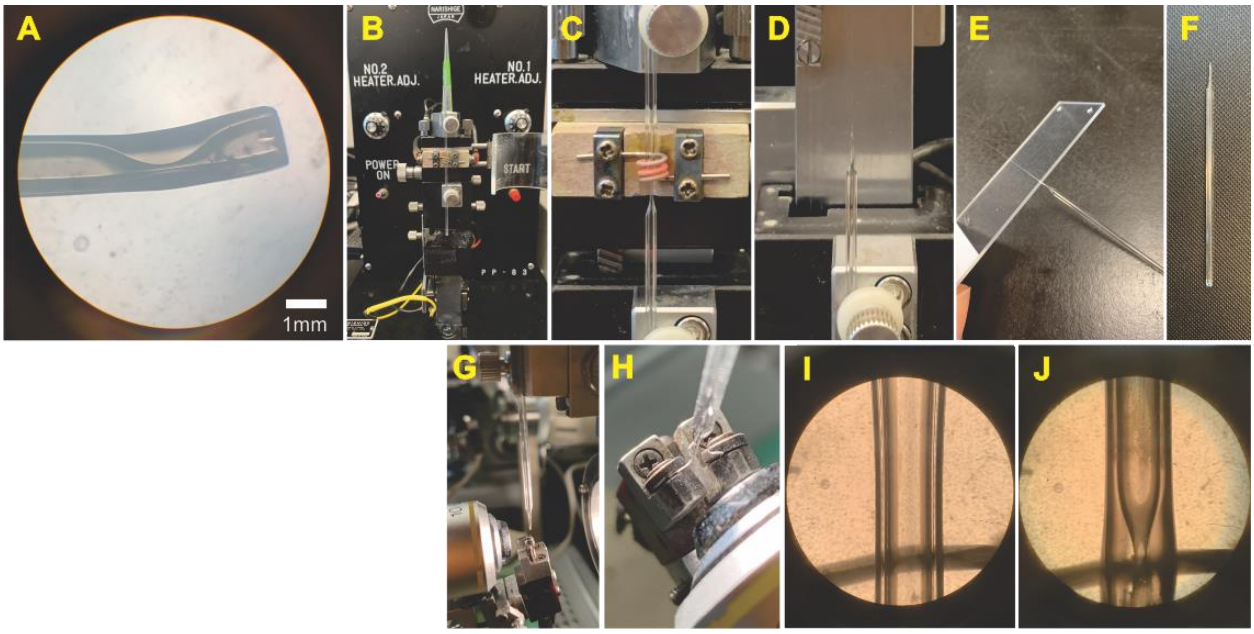

Figure 2.6 Manufacture of trumpet-shaped glass electrode

[A] Magnified view of the electrode tip used for recording and stimulating. **[B-J]** Manufacture of suction electrodes. For detailed instructions, see above **[B]** Glass capillary tube positioned on vertical puller. **[C]** Tube heated to form 1-2mm neck. **[D]** Tube heated to separate halves, keeping bottom half with the bulbous tip. **[E-F]** Glass slide used to score underneath the bulbous tip and break the tip. **[G]** Electrode placed in Microforge with a u-shaped filament. **[H]** Tip positioned at the center of the filament. **[I-J]** View of electrode in the Microforge before and after heating.

2.5.4 Manufacture of Sylgard-coated dissecting dish

1. Take the bottom half of a 100mm plastic Petri dish and set it on a flat surface.

2. Follow instructions found in the SYLGARD^{TM} 170 Silicone Elastomer Kit to mix 40 ml of encapsulant in a disposable plastic weighing dish.
3. Slowly pour encapsulant into Petri dish until the dish is filled halfway up (roughly 35 ml of encapsulate). Quickly pouring creates bubbles and an uneven surface for dissection.
4. Gently tap Petri dish on a benchtop to release bubbles trapped in the encapsulant.
5. Set the dish aside in an undisturbed location to allow the encapsulant to cure for 24 h at room temperature.

2.5.5 Manufacture of suction electrodes (Figure 2.1)

1. Cut a section of insulated shielded two-wire cable to the desired length. The length will vary depending on how far the amplifier is from the recording dish. Extra length will help the electrode cable to be slack and prevent tugging issues during recording.
2. Use the wire stripper to strip 1.5 inches of the outer PVC jacket at each cut end to reveal the braided shielding.
3. Cut away the braided shielding at one end to reveal the insulated copper cables (typically black and red). At the other end, unbraid the shield wire material from the pair of copper cables and re-twist into a point. Set cable aside.
4. Cut to free 5 inches of insulated copper wire. Use the wire stripper to strip 0.5 inches of insulation on both ends.
5. Splice together one end of the copper wire from Step E4 with the pointed shielding in step 3. Secure and insulate the spliced region with electrical tape.
6. Secure the other end of the copper to the single banana plug using a precision screwdriver to loosen the screw clamp in the plug to enable the copper wire to enter, then tighten to secure the wire.

7. Staying on the same side of the communication cable, use the wire stripper to strip 0.5 inches of insulation from the red and black wires. Secure the red and black wires to the double banana plug using the same procedure in Step E6.
8. Return to the side of the communication cable where the braided shielding was cut. Now use the wire stripper to strip 0.5 inches of insulation from the red and black wires. Using the D-sub crimping tool, crimp one D-Sub pin to each wire. The input cable is now complete and can be set aside.
9. To build the electrode holder, start by cutting a 1.5 inch piece from the plastic shaft of a cotton swab. Using a 25 G needle, gently poke a hole into the middle of the shaft, taking care not to poke through the opposite end.
10. Cut 4 inches of coated silver wire, thread it through the hole in the plastic shaft from the outside, and feed 3 inches through. Use epoxy to seal the hole and secure the wire tightly. Take care not to fill the shaft with epoxy as this will prevent you from applying suction to the electrode.
11. After the epoxy is set, cut 1 inch of silicone tubing and connect it to the end of the plastic shaft where the silver wire is protruding. The glass electrode will be placed on this end of the electrode holder.
12. Next, cut 1 foot of silicone tubing and connect it to the other end of the plastic shaft. Connect a blunted 25 G needle to the end of the silicone tubing and seal any gaps with epoxy. Connect a three-way stopcock to the 25 G needle. Connect a 5ml disposable syringe to the end of the stopcock.
13. Cut 4 inches of coated silver wire. Using a lighter, burn off 0.5 inches of the plastic coating on either end. Do the same for the epoxied silver wire in step 10. Coated wires that are bare

at the top provide more stable recordings if DC-like events are acquired. For example, artifacts caused by minor changes in bath volume can be minimized.

14. Use the crimping tool to crimp a connector socket to one end of the cut coated silver wire from Step E13 and coated silver wire from Step E10.
15. Chemically chloride the uncrimped ends of the silver wires by dipping the ends into Clorox bleach for 24 h.

2.5.6 Recipes

1. High-Mg^{2+}/Low-Ca^{2+} Microdissection Solution: 127.99 mM NaCl, 1.90 mM KCl, 6.5 mM $MgSO_4 \cdot 7H_2O$, 0.85 mM $CaCl_2 \cdot 2H_2O$, 1.20 mM KH_2PO_4, 9.99 mM 68 Glucose, 26.04 mM $NaHCO_3$. The pH is adjusted to 7.4 after saturation with gas (95% O_2, 5% CO_2) at room temperature. The recommended volume to prepare for this protocol is 250 ml.
2. Artificial Cerebrospinal Solution (aCSF) for Electrophysiological Recordings, 127.99 mM NaC, 1.90 mM KCl, 1.30 mM $MgSO_4 \cdot 7H_2O$, 2.40 mM $CaCl_2 \cdot 2H_2O$, 1.20 mM KH_2PO_4, 9.99 mM 68 glucose, 26.04 mM $NaHCO_3$. The pH is adjusted to 7.4 after saturation with gas (95% O_2, 5% CO_2) at room temperature. aCSF may be buffered with HEPES or bicarbonate. The recommended volume to prepare for this protocol is 500 ml.
3. Patch Electrode Solution: 140.0 mM K-gluconate, 11.0 mM EGTA, 10 mM HEPES, 1.32 mM $CaCl_2$. The pH is adjusted to 7.3 using KOH. Target osmolarity was 290 mOsm. In most recordings (25/39 cells), a support solution was added consisting of 4.0 mM ATP and 1.0 mM GTP. The recommended volume to prepare for this protocol is 3 ml.

2.6 Conclusion

Despite their physiological importance, our understanding of the function of paravertebral ganglia is based largely on work undertaken in larger mammalian models [54,64,176,187]. Greater

understanding of the operational properties of SPNs have not benefited from powerful molecular toolkits provided by molecular genetic approaches in mouse models [177]. Unlike in cervical and lumbar chain ganglia, thoracic PostNs are situated in a protected paraspinal and subpleural location on the ventral wall of the thoracic cavity. This makes *in vivo* electrophysiological studies difficult and explains the need for *ex vivo* approaches [25,54,187]. Moreover, as the largely transparent individual ganglia are very small (<200 μm in length) with the entire thoracic chain being <2 cm, dissection for study is challenging.

We also developed the *ex vivo* preparation to enable whole-cell recordings of tPostNs for assessment of membrane properties independent of impalement leak produced with sharp microelectrodes. The results indicated that the membrane resistivity was an order of magnitude higher than previously thought. This increase in resistivity was associated with enhanced excitability, a greater intrinsic capacity for synaptic integration, and the ability to sustain firing when measured during whole cell recordings [36].

To undertake whole-cell patch recordings, the chain is removed entirely from the vertebral column using fine iridectomy microdissection scissors and glass probes [36]. With this method, one can investigate multisegmental preganglionic actions in tPostNs in mice [25], including via optogenetic recruitment of preganglionic cholinergic axons using ChAT-CHR2 mice [188]. As there are several genetically distinct populations of sympathetic preganglionic neurons [20,175], various cre-based driver approaches can be leveraged to study multisegmental actions arising from different SPN populations. Capturing individual or population activity of genetically distinct tPostNs is also possible with the use of cre-based reporters or genetically-encoded Ca^{2+} indicators [177]. In summary, the described approach enables the use of mice for highly accessible

ex vivo studies for electrophysiology, calcium imaging, optogenetics, and pharmacology for cellular and circuit studies on input-output relations of the thoracic paravertebral chain.

3 Characteristics and Variability in SPN Axonal Conduction: Velocity, Myelination, and Branching Patterns

3.1 Abstract

The thoracic paravertebral sympathetic chain contains axonal projections from spinal cholinergic sympathetic preganglionic neurons (**SPNs**) that innervate postganglionic neurons and provide the primary sympathetic control of vascular function in the trunk and upper extremity. SPN axons extend across multiple paravertebral ganglia through an interganglionic nerve (**IGN**), offering multisegmental convergent and divergent input to postganglionic neurons.

Our understanding of SPN connectivity in thoracic ganglia is derived from classical *ex vivo* studies conducted at room temperature in guinea pigs. These studies involved stimulating SPN axons in ventral roots (**VRs**) and recording responses from postganglionic neurons across ganglia. Although it was previously assumed that axonal conduction across these projection territories was reliable, this chapter questions that assumption.

Using an *ex vivo* approach in mice (discussed in Chapter 2), we first confirmed that SPN axons projecting to the thoracic ganglia in mice have divergent projections like what is seen in other species. We anterogradely labeled mid- to lower-thoracic SPN axons in adult mice exiting the T7 or T10 VR (n=4). The labeled axons showed rostro-caudal multisegmental divergent projections spanning 10 segments and issued collaterals to form putative synapses in multiple ganglia.

Physiological studies then explored SPN axonal divergence by electrically recruiting their axons in VRs from mid- to caudal-thoracic spinal segments while recording their conduction to multiple ganglia along the chain. Obtained results confirmed axonal divergence across thoracic sympathetic chain ganglia (n=4). The largest evoked compound action potentials (**CAPs**) were typically recorded in the ganglia at the segment nearest to the stimulation site.

After blocking synaptic transmission, we studied the conduction velocity of evoked SPN CAPs in branching (IGN) and unbranching (splanchnic) axons. The T10 VR was stimulated, and the evoked CAP response was recorded at two sites just caudal to the T12 ganglion: the IGN and the adjacent splanchnic nerve. Both electrical (200μA, 500μs) and optical stimuli (6.6mW/μm², 20ms pulse) recruited SPN axons across a range of conduction velocities (**CVs**) (IGN: electrical [0.11-0.84 m/s] vs optical [0.10-1.08 m/s]; splanchnic: electrical [0.13-2.00 m/s] vs optical [0.11-6.13 m/s]; n=7). Notably, branching axon conduction velocities fell exclusively within the range for unmyelinated C-fibers.

To assess conduction reliability, we evaluated intertrial variability and observed significant response variability indicative of conduction failures, challenging the assumption that SPN spike propagation is reliable along its anatomical projections. When the evoked CAP was divided into epochs based on CV, we found that slower-conducting axons in both IGN and splanchnic nerves (n=7) showed higher coefficients of variation. We conclude that conduction failures must be incorporated into our understanding of the factors governing the magnitude of population encoded sympathetic drive to organ systems.

3.2 Introduction

SPNs are the final arbiters of CNS sympathetic output. SPN axons that project to paravertebral ganglia branch issue divergent multisegmental projections on postganglionic neurons in paravertebral sympathetic chain ganglia. Thoracic chain ganglia are intimately involved in the modulation of stress, metabolism, blood distribution and thermoregulation [6]. While thoracic postganglionic neuronal populations are comprised of 5 genetically distinct adrenergic subpopulations [177], little is known about their recruitment by SPNs, themselves comprising populations of predominantly unmyelinated axons that are almost as genetically diverse as the

hypothalamus [46,47]. SPN axons enter paravertebral chain ganglia via the white ramus and branch rostrocaudally across multiple paravertebral chain ganglia (see chapter 1 for more detail) [30]. Divergent projections from individual SPNs onto multiple postganglionic neurons provides a mechanism for amplification of CNS sympathetic commands to the numerically much greater postganglionic neurons (~200:1 in human & 14:1 in mouse) [66].

Approximately 99% of mouse SPN axons are unmyelinated with a mean diameter of 0.4 µm (much smaller than human) and branching diameters as low as 0.1 µm [73]. Such small axons are susceptible to activity-dependent hyperpolarization, conduction slowing and block [70 71]. Their small diameter may make them particularly sensitive to Na^+ channel inactivation [149] and to hyperpolarization by a $[Na^+]_i$ sensitive metabolic rheostat provided by the α3-Na^+/K^+ pump that tracks activity history [189,190] and may regulate autonomic activity dynamics [86]. Until now, conduction failure has not been considered a feature of the SPN output modifiability [3]

While SPN axons effectively amplify CNS sympathetic commands through their divergent projections, their branching architecture introduces a potential vulnerability. Axonal branch points are susceptible to conduction failure due to the geometrical factors of the primary axon and its branching collaterals. Therefore, various strategies are employed to control the safety factor and ensure successful signal transmission [72,92]. The presence of branch points can reduce conduction velocity [68] where a sudden decrease in axon diameter causes a decrease in both velocity and peak amplitude of the propagating spike [91]. Conduction failure at branch point has not been considered a feature of the SPN output modifiability [3].

This leads to the proposition that conduction along axons, including at axonal branches, may represent an important yet unexplored aspect of presynaptic control in sympathetic output. We explore whether spike conduction in SPN axons is reliable and hypothesize that propagation

along unmyelinated axons represent a physiologically relevant and modifiable site of conduction control, particularly across branch points [191]. To determine whether conduction failures are more prominent in branching axons we compare actions on SPN paravertebral branching axons recorded across ganglia in the interganglionic nerve (IGN) to SPN unbranching axons that project to prevertebral ganglia in the splanchnic nerve.

3.3 Materials and Equipment

3.3.1 Neurobiotin labeling to assess preganglionic divergence.

A ChAT-ChR2 mouse (driver line is ChAT-IRES-cre (JAX: 006410); reporter line is R26-ChR2-eYFP (JAX: 012569)) was euthanized with urethane (0.2mL, 50% solution). The vertebral column including ventral roots and sympathetic ganglia were dissected using the procedure described in chapter 2.5. Prepared tissue was placed in a circulating bath with aCSF containing (in mM): NaCl [127.99], KCl [1.90], MgSO4 ·7H2O [1.30], CaCl2·2H2O [2.40], KH2PO4 [1.20], glucose [9.99], and NaHCO3 [26.04]. ACSF pH was adjusted to 7.4 after saturation with gas (95%O2, 5%CO2) at room temperature. To obtain evidence of widespread SPN divergence, we labelled SPN axons in the T7, T9 or T10 ventral roots with Neurobiotin dissolved in distilled water (Vector Labs, 6%, RRID:SP110). This was loaded into an appropriately tapered glass capillary tube to enable root suction of the cut-end of either the T10 or T7 ventral root and left undisturbed for 6 hours at 22 °C. Subsequently, the preparation was removed from the perfusion chamber and fixed in 4% paraformaldehyde (0.5M phosphate, 4% paraformaldehyde, NaOH) for 2 hours. After fixation, the paravertebral thoracic chain was immersed in 20% sucrose solution and stored at 4°C. The sympathetic chain was subsequently isolated from stellate (T1 and T2) to T12/13.

The dissected chain was washed overnight in PBS with Triton (PBS-T) solution containing 20% DMSO and 0.3% Triton-X. It was then placed in sealed vials filled with the same PBS-T solution and incubated in a 37°C water bath overnight. To prevent any reaction of DMSO with oxygen, we minimized air exposure in the vials. A foam float ensured the vial was completely submerged in the water bath. This step was repeated using a second PBS-T solution (20% DMSO, 0.1% Tween20, 0.1% Sodium Deoxycholate, 0.1% Tergitol, 0.3% Triton X 80%) with the same precautions regarding air exposure. Next, the tissue was transferred to a third PBS-T solution (20% DMSO, 0.3 M Glycine, 0.3% Triton X 80%) for three hours at 37°C in the water bath. Following this, an overnight PBS-T wash and 3-4 subsequent hourly washes were performed to fully remove any DMSO residue. The chain was subsequently incubated for 5-7 days with ExtrAvidin Cy3 (Sigma, 1:000, RRID:E4142) and a primary antibody: chicken anti-Tyrosine Hydroxylase (Abcam, 1:100, RRID:AB_76442). This tissue then underwent six one-hour washes in PBS-T, followed by an overnight stay in the same solution followed by incubation for another 5-7 days in secondary antibody solution: Alexa 488 (Jackson Immunresearch, 1:100) and ExtrAvidin Cy3 (1:1000). The tissue was then washed in PBS-T (5 x 1hr), then 50mM Tris-HCl (2 x 1hr followed by 1 x overnight) then in 50mM Tris-HCl (2 hours) before mounting on prepared glass slides (four dots of nail polish were applied to the slides to slightly elevate the cover slip).

3.3.2 Myelin Basic Protein Stain and Channelrhodopsin/GFP dual immunolabeling

A ChAT-ChR2 mouse (see previous section for line details) paravertebral chain with attached roots was stained with rat anti myelin basic protein (Sigma, 1:50, MAB386) and chicken anti-GFP (Abcam, 1:100, AB3970). Whole mounts were washed overnight in PBS-T then incubated in primary antibodies for 3 days followed by wash in PBS-T (3 x 30 min). Tissue was incubated

for 3 hours in a secondary antibody solution: Cy3 donkey anti-rat (Jackson Immunoresearch,, 1:250, RRID:712-165-153) and FITC anti-chicken (Jackson Immunoresearch, 1:100, RRID:703-095-155). The tissue underwent a final wash in PBS-T (1 x 20 min) and 50mM Tris-HCl (2 x 20 min) before mounting on glass slides.

3.3.3 Assessment of axon counts and size.

A ChAT-TdTomato mouse (driver line is ChAT-IRES-cre (JAX: 006410); Reporter line is R26-ChR2-eYFP (JAX: 024109)) was dissected according to the procedure described in chapter 3.3.1. The T7 white ramus and the interganglionic pathway rostral and caudal to all paravertebral ganglia with Neurobiotin reaction were imaged for Neurobiotin-FITC on a Nikon Crest Spinning Disk Confocal (60x objective, NA 1.49, optical resolution 232 nm, 0.108 microns/pixels X-Y, 0.150-micron Z-steps). Image stacks were deconvolved (Microvolution) and analyzed in FIJI for manual axon counts (Tubeness, Reslice) and cross-section measurement (Stardist, Analyze Particles) of Neurobiotin^{+} axons. We analyzed 120 slices from each rostral-caudal tract for 3 IGN regions (T5-T4, T-6-T5, and T7-T6) to assess axon count, diameter, and number. The data from these slices were averaged to obtain a measurement for each segment. This analysis was conducted using FIJI software. To evaluate differences in diameter and CSA between IGN segments, we employed one-way ANOVAs followed by Dunn's pairwise multiple comparison procedures. Values are reported as mean ± standard error (SEM).

3.3.4 Electrophysiology

See chapter 2.5 for detail on *ex vivo* dissection. In cases where collagenase treatment is employed, the tissue is rinsed post-treatment before being secured in a perfusion dissection dish. A meticulous dissection ensues, aimed at revealing the midline and preparing the tissue for electrode placement. The vertebral column is bisected to expose the spinal cord, which is then

carefully removed to isolate the desired nerves. The tissue is given a rest period of one hour in the recording dish prior to electrode placement. We find the tissue maintains better health when introduced to the bath at the same temperature at which recording will occur, or at the highest temperature being tested if temperature is a variable in the experiments. The ganglia of the paravertebral chain are made visible and suction electrodes are placed delicately to ensure stable recordings. These recordings can be maintained for extended periods provided that the oxygenation and temperature are kept stable.

3.3.5 Quantification and analysis of evoked SPN CAPs

Evoked SPN CAPs, were recorded following VR stimulation once every 60 seconds. Recorded CAPs were divided into CV-subpopulations depending on latency of arrival from time of stimulation. For each CV population, 10 episodes were rectified and integrated using Clampfit software. At this point background noise was accounted for by subtracting an equal duration of baseline noise to provide a singular, comprehensive measure of CAP size. All 10 episodes were then averaged to ensure a more accurate representation of the CAP. Values are reported as mean percent of baseline ± standard error (**SEM**). If drugs were administered, student's t-test was employed to determine statistical significance in comparing drug conditions.

Statistical comparison of magnitude responses across preparations are complicated by various limitations of extracellular recordings of CAP events. This includes: (1) CAPs reflect the arrival of multiple extracellular spikes whose voltage waveform may differ in polarization leading to summed values that are smaller than the total number of axons; (2) larger amplitude spikes will have a more prominent contribution to overall calculated response; (3) recording quality and electrode size may differ across preparations, both leading to differences in the total number of axons sampled; and (4) observed variability in magnitude of evoked responses across

populations may lead to overrepresentation of an individual experiment in the total amplitude of evoked response.

3.3.6 Quantification of Coefficient of Variation

CAP subpopulations were classified according to their conduction velocities (see chapter 3.3.5). For each subpopulation, we conducted an analysis of 30 episodes within a 30-minute timeframe. All episodes underwent a process of rectification and integration, followed by a baseline subtraction to minimize noise. The average rectified integral for each epoch was determined for each CV category. The Coefficient of Variation (**CoV**) was then calculated, based on the average value of each CV category. The results are presented as the mean CoV. To determine statistical significance, we employed a one-way repeated measures ANOVA. For detailed pairwise comparisons, a Bonferroni t-test post hoc analysis was utilized.

3.4 Results

3.4.1 Assessment of complete synaptic block

A critical aspect of our investigation into SPN axons is the ability to differentiate directly recruited SPN axonal volleys from synaptically recruited postganglionic spiking activity. To achieve this, we used hexamethonium (50 or 100 μM) to inhibit nicotinic ganglionic transmission to isolate only SPN CAP spiking events. To confirm synaptic block, whole cell recordings were obtained from postganglionic neurons having ongoing spontaneous synaptic potentials (n=3). Hexamethonium (100 μM) eliminated or greatly depressed the amplitude of observed synaptic events, shown as excitatory postsynaptic currents (**EPSCs**) or excitatory postsynaptic potentials (**EPSPs**) in Figure 3.1A (Data from Dr. Celia Li). To further verify the efficacy of hexamethonium in blocking recruited postganglionic neurons, we compared responses to those observed following superfusion in a high-Mg^{2+}/low-Ca^{2+} solution previously reported to block synaptic transmission[192,193]. As shown in Figure 3.1B, hexamethonium

reduction in the evoked CAP response is on par with that of bath superfusion with the high-Mg^{2+}/low-Ca^{2+} solution, further supporting use of hexamethonium to isolate the preganglionic volley.

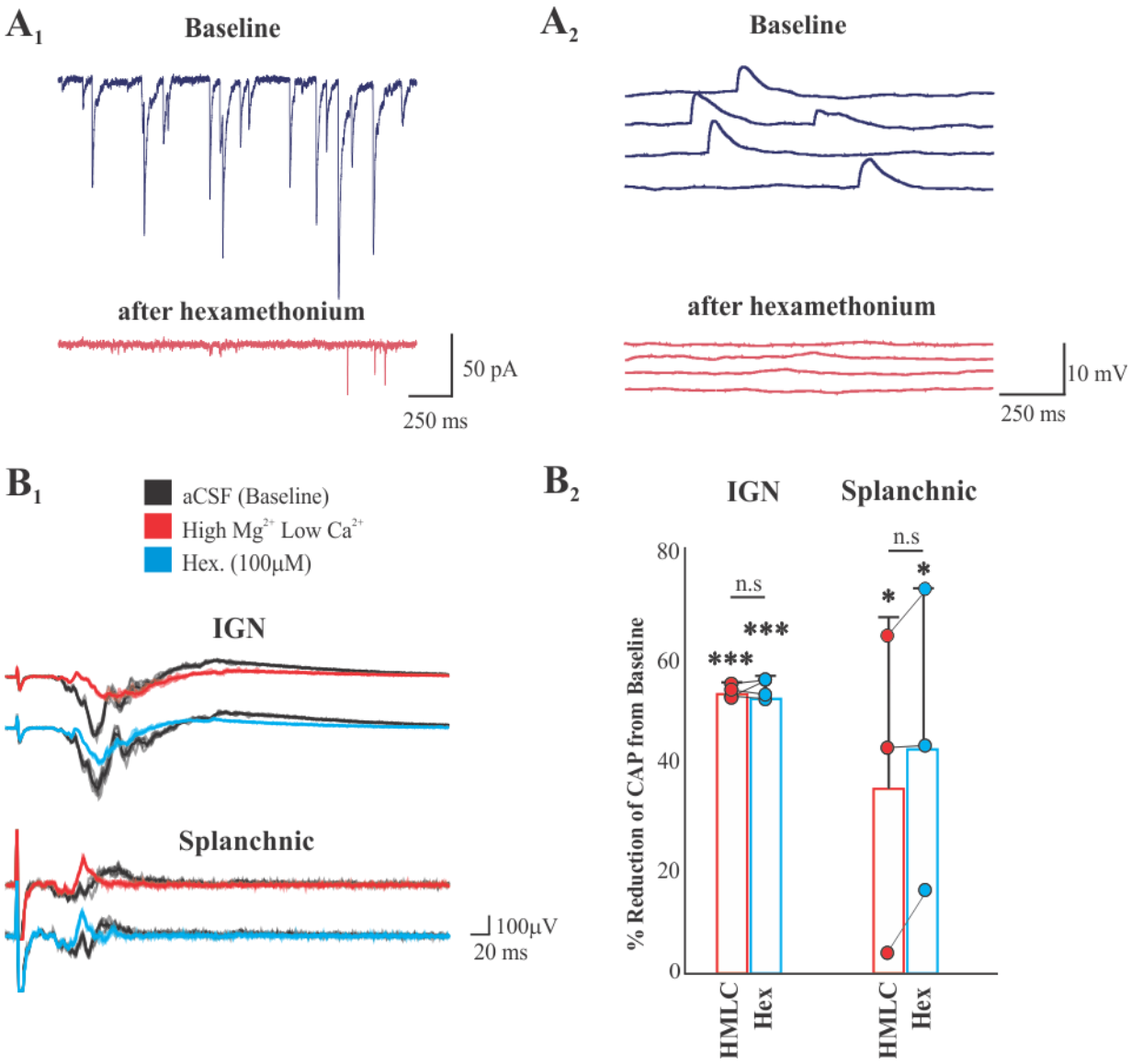

Figure 3.1 Hexamethonium and high-Mg^{2+} / low-Ca^{2+} bath replacement has similar effects on evoked response.

[A] Hexamethonium (100µM) blocks spontaneous synaptic activity in thoracic chain postganglionic neurons. Synaptic block is shown in two separate neurons recorded as loss of EPSCs in a voltage clamp recording (held at -90 mV) **[A_1]** and EPSPs in a current clamp recording **[A_2]**. **[B]** Comparing synaptic blocking actions of hexamethonium (100 µM) to high-Mg^{2+} (6.5mM) / low-Ca^{2+} (0.85mM) (HMLC) solution on amplitude of evoked response. At

room temperature in artificial cerebrospinal fluid (aCSF), electrical stimulation was applied to the T10 ventral root, with concurrent recordings taken from the T12 interganglionic and splanchnic nerves (200μA/500μs once every minute). Superfused aCSF was replaced with a high-Mg^{2+} / low-Ca^{2+} solution for a minimum duration of 30 minutes. Following this, the aCSF was reintroduced into the bath. Subsequently, 100 μM hexamethonium was administered to the bath and allowed to perfuse for 30 minutes. **[B_1]** Example showing hexamethonium and ionic block of synaptic transmission which led to comparable reductions in evoked response. **[B_2]** Hexamethonium and ionic block of synaptic transmission led to comparable reduction in evoked responses. The rectified integral of the entire CAP was calculated and then compared against the baseline values. The CAP of IGN SPNs reduced by 51.9 ± 0.8% ($p<0.001$) in HMLC and 51.0 ± 1.9% ($p<0.001$) in hexamethonium (n=4). CAP of splanchnic reduced by 34.4 ± 18.1% ($p<0.01$) and 41.6% 9 ± 16.9% ($p<0.01$) (n=3). Paired T-tests were used to assess the significance of CAP reduction from baseline. No significant differences were seen between synaptic blockers.

3.4.2 Recruitment profiles for SPN volleys

Experiments undertaken at 22°C first compared SPN axonal recruitment at multiple stimulus strengths and duration using both electrical and optical stimuli on T10 ventral roots while recording evoked responses; (i) in the IGN caudal to the T12 ganglia, and (ii) in the adjacent splanchnic nerve (Figure 3.2). Although lower intensity electrical stimuli recruited responses across a range of conduction velocities, there was preferential recruitment of faster conducting events (Figure 3.2A). Conversely, lower intensity optical stimuli tended to first recruit slower conducting events, consistent with past observations on ChAT-CHR2 optical axonal recruitment in order of size [188] (Figure 3.2B). Stimulation threshold was found to be ~50μA, 50μs in the T12 IGN and splanchnic nerve recordings in most preparations with maximal recruitment typically achieved at 200μA, 200μs stimulation (n=5). To ensure supramaximal recruitment of slow-conducting axons, electrical stimulation intensity for experiments in subsequent chapters was kept at 200μA, 500μs. While recruitment profiles using both anodal and cathodal stimulation were made, anodal stimulation always provided the largest response and was therefore used for all experiments in this thesis. Recruitment profiles were also compared at different optical

intensities and durations (5, 10 and 20 ms durations are shown in Figure 3.2B). In 4/5 experiments, a duration of 20 ms optical stimulation was needed to maximally recruit SPN populations at room temperature. Maximal recruitment was usually achieved at an optical intensity of ~6.3mW/μm^2 so 6.6mW/μm^2 was used for physiology experiments to ensure supramaximal recruitment with a 20 ms pulse duration.

To enable separate analysis of SPN axonal subpopulations, we divided the volley into populations based on conduction velocity. However, with optical stimulation requiring durations in the many millisecond range for complete recruitment, accurately pinpointing the onset of recruitment becomes challenging (as demonstrated in Figure 3.2B2). Responses could not be evoked by optical pulses shorter than 2ms (not shown). At a pulse width of 2ms, we initially recruited slow-conducting axons. The recruitment of the fastest unit was first observed with a 12ms pulse, although it is uncertain whether a 10ms pulse could have recruited this axon due to interference from the optical stimulus artifact. A peak response was typically achieved with a 20ms pulse. To obtain a consistent and comparable analysis of axonal recruitment between optical and electrical stimuli, optimal alignment was achieved by aligning the onset of the electrical stimulus artifact with a point 5 ms into the optical pulse.

.

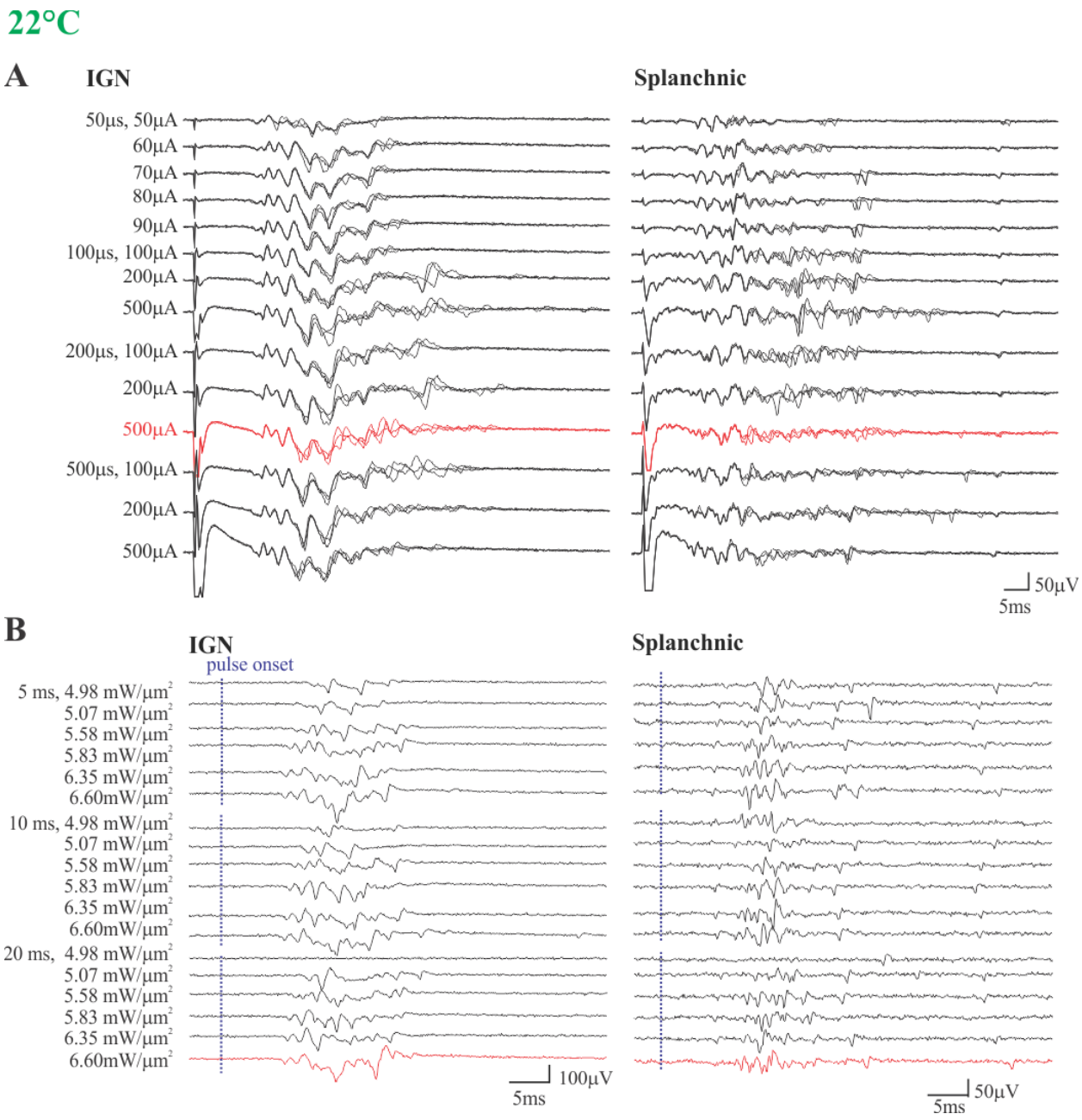

Figure 3.2 Recruitment of SPN axons with graded electrical and optical stimulation

Shown are evoked responses following stimulation of the T10 ventral root with concomitant recordings in T12 IGN and splanchnic nerves. **[A]** Responses to electrical stimulation at different intensities in one animal are shown as 3 overlapping events delivered 60 seconds apart. Stimulation below 50µA, 50µs recruited no SPNs in 6/6 animals for both IGN and splanchnic nerves. Supramaximal recruitment was usually achieved at a simulation intensity of 200µA, 500µs for both nerve-types (n=6). Traces in red represent stimulation intensities used in the

thesis unless otherwise stated. **[B]** Single episodes are shown following optical stimulation delivered for 5, 10, and 20ms the latter of which was previously determined to be the lowest optical stimulation duration to achieve maximal response. Traces in red represent stimulation intensities used in the thesis unless otherwise stated.

3.4.1 Anatomical assessment of CNS preganglionic (SPN) axon composition and projections.

3.4.1.1 SPN projections issue complex multi-segmental branching patterns into thoracic chain ganglia.

We utilized Neurobiotin intra-axonal labeling from ventral roots to understand the anatomical structure and projections of axons from mid to caudal thoracic spinal segments. While there was variability in distance associated with successful fills, several examples showed considerable rostrocaudal divergent projections (Figure 3.3A-B). Divergent projections are seen across many segments rostrally and caudally and reveal the structural intricacies of branching within the sympathetic ganglia (Figure 3.3B). Counts were made of axons entering and exiting across two rostral and one caudal ganglia segment in animal shown in Figure 3.3B (Table 3.1). Notably, many SPNs issued diverging rostrocaudal collaterals after exiting the T7 white ramus, seen as T-shaped branch points (Fig 3.3B2). Of the 165 SPN axons labeled in the T7 ramus, 109 axons projected rostrally into the T7-T6 interganglionic nerve (IGN), while 143 axons projected caudally into the T7-T8 IGN, indicating that most T7 axons bifurcated for rostrocaudal projections at this point (Figure 3.4B). This is in sharp contrast to a study on projections from T7 in embryonic rat that reported only 3% of axons bifurcate while the other axons only project rostrally or caudally [31]. We observed that rostral axonal projections include those that bypass the ganglia without entering and those that enter the ganglia to issue putative synapses. At least some of these axons can be seen to project rostrally back into the IGN. That greater numbers of rostrally projecting axons were seen exiting than entering both the T6 and T5 ganglia suggest that branching has occurred within these ganglia (Figure 3.3). Note that axon counts were always

lower in the IGN distal relative to proximal from injection site. This is consistent with distance dependent loss of Neurobiotin label in many axons and, if true the increased axon numbers across ganglia indicative of branching is likely to be considerably underestimated. Alternately, it is possible that many axons end blindly within the IGN. In comparison, caudally-projecting axons appear to have fewer axons entering the ganglion (T8) and had overall fewer axons exiting distally. This observed decrease could be indicative of either the termination of SPN axons at the T8 level or a progressive loss of Neurobiotin labeling with increased distance. The many axons that clearly bypass T8 identify them as unbranching axons projecting to the splanchnic nerve (Fig 3.2B1; Table 3.1).

In most physiological experiments described in this thesis, the focus was on the recruitment of SPN axons at the T10 ventral root. Recordings were primarily conducted from the IGN caudal to the T12 ganglion and from the splanchnic nerve adjacent to it. Complementing these physiological studies, anatomical examinations using Neurobiotin labeling of SPN axons from the T10 ventral root corroborated the SPN trajectories explored in this research, as depicted in Figure 3.5.

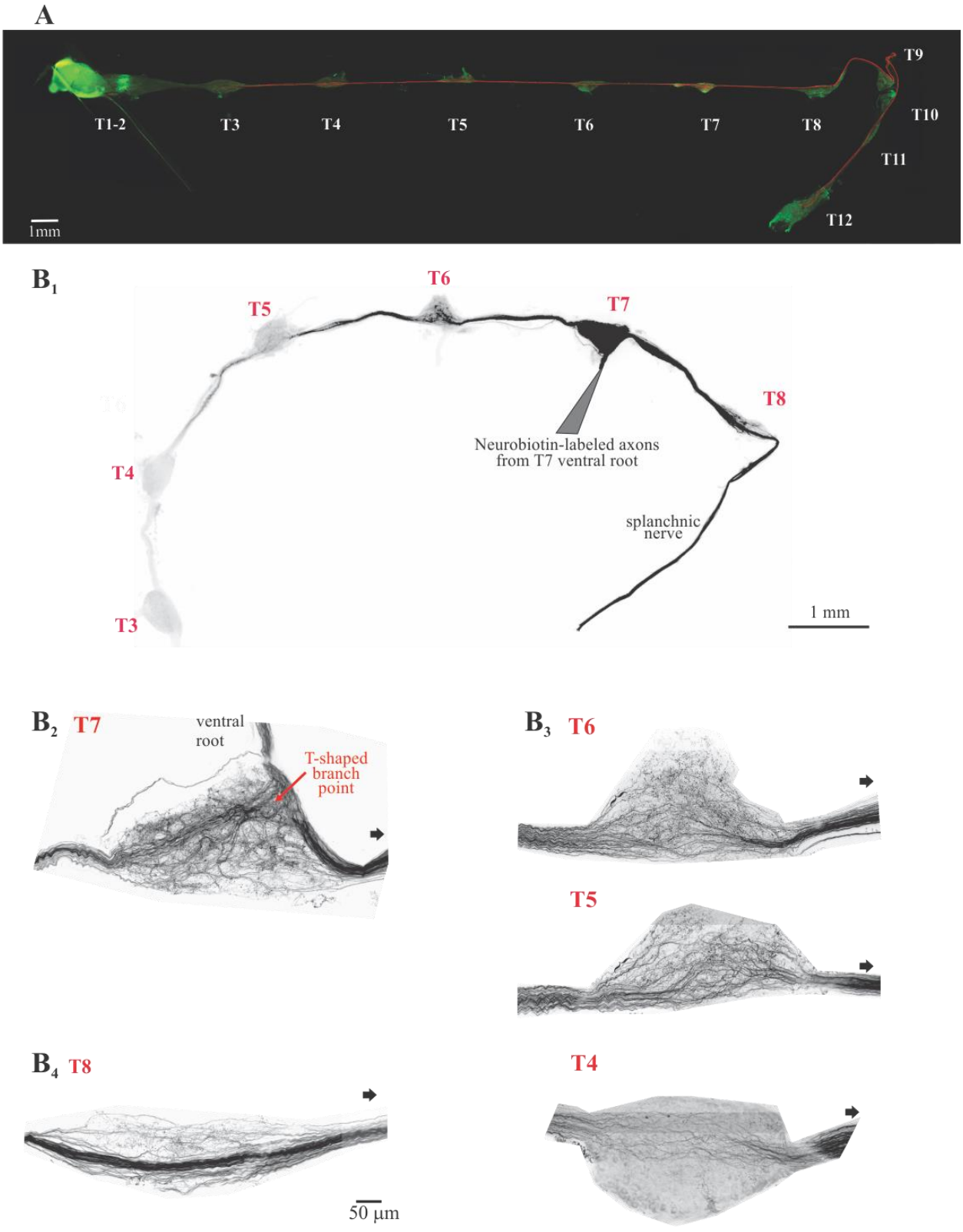

Figure 3.3 Thoracic SPN axons originating at the T7 spinal segment have broad multi-segmental divergent projections with multiple branching patterns.

T7 SPN axons were labeled with Neurobiotin after diffusion from the T7 ventral root (n=2). **[A]** Divergent rostral- and caudal-going NB^+ labeling (red) can be seen along the length of the thoracic chain ganglia containing TH^+ postganglionic neurons (green). **[B_1]** In another mouse NB^+ labeling is seen along T3-T8 chain ganglia and in the splanchnic nerve [T9-12 ganglia are missing]. **[B_2]** T7 SPN axons form a 'T' shaped branch point junction. **[B_3]** Many T6 and T5 axons issue collaterals to form putative synapses before projecting to further rostral sites. Far fewer axons remain at T4. **[B_4]** Most SPN axons that travel caudally are unbranching and may contribute to the splanchnic nerve which predominantly innervates the celiac ganglion. In panels B_{2-4}, caudal direction is shown by a black arrow.

A

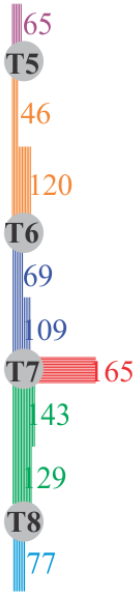

B

IGN Location	# of NB+ Axons	% change from site adjacent and proximal to site of injection
T5R	65	+41% *
T5 ganglion		
T5C	46	-62%
T6R	120	+74% *
T6 ganglion		
T6C	69	-37%
T7R	109	
T7 ganglion	165	Axons in the T7 White Ramus
T7C	143	
T8R	129	-10%
T8 ganglion		
T8C	77	-40%

Figure 3.4 SPN axon counts in IGN segments rostral and caudal to ganglia show high degree of variation.

This figure presents neurobiotin-labeled axons originating from the T7 ventral root and their branching patterns at T7, T6, and T5 ganglia. **[A]** Schematic of degree of branching indicated by increased counts of labeled axons exiting compared to those entering the rostral ganglia (asterisks). That there is also a distance-dependent reduction in axonal labeling may be caused by incomplete labeling of many axonal projections. **[B]** Table exemplifies degree of branching by calculating percent change in axon counts as labeling traverses a ganglion or IGN segment. Gray boxes depict segment of Neurobiotin labeling.

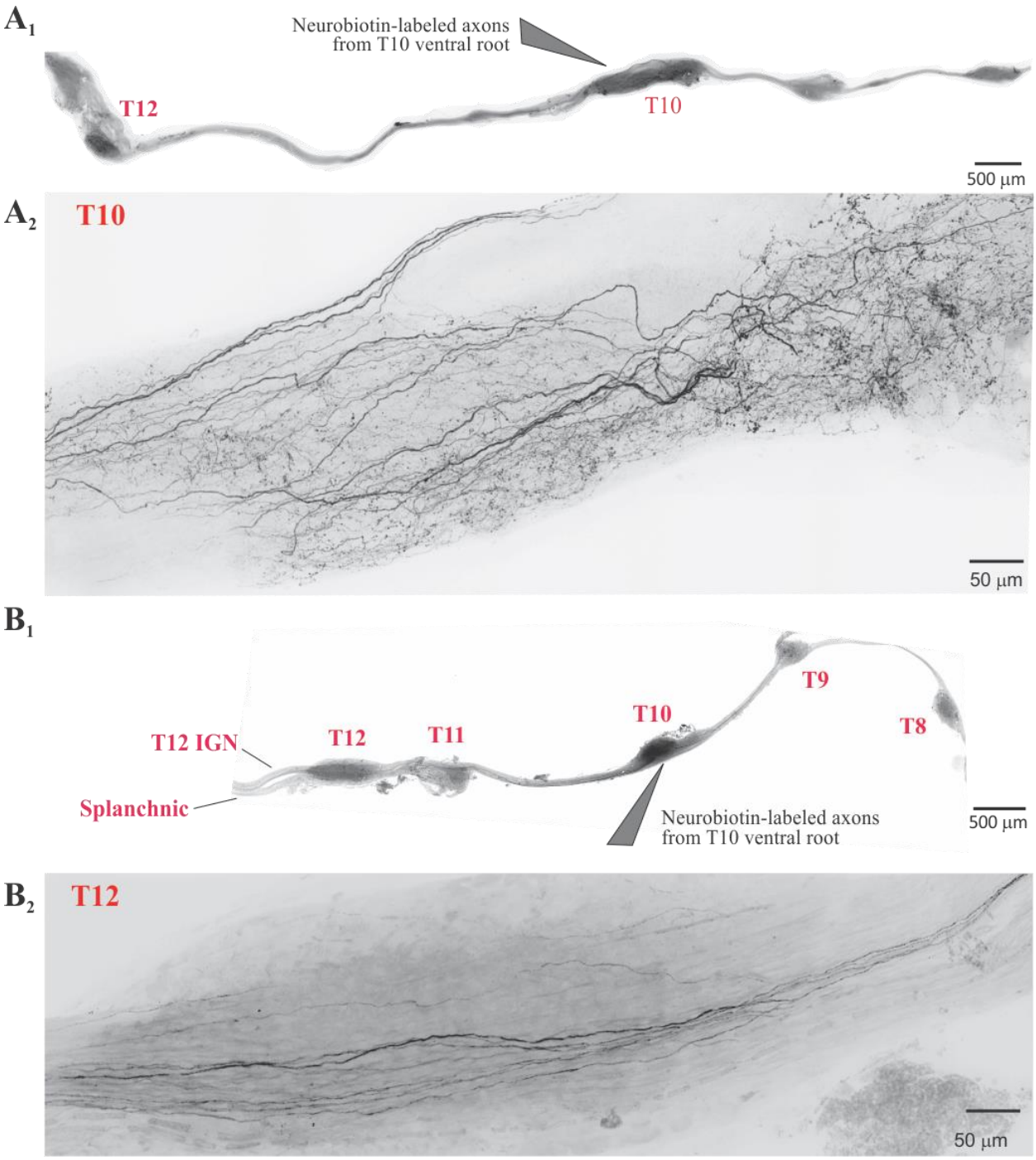

Figure 3.5 Neurobiotin diffusion at T10 ventral root labels rostral and caudal going SPN axons.

[**A**$_1$] Neurobiotin labeling of the T10 ventral root reveals axons extending toward the T12 interganglionic nerve (IGN). [**A**$_2$] A detailed view of the T10 ganglion highlights collateral branches of SPN axons within the ganglion. [**B**$_1$] In a separate specimen, Neurobiotin labeling of the T10 ventral root illustrates SPN axons projecting both rostrally to T8 and caudally to T12

IGN. Notably, the caudal projection is seen extending to the T12 IGN and the splanchnic nerve. [**B**$_2$] A closer examination of the T12 region reveals Neurobiotin-labeled SPN axons passing through the T12 ganglion with comparatively fewer branches, likely due to their projection toward the splanchnic nerve.

To determine whether axon size, namely cross-sectional area (**CSA**) or diameters change as the axon is measured further from the segment of SPN entry into the sympathetic chain, we conducted a population analysis by looking at cross sections of axons along the interganglionic pathway between T7-T6, T6-T5 and T5-T4 in one animal (figure 3.6) (Data from Dr. Alan Sokoloff). The observed increase in axon counts further from the diffusion site (T7-T6: 73.2 ± 0.3, T6-T5: 64.4 ± 0.7, T5-T4: 110 ± 2.0, $P<0.001$) suggests enhanced axonal branching. Additionally, a slight decrease in cross-sectional area from T7-T6 (0.6 μm^2 ± 0.06) to T6-T5 and T5-T4 (0.50 μm^2 ± 0.07, $p<0.01$) indicates similar, but statistically different axon sizes between segments.

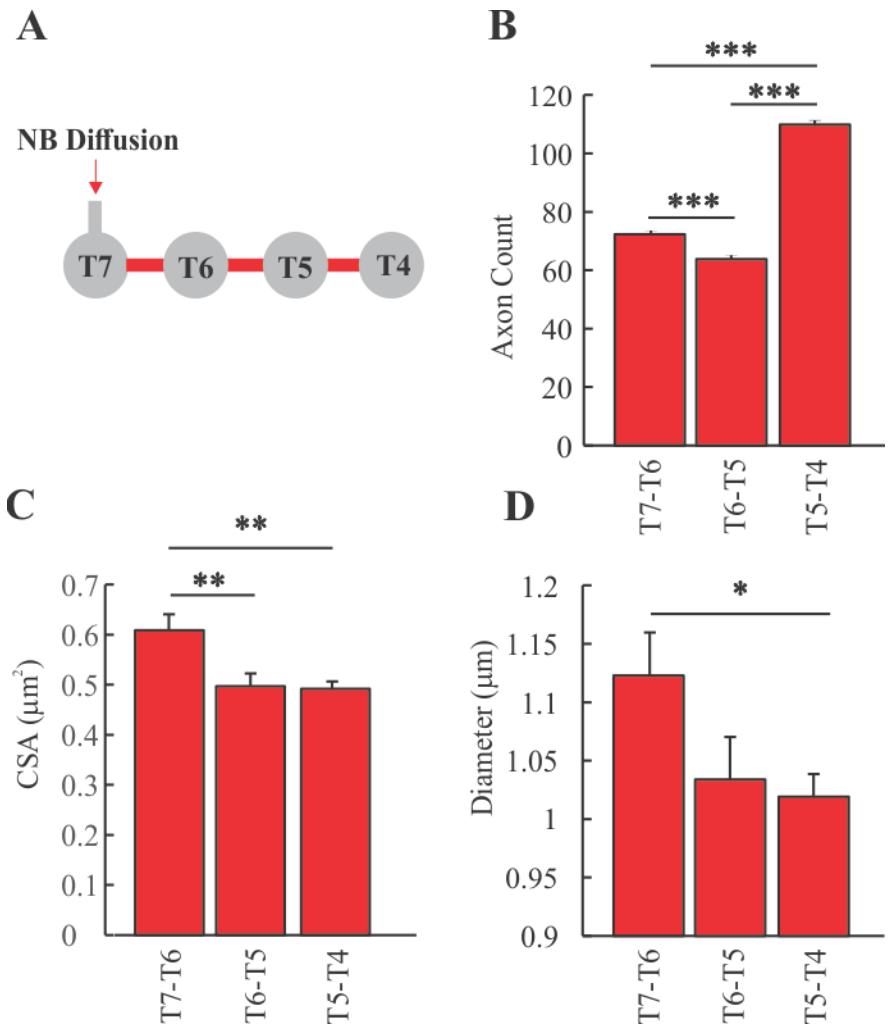

Figure 3.6 As axon branching increases, diameter and CSA reduce further from NB diffusion site.

[A] Experiment schematic showing NB diffusion at the T7 ventral root. For all graphs, cross sections of the IGN between ganglia (red) were measured for axon count, mean cross sectional area and mean diameter of axons. [**B]** Progressive increase in number of axons counted away from diffusion site suggests more axonal branching. Axon counts are as follow: T7-T6 (73.2 ± 0.3), T6-T5 (64.4 ± 0.07), T5-T4 (110 ± 2.0) ($P<0.001$). **[C]** Cross sectional area of T6-T5 and T5-T4 (0.50 μm^2 ± 0.07) are smaller than T7-T6 (0.6 μm^2 ± 0.6) ($p<0.01$) would suggest axon size reduces within the first IGN segment **[D]** Differences were seen in diameter between T7-T6 (1.1 µm ± 0.04) and T4-T5 (1.0 µm ± 0.04). One-way ANOVAs were used to assess significance.

3.4.1.2 Myelinated and unmyelinated axon composition

The anatomical and physiological characteristics of spinal cord SPNs in the mouse paravertebral thoracic chain's branching patterns remain largely unexplored. This thesis aims to delve into the factors that influence the conduction of SPN spikes across segmental ganglia, and in support of this goal, we present studies that explore the anatomical and physiological underpinnings relevant to our research focus. Previous reports have indicated that in the superior cervical ganglion[73], about 99% of mouse paravertebral SPN axons are unmyelinated. Our research, utilizing ChAT-YFP transgenic mice to highlight cholinergic axons, confirms a similar composition in the thoracic SPNs of mice. Immunostaining for myelin basic protein allowed us to identify four myelinated axons within the white commissure (refer to Figure 3.7). Additionally, high-resolution axon counts in another mouse estimated a total of 165 axons (shown in Figure 3.6), suggesting that approximately 2.4% of these axons are myelinated. This discovery of a minor population of myelinated axons aligns with electrophysiological findings, indicating that a few axons exhibit conduction velocities consistent with those of slowly conducting myelinated axons.

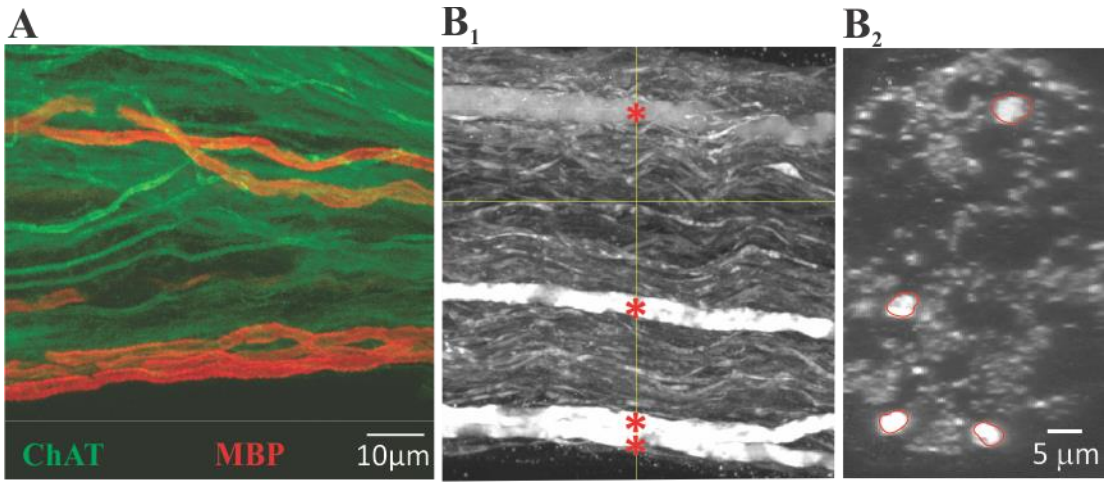

Figure 3.7 Thoracic SPN axons are predominantly thin and unmyelinated.

The composition of SPN axons is primarily characterized by thin-diameter, unmyelinated fibers. **[A]** The ChAT-YFP mouse reveals both unmyelinated (displayed in green) and myelinated SPN axons within the white ramus, the latter being identified with immunolabeling for myelin basic protein (MBP; red). **[B_1]** Confocal scan of the white ramus, showing both myelinated (red stars) and unmyelinated axons. **[B_2]** The yellow line in [B_1] demarcates the cross-sectional area of the ramus displayed in this panel, where myelinated axons are encircled in red.

3.4.1.3 Recording divergence and convergence patterns using optogenetic recruitment of CNS preganglionic (SPN) axons

To demonstrate the functional capacity of observed multisegmental SPN axonal projections we undertook electrophysiological studies on axonal divergence and convergence across the thoracic sympathetic chain originating from several mid- to caudal- thoracic spinal segments. SPNs were recruited via optogenetic stimulation (ChAT-ChR2 mice) in thoracic ventral roots, while CAPs [194] were recorded via electrodes suctioned directly onto various thoracic chain ganglia. Evoked responses in ganglia were predominantly due to recruitment of postganglionic neurons as separate experiments undertaken with hexamethonium had greatly reduced these responses (Figure 3.1). In our experiments conducted at room temperature, it was evident that SPN axons originating from various thoracic ventral roots exhibited patterns of both convergence and divergence across multiple ganglia (Figure 3.8A). Notably, the largest CAPs generally occurred in the nearest ganglia. The T12 ganglion consistently received convergent input from all rostral segments up to T6 (n=4/4), while convergence from further rostral segments was not consistent (T5 – n=3/4; T3 – n=1/4; Figure 3.8A-B). This distribution is consistent with that previous reported in guinea pig [25]. Overall, these results demonstrate that SPN axons project to influence multiple segments and can establish divergent connections to multiple ganglia.

22°C

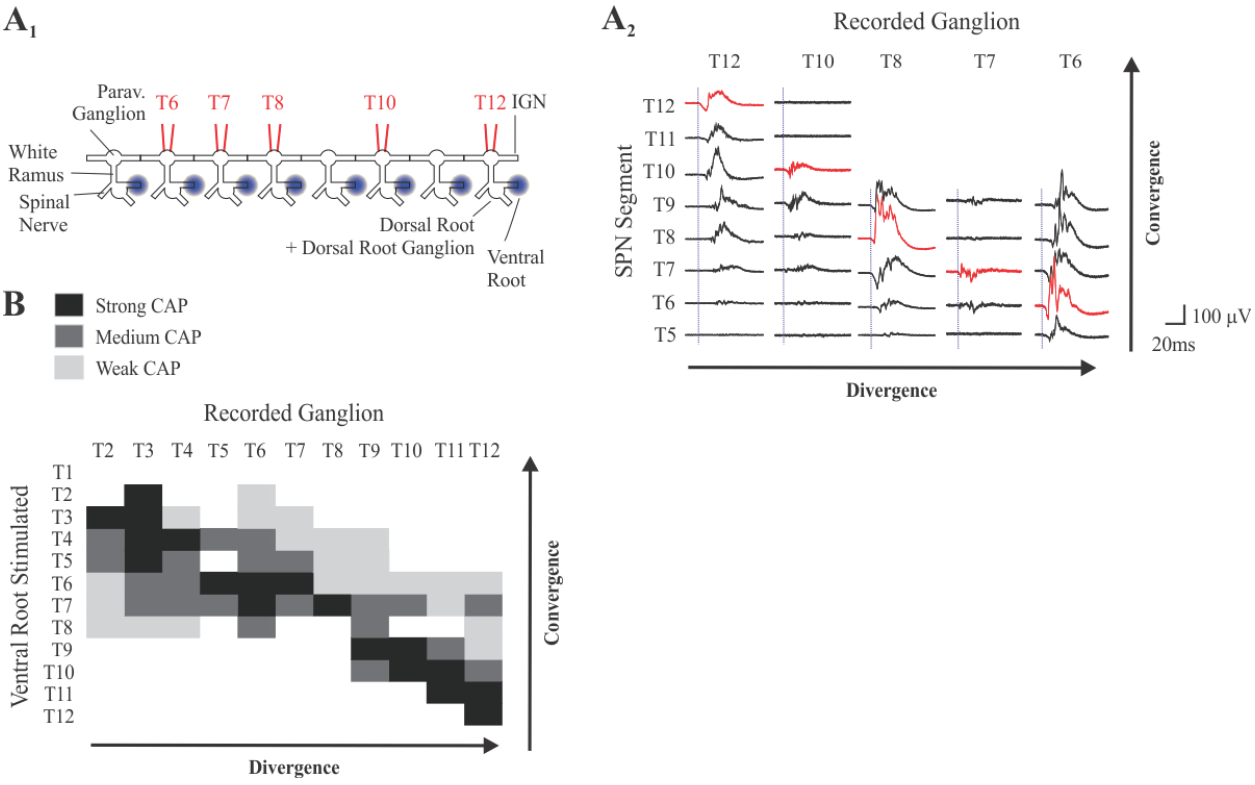

Figure 3.8 Observation of multisegmental convergence and divergence in thoracic SPN axons.

[A1] This experimental schematic depicts optical stimulation (6.6mW/µm², 20 ms pulse, represented by blue dots) applied to the mid to lower thoracic ventral roots. En passant ganglia recordings were performed using glass suction electrodes (illustrated in red), capturing the direct recruitment of SPN axons and an EPSP, without the use of hexamethonium to inhibit synaptic transmission. **[A2]** Displayed are three overlapping episodes from optical stimulation experiments. The traces in red indicate stimulation of the same segment, typically exhibiting the largest responses (n=1) **[B]** This map details the convergence and divergence patterns observed in a different animal, recorded using supramaximal electrical stimulation (1ms, 1mA). Like figure A_1, this map shows the highest CAP was seen at or adjacent to segment of stimulation. Similar experiments were conducted on 4 animals.

3.4.1.4 Identification of axon populations by conduction velocity.

All studies on the conduction velocities of SPN axonal populations were undertaken at supramaximal stimulation of T10 ventral roots following block of synaptic transmission with

hexamethonium (See Figure 3.2) while independently recording from the IGN caudal to the T12 ganglia (i.e. across 3 ganglia) and the adjacent splanchnic nerve of the same length. The splanchnic nerve is composed of unbranching SPN axons that project to prevertebral ganglia. As such it provides comparison of spike conduction properties to branching IGN axons, as well as insight into possible functional differences SPNs innervation para- vs pre-vertebral ganglia. The measured distance from the T10 ventral root to the splanchnic or IGN was determined to be 5mm. Conduction velocities (CV) for electrically and optically stimulated SPNs were determined at 22°C (n=7). This was achieved by calculating the CV of the earliest and latest units arriving in the CAP, as detailed in Table 3.3. Conduction velocity for electrically stimulated responses was determined by calculating the latency from the end of the stimulus artifact to the onset of the compound action potential (CAP), and then dividing this value by the distance of 5 mm. For optically stimulated responses, the CV was assessed by measuring the latency from 5 ms into the 20 ms optical pulse to the onset of CAP. This method was based on an analysis aimed at optimally aligning the characteristics of optical and electrical CAPs, as depicted in Figure 3.2C. Whether stimulated optically or electrically, the splanchnic nerve possesses fibers that conduct at faster velocities compared to those in the IGN, but also contain axons of slower CVs seen in the IGN (Table 3.3).

Table 3.1 Conduction velocity range of thoracic SPN axons in mouse.

	Electrically Evoked	Optically Evoked
22°C		
Interganglionic Nerve	0.11-0.84	0.10-1.08
Splanchnic Nerve	0.13-2.00	0.11-6.13

3.4.2 Evoked response fidelity is high in the fastest axons whereas the slowest axons have high response variability indicative of high rates of conduction failures.

Considering the incredibly fine diameters of SPN axons and their extensive branch patterns, we hypothesized that the conduction in SPN axons would be vulnerable to propagations failures, contrary to the previously assumed viewpoint of reliable conduction. To investigate this, we first recruited SPN axons using supramaximal electrical and optical stimuli alternating every 30 seconds so that each stimulus type was delivered every minute, for a duration of 40 minutes. These axons were then observed at either the caudal-end of the T12 ganglion (T12 IGN) or the splanchnic nerve emerging from the T12 ganglion, all under room temperature conditions (as illustrated in Figure 3.9A). Over this period, our data showed that SPNs in both splanchnic and IGN have greater intertrial response variability in slower conducting responses (see shaded bars in Figure 3.9B).

To further identify the fibers linked to the time-variant loss and emergence of SPN conduction, we divided the evoked CAP into four categories separated by conduction velocity. These categories align with conduction velocities previously identified with specific afferent fiber types at room temperature[77]. The fasted fibers are likely to be lightly myelinated, possessing conduction velocities resembling those of Aδ fibers (0.8< m/s). Notably, these fibers appear exclusively in splanchnic nerve recordings, with an absence in IGN recordings. The other three CV classifications probably represent thin, unmyelinated axons, fitting within the C-fiber conduction speed range. C-Fibers are evident in both splanchnic and IGN recordings (refer to Figure 3.3C-D). To assess whether differences are seen within the C-fiber class, we divided the C-fiber component of the CAP into 3 epochs and labelled them as fast C-fibers (0.3-0.8m/s), slow C-fibers (0.17-0.3m/s), and extra-slow C-fibers (0.10-0.17m/s).

We compared variability in the rectified integral CAP amplitude responses across these fiber types, gathered every minute over 30 minutes. Figure 3.9C plots percent change from mean across time for each fiber in the experiment. Note that there is much greater time-dependent variability in the later arriving fiber types. The variability in fiber type responses between T12 IGN and splanchnic nerves is illustrated through histograms in two separate experiments, showcasing the diversity in percent change from the mean and the similarity in distribution across different animals (Figure 3.9C2).

To assess how consistent differences in variability across nerve fiber types were seen, inter-animal variability was compared as the coefficient of variation (**CoV**) across fiber types in 7 mice (Table 3.2). We observed a trend where all components of the CAP exhibited deviations from the mean, with increasing CoV values correlating with decreasing conduction velocity. This pattern was consistently observed in both splanchnic and IGN axons. Post-hoc analysis showed that C-fibers exhibited higher coefficients of variation (CoV), with notable distinctions between extra-slow fibers and all other groups within the splanchnic nerves, as well as between extra-

slow fibers and slow-C fibers in IGNs.

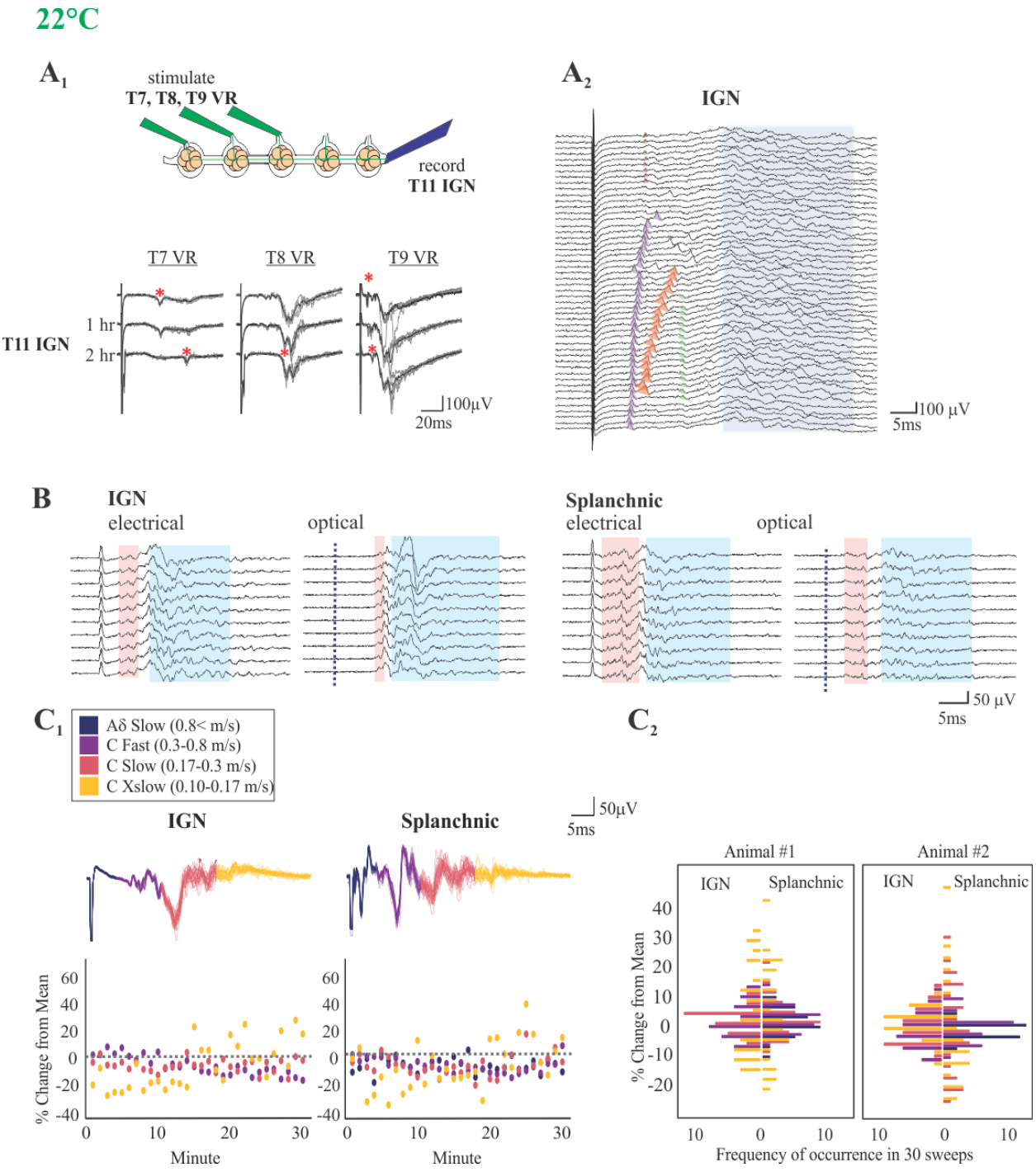

Figure 3.9 Spontaneous conduction block and emergence is seen in all fiber types.

[A1] Experimental setup and the recording of CAPs from converging SPN axons at T11 IGN, originating from T7, T8, and T9 ventral roots. It demonstrates that the evoked responses are larger when the stimulation site is closer to the recording site, with stimuli delivered every 1/30

seconds. Notably, the red asterisks indicate instances where spontaneous changes in conduction were observed over a two-hour period. **[A_2]** Shown is a raster plot of individual CAP records following T9 VR stimulation at one-minute intervals for 45 minutes (episodes are ordered chronologically from top to bottom). The emergence of two larger early units with progressively earlier latency is highlighted, suggesting increased conduction security (purple and orange underlining). Other emergent or lost events are marked in pink or green, with the high variability in the later arriving unmyelinated axons (blue shaded region) impeding individual assessment but quantifiable through rectified integral comparisons. **[B]** a raster of 10 episodes recorded at 1/90 seconds, this panel illustrates the ongoing emergence of conduction variability in IGN and splanchnic nerve across different stimulation methods. The time-dependent changes in conduction are more prevalent in slow-conducting axons (blue boxes) compared to fast-conducting ones (red boxes). **[C_1]** Showcase of CAPs recorded with electrical stimulation, divided into epochs based on conduction velocity. Ten superimposed episodes illustrate the increased jitter between episodes as conduction velocities decrease. A-δ fibers, exclusive to the splanchnic nerve, are shown. Time-series plots from one animal demonstrate CAP rectified integral variations from the mean over 30 minutes. **[C_2]** This panel presents histograms plotting the percentage change from the mean in two different animals, highlighting the variability across fiber types. Inter-animal variability is commonly noted, with extra-slow C fibers typically showing the largest percentage change from the mean. The conditions include 100µM Hexamethonium in the bath and varying stimulation parameters as noted for each panel, with the onset of a 20ms optical pulse marked by a blue dotted line.

Table 3.2 Inter-animal variability and coefficient of variation across fiber types

The coefficient of variance was calculated for all fiber types by dividing the standard deviation by mean (n=7). Mean CoVs were calculated (n=6) and show highest variance in extra-slow C Note: All CAPs were recruited supramaximally (200uA/500us for electrical) at 22°C. Statistical significance for the (CoV) was determined using t-tests, comparing each CoV value to the overall mean CoV (**p<0.05, **p<0.01, ***p<0.001).

	Splanchnic				**IGN**		
	Aδ	C-Fiber			C-Fiber		
CoV (%)		Fast	Slow	Xslow	Fast	Slow	Xslow
Animal 1	2.4	5.1	15.1	23.3	6.1	6.5	5.4
Animal 2	5.7	5.3	8.0	18.2	7.1	4.8	17.6
Animal 3	10.4	3.6	13.2	18.4	12.5	6.6	19.7
Animal 4	5.8	14.1	11.3	15.2	15.8	11.3	10.8
Animal 5	3.5	11.7	12.0	13.2	9.9	8.4	15.0
Animal 6	18.0	13.0	15.6	29.1	25.6	25.7	48.0
Animal 7	-	-	23.7	-	12.9	7.5	11.9
Mean CoV (%)	**7.6***	**8.8****	**14.1*****	**19.6*****	**12.8****	**10.1*****	**18.4*****

3.5 Discussion

3.5.1 Mouse thoracic SPN axons exhibit broad divergence and are largely unmyelinated.

3.5.1.1 SPN axons exhibit widespread divergence.

Our study utilized Neurobiotin intra-axonal labeling from ventral roots to explore the anatomical projections of SPN axons in mice. We observed extensive divergent projections both rostrally and caudally, with most SPNs forming bifurcations at the T7 white ramus for rostrocaudal projections. This divergence appears more pronounced than previously reported in guinea pig [54] and rat [31]. Though the magnitude of pre- to postganglionic neuron ratios that are often used for estimates of SPN divergence [195], it is clear that magnitude of observed anatomical divergence and the reliability of spike propagation along its divergent projections represent important variables in the recruitment of postganglionic activity and these variables may differ between the ganglia studied, individual animals, by sex, developmental stage, and between species.

We observed all three kinds of SPN axonal branches previously described outside of the spinal cord: terminal branches close to postganglionic soma; bifurcating branches within autonomic nerves remote from their targets [196]; and collateral (*en passant*) branches distributing to several ganglia of the sympathetic chain [5,65]. Our anatomical labeling of T7 SPN axons revealed intricate branching patterns within the thoracic chain ganglia with notable 'T' shaped branch points within the T7 ganglia to enable rostral and caudal projections. Analysis of rostral projections show that many axons branched to form synapses at T6 and T5 before continuing rostrally with a significant decrease in axon number observed by T4. Axon counts and cross-sectional area measurements showed increased branching and reduction in axon size along the interganglionic pathway.

Our electrophysiological studies revealed that SPN axons, originating from mid- to caudal-thoracic spinal segments, demonstrate significant multisegmental convergence and divergence across the thoracic sympathetic chain as demonstrated previously in guinea pig [25]. Notably, the T12 ganglion showed convergence from segments rostral to T12 up to T6 consistently, but this pattern varied above T6. Our finding that SPN axons influence multiple segments through divergent connections to ganglia, with the largest CAPs typically observed in the nearest ganglia is consistent with previous reports in guinea pig thoracic ganglia [25].

Consistent with previous reports in superior cervical ganglia [73], SPNs in the mouse paravertebral thoracic chain were shown to be overwhelmingly unmyelinated, with only a small number of myelinated axons present. This was consistent with the predominantly C fiber conduction velocity measures obtained in SPN axons recorded in splanchnic (unbranching) and IGN (includes branching) axons. Both IGN and splanchnic had a comparable range of slower conducting axons whose velocities were consistent with those of unmyelinated C-fiber axons, while only the splanchnic nerve contained faster conducting axons consistent with Aδ fibers [197].

3.5.2 At room temperature, variability of SPN conduction correlates to conduction velocity

When single evoked responses were delivered at 60-second intervals, the myelinated and fastest conducting unmyelinated responses remained largely consistent, while the slower/extra-slow C-fibers had significantly greater variability.

It was unexpected to discover that slower conducting axons demonstrated variability in response at room temperature, a condition under which we would anticipate more consistent spike conduction owing to a presumed higher safety factor[198] . Furthermore, splanchnic SPNs, which do not have branching axons, also show a similar degree of variability as seen in slow conducting axons. This suggests that fiber diameter, rather than branching, may be the primary

factor influencing physical constraints on spike propagation. Alternately, recordings obtained from the T12 IGN may also be largely comprised of unbranching axons. This latter possibility is unlikely as Neurobiotin labeling of SPNs in the T10 VR demonstrated that caudally-directed axons included branching axons.

3.5.2.1 Conduction variability

It has been assumed that once an SPN was activated in the spinal cord, spike conduction along the axon is reliable with consequent actions on postganglionic neurons (via the n+1 rule) being robust and reproducible [3,56], but this may be influenced by the experimental approach. The only other study that assessed divergence and actions across thoracic ganglia undertook studies at reduced (room) temperature [25], having larger and wider spikes[198], expected to increase safety factor for spike propagation including at branch points. Conduction was likely additionally improved due to a decrease in the temperature-sensitive K_2P TREK-1 K_{leak} conductance, leading to increased membrane resistivity and depolarization.

Given the remarkably thin diameters and complex branching patterns of SPN axons, it is reasonable to consider that the conduction through SPN axons may be more variable than previously believed. We speculate that spikes within these small-diameter SPN axons travel with low safety above the threshold level, precariously close to failing – meaning that minor changes in channel dynamics along the axon could impact conduction. Additionally, the branching nature of SPN axons further contributes to the reduced reliability of SPN spike propagation, underscoring the low safety factor inherent in the system. Indeed we observed considerable variability in conduction, consistent with this view. Assuming high conduction failure rates are a prominent feature of SPN axons, it suggests that sympathetic drive is encoded by alterations in net population activity, a feature explored in more details in subsequent chapters.

3.5.3 Differential recruitment of SPN axons by electrical and optical stimulation

We observed distinct patterns of SPN axonal recruitment when using both electrical and optical stimuli on T10 ventral roots. Electrical stimuli were found to preferentially recruit faster conducting events, while optical stimuli favored slower conducting events. A stimulation threshold was identified at approximately 50µA, 50µs for T12 IGN and splanchnic nerve recordings, with maximal recruitment typically achieved at 200µA, 200µs. For optical stimulation, a pulse duration of 20 ms at an intensity of around 6.3mW/µm² was necessary for maximal recruitment.

As depicted in Figure 3.2, we indeed found that optical stimulation can recruit slower conducting axons first. Although it's evident that SPN axons recruited via optical means exhibit comparable arrival times compared to those recruited electrically, determining the precise conduction velocities of the optically recruited SPN populations remains challenging. The extended duration of the stimulation pulse hinders accurate measurement of the exact moment of axon recruitment. To enhance the accuracy of comparisons between optical and electrical responses, additional experiments focusing on measuring optical duration are essential. Recognizing the unique differences in axon populations activated by each method, we designed our experiments in this thesis to include both optically and electrically recruited SPNs, employing supramaximal recruitment strategies to ensure all SPN populations are captured for analysis.

The preferential recruitment of slow-conducting axons in response to optical stimulation can be attributed not only to the extended axonal activation times provided by optical pulses but also to differences in axonal structure. In peripheral nerves, unmyelinated axons, typically of smaller diameter, show increased responsiveness to optogenetic activation [199]. On the other hand, electrical stimulation is less effective in these smaller, unmyelinated axons due to their lack of

myelin and distinct biophysical properties [200]. It has been shown that in ChAT-CHR2 mice optical stimuli recruit the slowest conducting axons first in contrast to electrical stimulation which recruits in reverse side order [188].

3.6 Conclusions

These results provide significant insights into the complexities of SPN axon pathways and their conduction properties. Our findings from Neurobiotin labeling of SPN axons from individual spinal segments (ventral roots) reveal that these axons branch off from spinal segments and innervate multiple ganglia within the paravertebral chain, indicating a complex network where a single ganglion may receive inputs from numerous thoracic spinal segments. Projections were more extensive than previously reports on multisegmental divergence by electrophysiological studies in guinea pig. Overall, mouse SPN axons were shown to have an extensive network of projections across numerous thoracic ganglia.

Measured conduction velocities of SPN axons range from those comparable to slow Aδ fibers to the much slower C-fibers, consistent with our observations that SPN axons possess extremely fine diameters, measuring around 0.1 micrometers. The combination of such slender axonal diameters with branching morphologies significantly raises the potential for conduction block. Indeed, slower-conducting axons displayed more variability in response at room temperature indicative of multi-axon conduction failures, despite the expectation of more reliable spike conduction at reduced temperature. It supports a view of distance-dependent spike conduction failures and the possibility of branch points as potential sites of failure and neuromodulatory control [72,92]. The comparison between splanchnic and IGN axons further emphasizes this point, revealing how physical attributes of axons can impact their conduction efficiency and reliability.

Additionally, the use of both optical and electrical stimulation to preferentially recruit distinct SPN axons introduces a novel approach to explore differences in action of SPN subpopulations.

4 SPN sensitivity to temperature and frequency

4.1 Abstract

This chapter focuses on the temperature and activation history dependent changes in population evoked SPN axonal responses recorded in the T12 IGN and splanchnic nerves following supramaximal recruitment of their axons from the T10 ventral root. To compare temperature dependent effects in population recruitment, we scaled evoked response amplitude and duration between 22° and 36°C. We observed that electrically-evoked response magnitude was significantly reduced at 36°C in both faster- and slower-conducting axons from both nerves. Slower-conducting axons of the IGN were the most profoundly depressed. Optically-evoked responses were commonly completely blocked at 36°C.

To compare the effect of activation history on response magnitude, conditioning stimulus trains (2 or 20s duration) were delivered at a range of physiological frequencies (5, 10 and 20 Hz) beginning 1s after a baseline response. At 22°C and 5Hz, electrically-evoked responses were significantly depressed in the slower-conducting axons of the IGN with a similar trend seen in splanchnic axons. Optical stimulation led to more profound depression of slower-conducting responses in the IGN while depressing both faster- and slower conducting responses in the splanchnic nerve. At 36°C and 5Hz, electrically evoked responses did not undergo depression, but at 20Hz faster-conducting axons were depressed in both nerves. The absence of depressive effect on slower-conducting responses may relate to their prior temperature-dependent block. Longer-duration trains (20s) led to greater response depression at 22°C and post-train facilitation at 36°C. Overall, these findings not only contribute to our understanding of the impact of temperature and activation history on SPN axonal conduction but also open avenues for exploring unique sensitivities of distinct axonal populations.

4.2 Introduction

SPN axons in mouse are overwhelmingly unmyelinated[73], and unmyelinated axons are very sensitive to temperature (T°) increases that can lead to conduction block [83,92,202]. The mechanism by which high T° elicits conduction failures includes reduction in spike width and amplitude [198]. Conversely, it may be expected that a lower T° reduces conduction failures by increasing spike amplitude and duration, as may also be accomplished with block of potassium (K^+) currents [63,201]. T° sensitive differences are particularly relevant to our understanding of transmission across SPN branch points as prior thoracic chain recordings of multisegmental actions were undertaken *ex vivo* at room temperature [25-27,54,202].

It is thought that preganglionic signals are distributed widely through paravertebral ganglia with little modification [3]. Yet elsewhere, axonal branch points are prone to conduction failure and are under modulatory control [72,92]. Almost all (99%) mouse paravertebral SPN axons are unmyelinated with mean diameter of 0.4 µm and branch diameters can be as low as 0.1 µm [73]. One prominent feature of unmyelinated axons is frequency-dependent hyperpolarization, conduction slowing and block [70,148,149,203,204]. In the absence of ability to record from individual axons, differences in population changes in activity may deepen our understanding of the rules governing population circuit dynamics. Further insight may be derived from realistic computational modeling of factors contributing to conduction failures in individual axons. This includes: (a) T°-, frequency-, and history-dependent mechanisms, (b) geometry changes including those seen at axonal branch points, and (c) behavioral state-dependent gain modulation in continuously active SPNs (e.g. baroreflex [6]) or in unique groups of accessory SPNs (e.g. during conditions of stress [44,205]).

This study focuses on SPNs innervating paravertebral thoracic chain ganglia. We developed an *ex vivo* adult mouse that has access to thoracic sympathetic chain with intact ventral roots and enables T°- and activity-dependent assessment of SPN conduction using electrical and optical stimulation of the ventral roots. To identify white ramus myelinated and unmyelinated cholinergic SPNs we used $ChAT^{+}$ transgenic mice and observed the expected low incidence of larger diameter myelinated axons. We assert that control of conduction along SPN multisegmental axonal branches is an overlooked but important physiologically modifiable presynaptic feature in output control.

4.3 Methods

4.3.1 Multisegmental *ex vivo* paravertebral preparation

Adult (8 weeks+) C57Bl/6 mice of both sexes were anesthetized with ketamine (100mg/kg) and xylazine (10mg/kg) mix by intraperitoneal injection, following light anesthetization in an isoflurane chamber. The thoracic vertebral column and adjacent ribs are excised and transferred to a Sylgaard dish containing ice cold, oxygenated (95% O_2 / 5% CO_2) high-Mg^{2+}/low-Ca^{2+} artificial cerebral spinal fluid (aCSF) containing (in mM), [NaCl 128, KCl 1.9, $MgSO_4$ 13.3, $CaCl_2$ 1.1, KH_2PO_4 1.2, glucose 10, $NaHCO_3$ 26]. Following a complete laminectomy and vertebrectomy, the spinal cord (SC) and dorsal roots (DR) are exposed and removed. The remaining thoracic chain ganglia, in continuity with communicating rami, spinal nerves and ventral roots are cleaned of excess fat and muscle. The tissue is transferred to a Sylgaard recording chamber superfused with oxygenated aCSF containing (in mM), [NaCl 128, KCl 1.9, $MgSO_4$ 1.3, $CaCl_2$ 2.4, KH_2PO_4 1.2, glucose 10, $NaHCO_3$ 26], at ˜40ml/minute at 28C and allowed to rest for 1 hour.

4.3.2 Electrophysiology

Temperature and activity-dependence experiments: Glass recording electrodes were placed on the caudal cut ends of the T12 ganglion, splanchnic nerve, and rostral cut-end of the T5 ganglion for temperature and frequency studies. Glass suction recording electrodes were positioned on thoracic ventral roots for stimulation (200-250 μm tip diameter). Optogenetic stimulation was performed using calibrated Clampex-controlled laser diode boxes built by lab engineer Bill Goolsby (voltage range 1-5V corresponding to 0-1500mW). ThorLabs M61L01 fiber optic cables (105 µm, 0.22 NA) were used in all experiments. For temperature experiments, bath temperature was maintained at 36°C by a Peltier device (built in-house by Mr. Bill Goolsby) prior to start of experiment. During the experiment, the bath was cooled at regular intervals to assess temperature-dependent changes in preganglionic conductance. The tissue was allowed to stabilize for at least 15 minutes before data acquisition. For activity dependent experiments, bath temperature was maintained at 28C unless otherwise stated. All recorded data were digitized at 50 kHz (Digidata 1322A 16 Bit DAQ, Molecular Devices, U.S.A.) with pClamp acquisition software (v. 10.7 Molecular Devices). Recorded signals were amplified (5000x) and low pass filtered at 3 kHz using in-house amplifiers.

4.3.3 Pharmacology

As recordings of population axonal spiking could include synaptically-mediated responses, we block synaptic activity, either with the nAChR receptor antagonist hexamethonium bromide (100 µM) [206]. Application of pancuronium bromide was used to block activity of the intercostal muscle.

4.3.4 Analysis

For detailed methodology on CAP quantification, see Section 3.3.2. In the analysis of T° effects, we employed paired t-tests to evaluate the significance of differences between T° as well as between CAP epochs within each nerve. Regarding the frequency analysis, we utilized a repeated measures ANOVA. This was complemented by Tukey's post hoc comparisons, applied as appropriate, to identify significant variations across different pulses during and after the train. Values are represented as mean percent of baseline ± SEM.

4.4 Results

4.4.1 Population recruitment of SPN axons is altered at elevated temperatures.

Our initial hypothesis posited that disruptions in conduction would be most pronounced in branching axons recorded at the T12 IGN. Such failures may not have been seen in previous studies undertaken in guinea pig at 22°C due to an increased safety factor provided by larger and broader action potentials seen at 22°C compared to body temperature [25-27]. Conversely, temperatures above normal body levels, have been linked to a heightened risk of conduction failure [83,207], indicating a potential temperature sensitivity in signal conduction at SPN branching points.

In our experiments, following the methodology outlined in Chapter 3, we initially recorded evoked responses at 36°C, followed by recordings at a reduced bath temperature of 22°C. To ensure a valid comparison of signal conduction at these temperatures, we scaled responses to account for temperature-dependent changes. Generally, nerve conduction velocity (CV) increases with temperature[198]. Our findings corroborate this, showing elevated conduction velocities in SPNs at higher temperatures (Table 4.1). Notably, at 32°C, the conduction in fibers of the splanchnic nerve was faster than that in the interganglionic nerve, consistent with the presence of a faster conducting Aδ population in splanchnic demonstrated in Chapter 3.

Table 4.1 Conduction velocity range (in m/s) of thoracic SPN axons at 22° and 32°C

	Electrically Evoked	Optically Evoked
22°C		
Interganglionic Nerve	0.11-0.84	0.10-1.08
Splanchnic Nerve	0.13-2.00	0.11-6.13
32°C		
Interganglionic Nerve	0.20-1.59	0.23-1.45
Splanchnic Nerve	0.21-3.24	0.26-3.57

In contrast to the methodology employed in Chapter 3, where we divided our analysis into four CV classes, we chose a different approach for these frequency-dependent studies. This decision was made to accommodate potential changes in axonal conduction velocity that could arise from varying frequencies. Consequently, we categorized the signals recorded at room T° into two groups—those with faster conduction and those with slower conduction—based on their CV. Utilizing the framework provided by Pinto and Sarvanov [77], which details T°-dependent changes in nerve fiber signal speeds, we adjusted the spike CV from 36°C to 22°C (Figure 4.1). Then, we scaled the amplitude and width by factors of 1.53 and 1.87, respectively, corresponding to the T° decrease from 36°C to 22°C, using reference data from Hodgkin and Katz (1949) and Stegeman and De Weerd (1982) [198,208] (Figure 4.1). These established benchmarks were then applied to our recordings in mice to compare T°-mediated differences in recruitment between 36°C and 22°C.

Upon scaling our data to account for T° induced differences in the CAP size, we conducted a comparative analysis between the fast and slow-conducting epochs of the CAP at 36°C and 22°C. Our analysis revealed a marked reduction in responses across all axon types at 36°C ($p<0.001$). The IGN slower-conducting axons exhibited a substantially higher % reduction in evoked response (51.5 ± 6%) compared to that seen in faster-conducting axons (24.7 ± 6%; $p<0.05$; Figure 4.1D). For the splanchnic nerve these values were reduced by 50 ± 8% and 36 ±

6%, respectively. The difference in observed reductions in CAP responses for both faster and slower responses between IGN and splanchnic could be attributed to variations in the axonal composition between these nerves (Figure 4.1D).

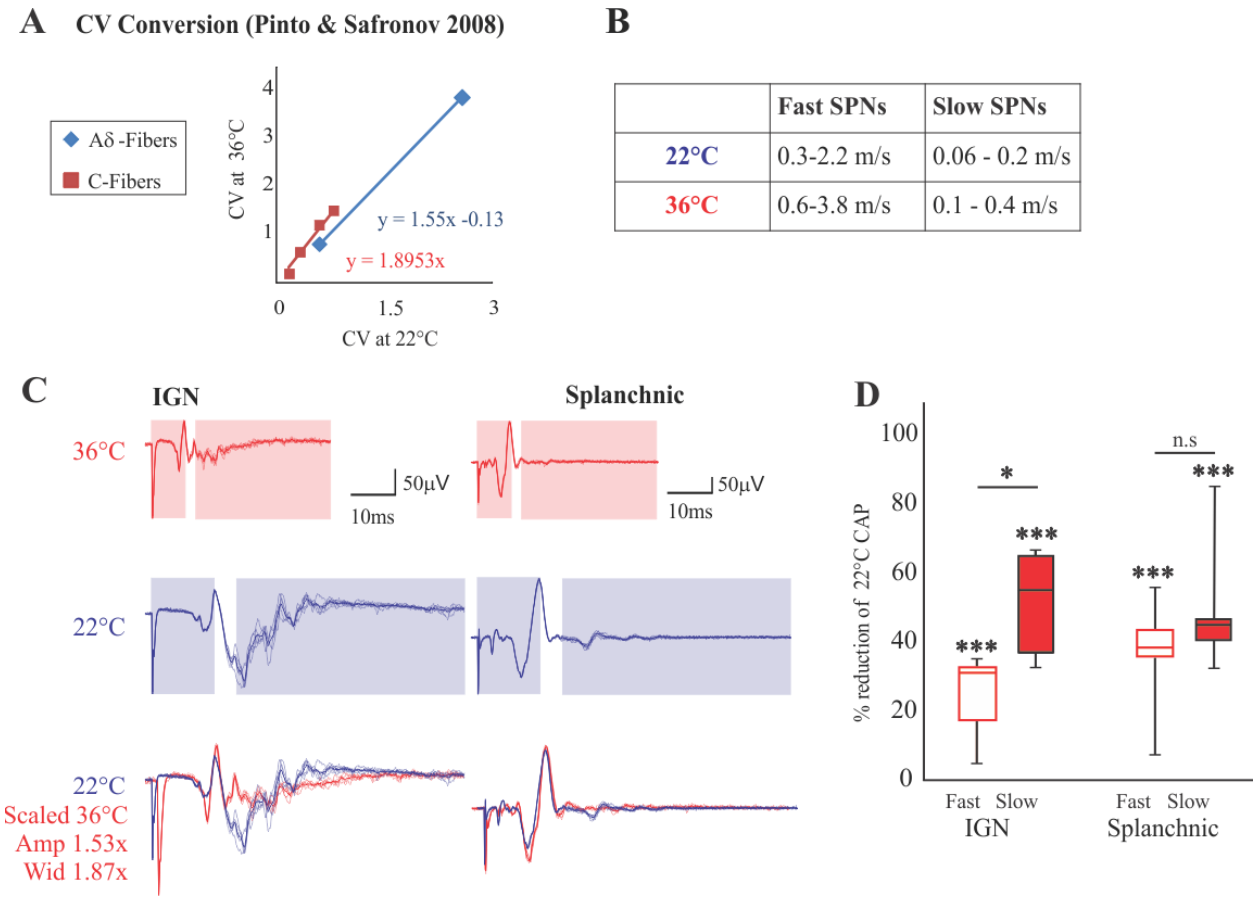

Figure 4.1 Increased temperature leads to reduced axonal recruitment.

[A] Graph derived from Table 1 in Pinto and Safronov 2008, estimating the changes in conduction velocity for A-δ and C-fibers, which exhibit conduction velocities comparable to SPN fibers observed in mice. **[B]** Using trend line formulas and experimental data collected at 36°C, predicated changes to conduction velocity ranges were extrapolated for 36°C. **[C]** Example of evoked responses at 36°C and 22°C are shown. The volley at 36°C was scaled using pre-determined scale factors and shown superimposed on 22°C evoked response to highlight loss of units at 36°C in both splanchnic and IGN with a greater degree of failure seen in IGN. Early and late SPNs are highlighted with boxes. **[D]** Evoked responses from 36°C and 22°C were rectified, integrated, scaled, and compared. The percent reduction in magnitude of evoked response was determined for fast and slow-conducting epochs of the CAP (n=5). (supramaximal electrical stimulation was delivered at 200µA/500µs.) Paired t-tests were used to assess significance between baseline and nerve, and across fiber types for each nerve.

4.4.2 Slower conducting SPN axons that branch exhibit depression during a 5Hz train.

The effect of activation history on the recruitment of evoked responses was investigated by delivering stimuli at varying frequencies and train lengths, with a comparison of responses between IGN and splanchnic axons. Activation history can alter spike conduction properties, including changes in the probability of recruitment as well as in conduction velocity (CV) [209], and may, therefore, be physiologically relevant to the recruitment of postganglionic neurons. We initially explored the impact of frequency-dependent conditioning stimuli on the magnitude of evoked responses, which were delivered at either 5Hz or 20Hz at 22°C. Frequency-dependent changes in the evoked response plateaued by the 6th pulse for both frequencies tested, as illustrated in Figure 4.2.

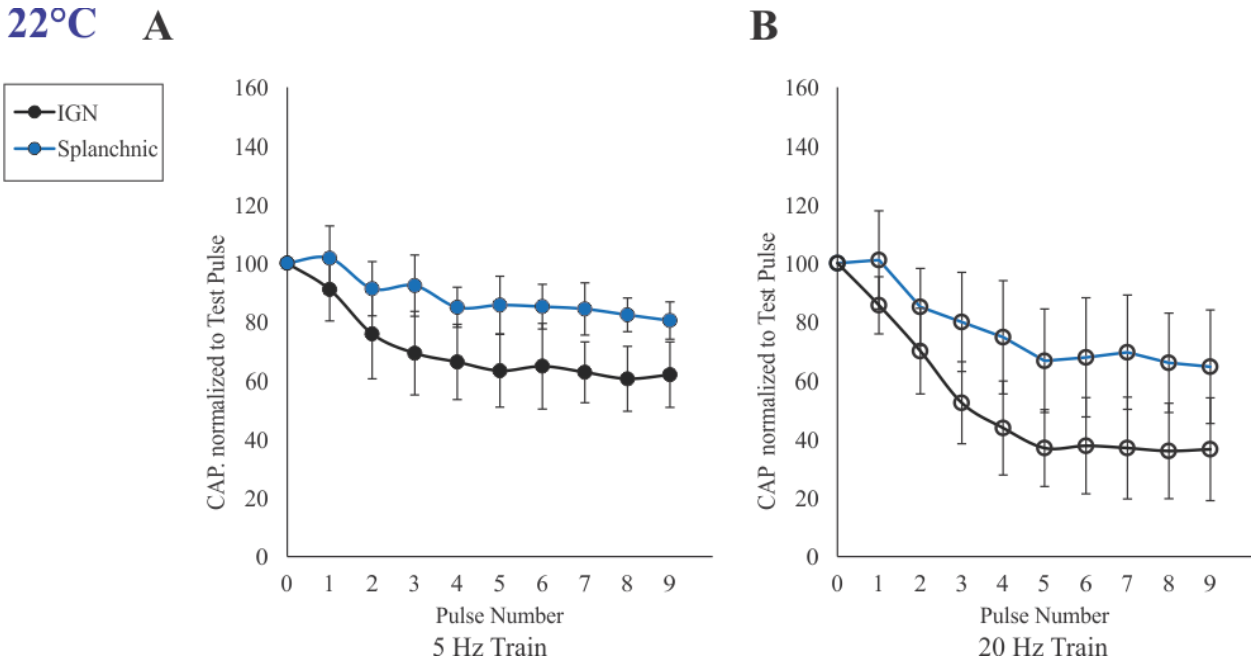

Figure 4.2 Effect of pulse number on change in evoked CAP response amplitude during 5Hz and 20Hz stimulation.

The responses throughout the stimulation train are normalized to the initial test pulse, elicited by a 200µA, 500µs electrical stimulus applied 1 second prior to the train. Percentage changes in CAP responses relative to the test pulse are depicted for frequencies of 5Hz **[A]** and 20Hz [**B**]. Typically, maximum depression response was seen by 6th pulse for both frequencies and both nerve types. Statistical significance is not reported due to an underpowered sample (n=4).

Quantification of activity-dependent changes in the CAP at 22°C were based on the experimental design shown in Figure 4.3A. A rest period of 90 seconds between trials ensured recovery to baseline response. As shown, we compared the pre-train test pulse CAP, evoked one second before the sequence began, to the 1^{st}, 6^{th} and 10^{th} pulses within the 2s 5Hz stimulus train, and also to a response evoked two seconds after the train (the post-train conditioned response). Example raw electrically- and optically evoked responses are illustrated in figure 4.3B and 4.4B, respectively. All signals were high pass filtered at a frequency of 25Hz.

For electrically-evoked responses, frequency-dependent decreases were preferential to slower-conducting events in the IGN and only during the stimulus train (Figure 4.3B, C). The average response of slow IGN axons dropped to 55±1% of the test pulse for pulse B and 59±11% ($p<0.001$, $n=4$) for pulse C.

For optically-evoked responses, all axon groups showed a significant decrement from the baseline, except for the fast-conducting axons in the IGN (Figure 4.4C). After the first pulse following the test pulse, the response of slow axons in both IGN and splanchnic nerves was significantly diminished to 48±12% and 51±8%, respectively ($p<0.001$). Fast-conducting splanchnic axons experienced a reduction to 32±16% with optical stimulation at the first pulse ($p<0.001$). This diminishing trend persisted through the stimulation train, with the final pulse eliciting a response significantly lower than the test pulse: 17±5% for slow IGN, 14±5% for fast splanchnic, and 22±5% for slow splanchnic axons ($p<0.001$). Notably, except for the fast IGN axons, which maintained their baseline levels throughout the 5Hz optical stimulation train, no recovery to baseline was observed following optical stimulation. Notably, the fast IGN axons were insensitive to depression via both stimulation types.

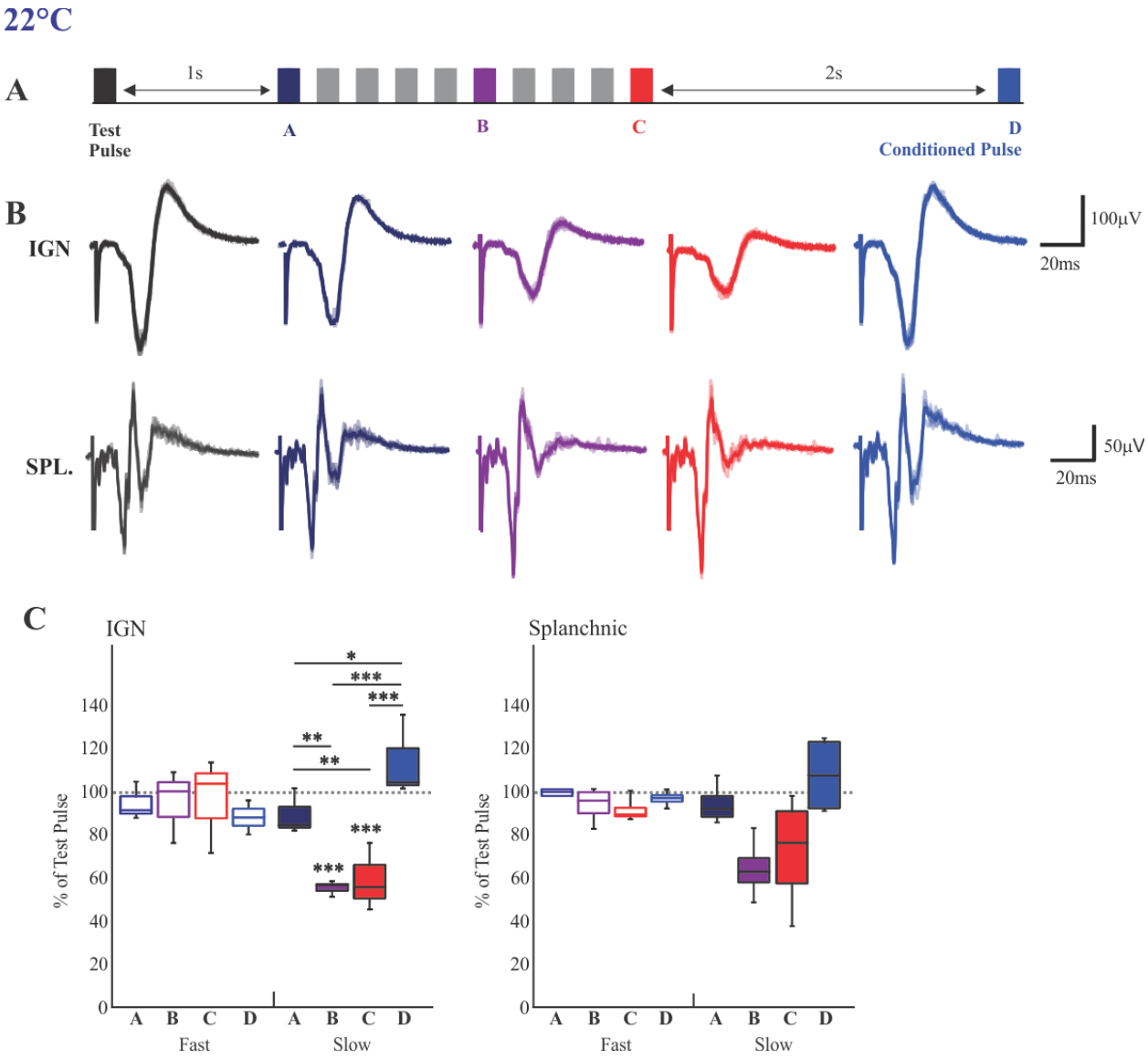

Figure 4.3. Slower-conducting IGN axons undergo preferential depression following 5Hz electrical stimulation at 22°C.

[A] This experiment's schematic illustrates a 5Hz stimulation protocol lasting 2 seconds. We focused our analysis on epochs A, B, C, and D, comparing each to the initial test pulse. Specifically, we examined epoch D for any history-dependent changes occurring 2 seconds post-stimulation train**.** Evoked responses for each epoch were divided into fast and slow conducting components. **[B]** The figure presents raw trace examples from both the IGN and splanchnic nerve in the same subject, recorded during key epochs after electrical stimulation. These traces highlight the response patterns during critical moments of the experiment. **[C]** We analyzed the rectified integral values of both fast-conducting and slow-conducting components from key epochs, expressing them as a percentage of the test pulse's corresponding rectified integral

values. Notably, frequency-dependent depression was observed exclusively in the slow-conducting sympathetic preganglionic neurons (SPNs) of the IGN, particularly in epochs B and C ($p<0.001$). While epochs B and C showed significant changes compared to epochs A and D, they did not significantly differ from each other. Late SPN depression in splanchnic was not found to be significant. However, Chi-square= 10.400 with 4 degrees of freedom ($p=0.034$) suggesting median values among the epochs are significantly different. Statistical analyses were performed using a repeated measures ANOVA, with post hoc comparisons where applicable, to determine significant differences across groups (n=4). The conditions include 100µM hexamethonium in the bath.

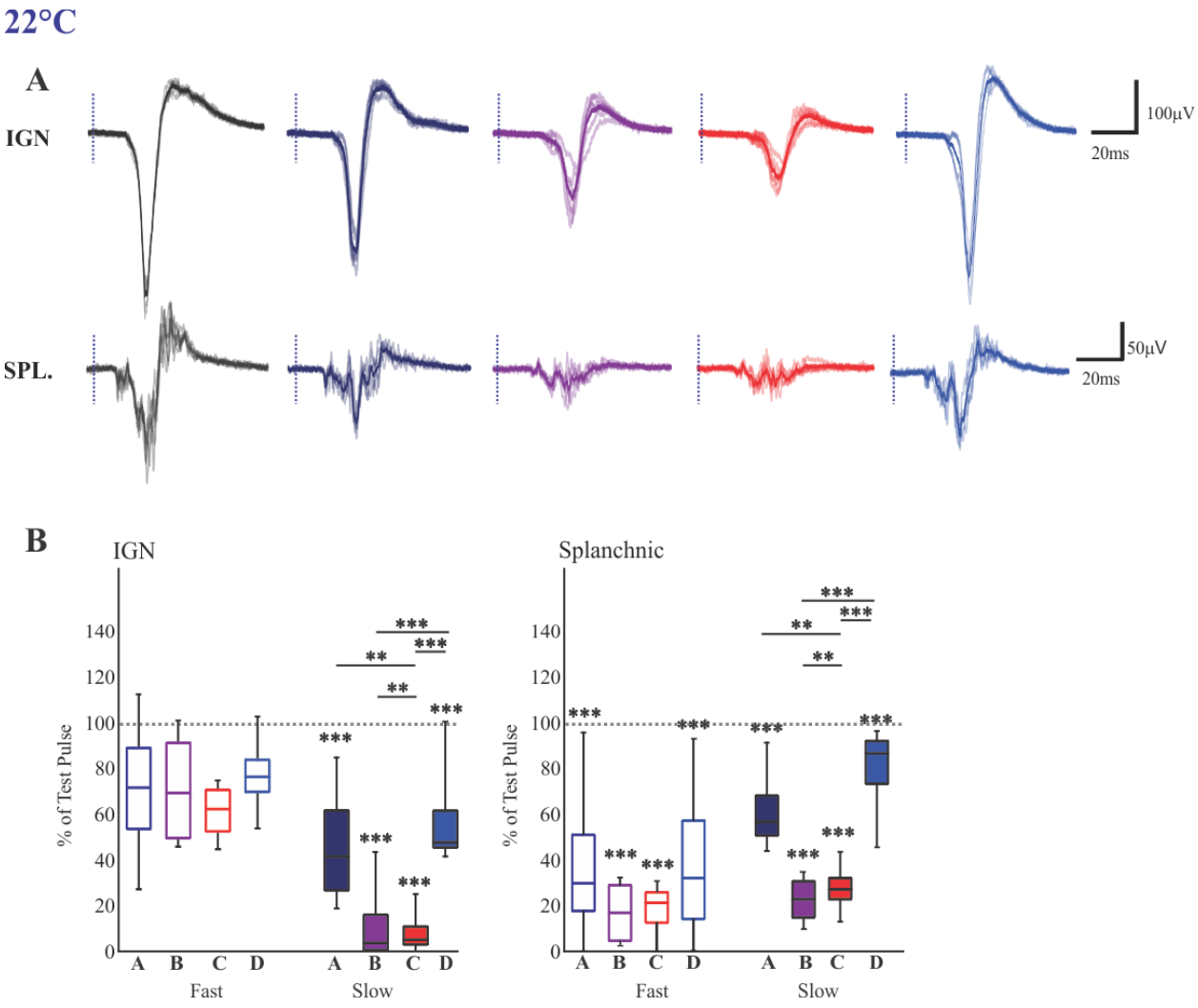

Figure 4.4. Optical Recruitment of SPNs show greater and broader levels of depression than electrical recruitment.

[A] The figure presents raw trace examples from both the (IGN and splanchnic nerve in the same subject, recorded during key pulses after supramaximal optical stimulation of 6.6mW/µm^2 for a

pulse duration of 20ms (dotted line). These traces highlight the response patterns during specific epochs of interganglionic and splanchnic nerves in one animal. **[B]** We analyzed the rectified integral values of both fast-conducting and slow-conducting components from key epochs, expressing them as a percentage of the test pulse's corresponding rectified integral values. Except for fast conducting IGN SPNs, all SPN populations optically recruited during a 5Hz train were significantly reduced from baseline. Slow conducting SPNs recruited at epochs B and C were significantly different from epoch A and D. Statistical analyses were performed using a repeated measures ANOVA, with post hoc comparisons where applicable, to determine significant differences across groups. (n=4). The conditions include 100µM hexamethonium in the bath.

4.4.3 A sub-population of slow-conducting SPN axons are resilient to 5Hz but exhibit depression at 10Hz.

We next compared the effect of 10Hz stimulation to that of 5Hz (Table 4.2). Our findings showed that the results for 5Hz and 10Hz stimulations were largely similar, with a few significant distinctions. Notably, in slow-conducting populations, Epochs B and C demonstrated more pronounced depression under 10Hz stimulation than at 5Hz, across all stimulation types. During 5Hz stimulation, no significant differences were observed in Epochs B and C with electrical stimulation, indicating that maximum depression levels were likely reached within 1 second. However, under 10Hz stimulation, the mean values for these epochs were further diminished. This suggests the existence of a subset of slow-conducting SPN axons that are resilient to 5Hz but exhibit increased sensitivity to 10Hz stimulation.

Table 4.2 Comparing percent electrical and optical evoked response magnitude relative to baseline following 5Hz or 10Hz stimulation at 22°C.

Epochs A-C provide the amplitude responses of the 1st, 6th, and last pulse in the train, respectively. Epoch D reports the amplitude value 2s after train completion. Values represent the mean % of baseline magnitude ± SEM with significance reported as; * $p<0.05$, ** $p<0.01$, and *** $p<0.001$.

A. Electrical Recruitment

	Fast SPNs (0.3-2.2 m/s)		Slow SPNs (0.06-0.2 m/s)	
	5Hz	10Hz	5Hz	10Hz
IGN				
A	94.4 ± 8.5	92.5 ± 14.6	89.1 ± 10.5	85.0 ± 12.9
B	94.9 ± 16.7	207.6 ± 113.0	55.0 ± 3.3***	30.3 ± 11.1***
C	96.0 ± 21.8	188.6 ± 90.6	58.9 ± 15.9***	25.4 ± 11.6***

D	88.0 ± 7.9	85.7 ± 15.5	113.7 ± 19.0	110.2 ± 24.6
Spl.				
A	97.8 ± 3.52	100.4 ± 6.7	92.9 ± 9.5	67.5 ± 45.8
B	92.6 ± 8.3	97.5 ± 10.1	62.9 ± 14.3	31.8 ± 29.5
C	90.2 ± 6.0	91.6 ± 10.9	70.7 ± 27.1	51.1 ± 27.7
D	95.4 ± 3.6	100.9 ± 9.0	106.5 ± 18.3	73.8 ± 50.3

B. Optical Recruitment

	Fast SPNs (0.3-2.2 m/s)		Slow SPNs (0.06-0.2 m/s)	
	5Hz	10Hz	5Hz	10Hz
IGN				
A	68.1 ± 29.2	61.1 ± 24.5*	48.5 ± 24.1***	44.1 ± 24.3***
B	68.6 ± 22.3	36.7 ± 26.2**	19.1 ± 16.8***	5.6 ± 3.6***
C	60.0 ± 11.1	46.8 ± 18.5*	17.4 ± 9.1***	5.4 ± 2.6***
D	73.4 ± 16.4	71.1 ± 9.0	58.7 ± 22.5***	46.3 ± 23.6***
Spl.				
A	32.0 ± 33.6***	37.9 ± 22.8***	51.2 ± 17.0***	48.5 ± 18.6***
B	13.6 ± 13.1***	21.4 ± 14.9***	18.5 ± 9.3***	9.3 ± 8.4***
C	14.1 ± 10.0***	19.9 ± 13.0***	22.8 ± 10.3***	9.0 ± 5.8***
D	32.4 ± 33.2***	30.9 ± 20.7***	64.9 ± 18.8***	66.6 ± 13.2***

4.4.4 Further comparison of effects of pulse train duration and subsequent assessment of temperature dependence of these changes at 22°C and 36°C.

We next explored the effects of higher frequency (20Hz), longer duration pulse trains (20s), and elevated temperature 36°C on response amplitude and history-dependence. We restricted our analysis to electrical stimulation as optically evoked responses were not reliably seen at physiological temperature without pharmacological intervention (see discussion in Chapter 5). To enable comparison to the 2s pulse trains described above, we quantified the first pulse in the train, then 1s into the train (6^{th} pulse at 5Hz, 21^{st} pulse at 20Hz) and then the last pulse in the train. Note that at 20Hz we were unable to quantify the slower-conducting volley components during the train due to overlap with stimulus artifact. Thus, comparison of 'test' evoked responses are to the final response in the pulse train (epoch C) and the subsequent conditioned response (epoch D) two seconds later (see lettering in Figure 4.3).

As with 2s trains at 22°C, during the 5Hz-20s train evoked faster-conducting responses in both the IGN and splanchnic nerves underwent no significant change. However, slower-conducting axons showed variability in their response; there was a noticeable transient reduction in CAP amplitude throughout the duration of the train. Notably, slower-conducting IGN axons experienced a depression in CAP size to 40 ± 4% ($p<0.05$) and 29 ± 7%($p<0.001$) during epochs B and C, respectively, as did splanchnic (65 ± 6%; $p<0.01$ and 65 ± 10%; $p<0.01$). However, unlike effects after 2s the post-conditioning response recovered 2 seconds after the train.

Shifting to a higher frequency of 20Hz, faster-conducting axons in both IGN and splanchnic nerves continued to show resilience with no significant changes, and slow axons continued to be significantly depressed in IGN (23 ± 9%; $p<0.001$) and splanchnic (65 ± 10%; $p<0.01$). However, the conditioned pulse (Epoch D) did not show a recovery in IGN, where the response remained reduced to 50 ± 17% ($p<0.01$). This would imply that prolonged high frequency stimuli recruited additional factors responsible for depression in the IGN.

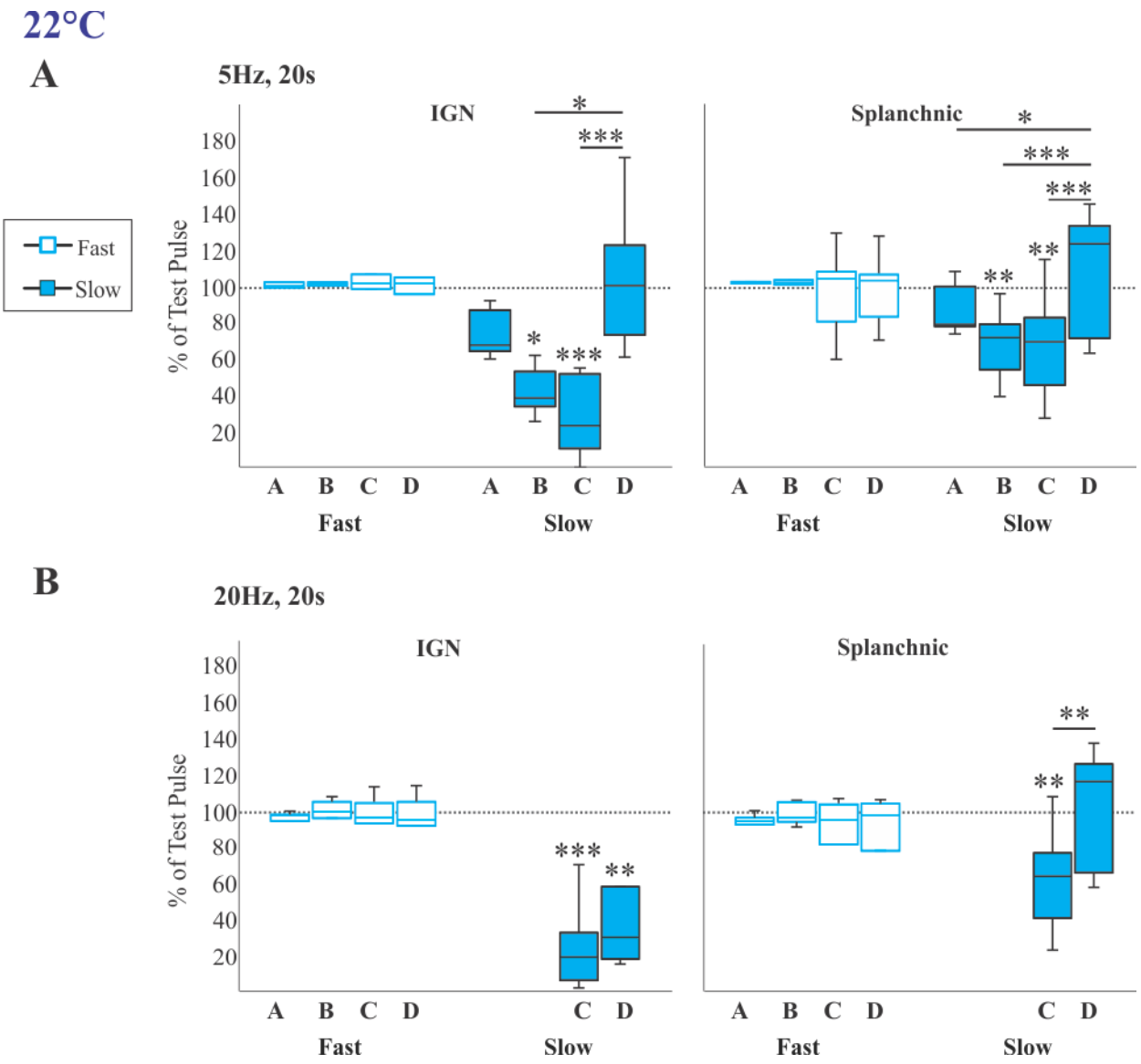

Figure 4.5. Slower-conducting SPN axons fatigue at 5 and 20Hz at 22°C with longer duration (20s) trains.

Shown are changes in electrically evoked responses relative to baseline at epochs A, B, C, and D (defined in Figure 4.3A). We particularly evaluated epochs C & D history-dependent effects observed following prolonged stimulus train delivery (20s). The rectified integral values of both faster- and slower-conducting CAP components from these key epochs are presented as percentages of the rectified-integral values of the baseline 'test' pulse. **[A]** Faster axon CAPs were unaffected by the 5Hz stimulation train in both IGN and splanchnic nerves. Slower axons exhibited a transient decrease in CAP magnitude during the train, with a subsequent recovery after 2 seconds. Specifically, slow IGN axons displayed a reduction to 40 ± 4% and 29 ± 7% in epochs B and C, respectively ($p<0.05$, $p<0.001$), while splanchnic slow axons demonstrated a consistent depression to 65 ± 6% and 65 ± 10% in the same epochs ($p<0.01$). **[B]** At 20Hz stimulation, faster axons in both IGN and splanchnic nerves showed no significant changes,

whereas pulse C indicated a notable reduction to 23 ± 9% in IGN ($p<0.001$) and to 65 ± 10% in splanchnic ($p<0.01$). The conditioned pulse (Epoch D) saw a recovery in splanchnic slow axons but remained diminished at 50 ± 17% for IGN ($p<0.01$). Note: Slow-conducting units from Epochs A-B were excluded in the 20Hz stimulation analysis because the CAP arrival was slower than the subsequent pulse in the train.Statistical significance was assessed via repeated measures ANOVA and post hoc tests where relevant (n=7).

We next examined 5Hz frequency-dependent actions at 36°C. To ensure epochs tested could be compared across 22°C and 36°C, we made a cursory assessment of maximum depression seen at both temperatures and found that, like 22°C, at 36°C, maximum depression is seen by the 6th pulse regardless of nerve or temperature (figure 4.6A). In contrast to that seen at 22°C, faster-conducting axon response amplitudes did not change during 5Hz stimulation at 36°C . Also, for slow-conducting axons, there were no significant changes from the baseline during epochs A through C. However, epoch D was facilitated by 37±27% ($p<0.001$) for IGN and 34±11% ($p<0.001$) for splanchnic.

Upon increasing the stimulation frequency to 20Hz, a different response emerged (Figure 4.6C). Fast axons in both IGN and splanchnic nerves experienced a significant uptick from the baseline in epochs C and D. Specifically, IGN fast axons were facilitated by 27±6% in epoch C, with this elevated response persisting 2 seconds post-train (27±4%, $p<0.001$). Splanchnic fast axons also demonstrated a facilitation of 18±4% during the train, which remained at a facilitation of 16±5% following the train ($p<0.01$). However, the slow axons presented a different profile. With 20Hz stimulation, no significant differences were detected from the test pulse in the responses of slow IGN and splanchnic axons due to the high level of variability in response.

One plausible rationale for the observed attenuation of frequency-dependent depression at elevated temperatures could be as follows: There may exist subsets of axons that are particularly

temperature-sensitive and preferentially blocked at 36°C, leaving behind a cohort of SPN axons that are more resilient to frequency-dependent conduction failure. This possibility is consistent with results obtained in Figure 3.6, which demonstrated that an increase in temperature disproportionately depressed recruitment of slower-conducting axons – the remaining population may be less susceptible to frequency-induced depression. Consequently, this could account for the maintained neural responses observed even during prolonged high-frequency stimulation at higher temperature settings.

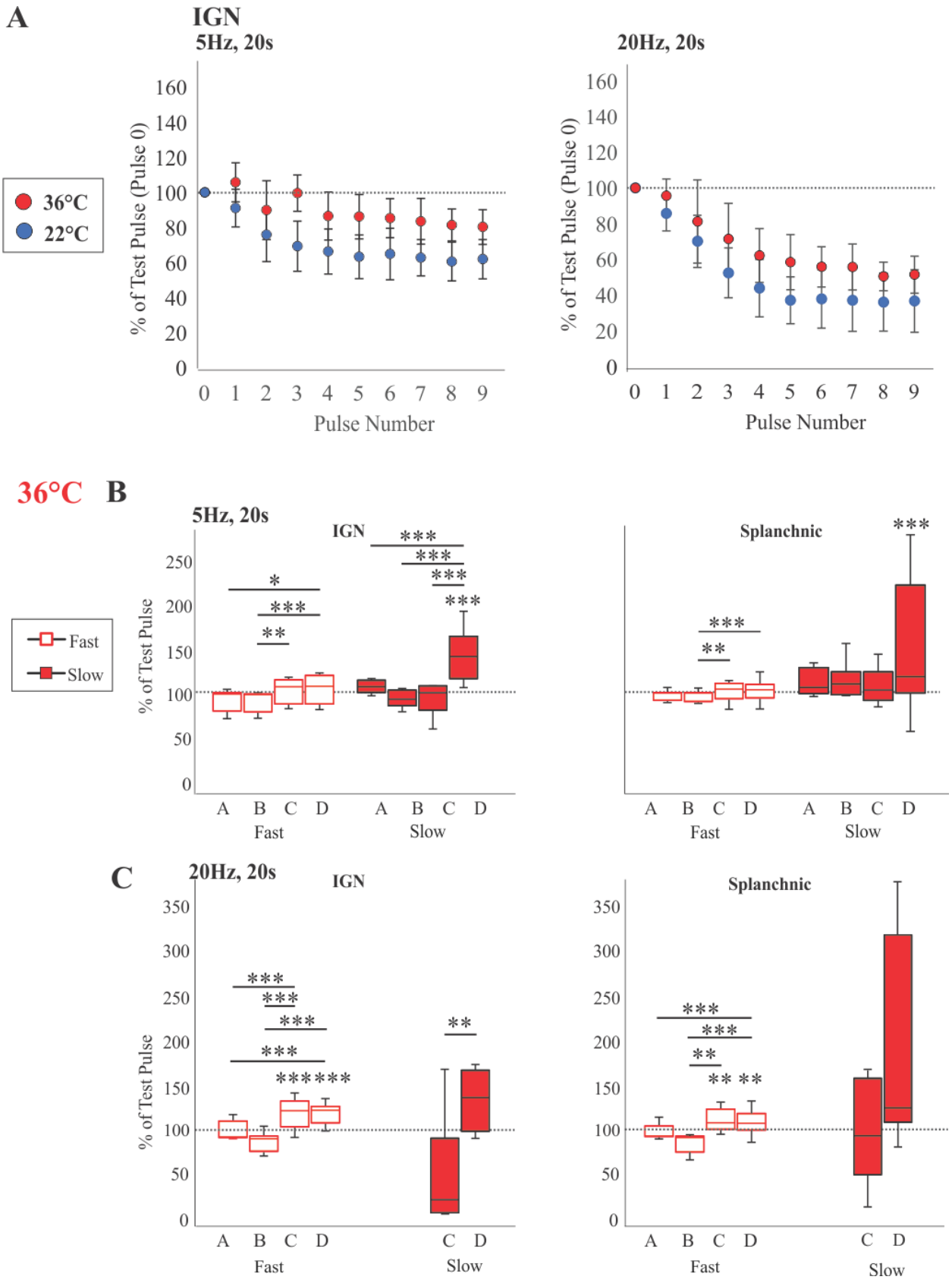
A
IGN
5Hz, 20s
20Hz, 20s
36°C
22°C
% of Test Pulse (Pulse 0)
Pulse Number
36°C B
5Hz, 20s
IGN
Splanchnic
Fast
Slow
% of Test Pulse
C
20Hz, 20s
IGN
Splanchnic

Figure 4.6. SPN axons recruited at 36°C are more resilient to 5Hz and 20Hz trains

Epochs A, B, C, and D, as depicted in Figure 4.3A, were analyzed against the initial test pulse for potential history-dependent effects, particularly at epoch D occurring 20 seconds post-stimulation. The rectified integral values for fast and slow CAP components are expressed as percentages of the test pulse. **[A]** CAP depression across 9 pulses was normalized to the test pulse (pulse 0), revealing that maximum depression occurs by pulse 6, consistent across both temperatures of 36° and 22°, as well as independent of stimulation frequency. Only IGN is shown here but splanchnic nerve showed a similar trend. **[B]** At 5Hz, fast axon CAPs in both IGN and splanchnic nerves remained unaffected; however, significant facilitation from baseline was noted in epoch D for both splanchnic and IGN slow axons (34% ± 11% and 37% ± 27%, respectively; $p<0.001$). **[C]** With 20Hz stimulation, fast axons in both nerves exhibited a significant increase from baseline in epochs C and D, with IGN fast axons showing 27% ± 6% facilitation in Epoch C and a sustained enhancement of 27% ± 4% after the train ($p<0.001$). Splanchnic fast axons experienced an 18% ± 4% facilitation during the train, remaining elevated at 16% ± 5% post-train ($p<0.01$). Slow axons in IGN and splanchnic nerves, however, did not display significant deviations from the test pulse under 20Hz stimulation. Statistical assessments were performed using repeated measures ANOVA with subsequent post hoc tests (n=7).

4.5 Discussion

In this study, we revealed that evoked response magnitude has strong T° and activation history dependence. Slower-conducting axons were particularly vulnerable to depression at higher T°. The loss of a significant fraction of SPN axons due to conduction failure at 36° compared to 22°C has important implications on our understanding of distant-dependent conduction failures as the only prior study on SPN divergence was undertaken at 22°C[25-27,54,202]. This study may have greatly overestimated the influence of SPN actions on postganglionic neurons in more distant chain ganglia. Relating the present data at 36° to that obtained *in vivo,* would suggest that SPN signaling capacity would be highly compromised. Indeed, our results could explain why 40–70% of SPNs appear to be silent (lack ongoing or reflex activity)[210].

As SPNs can fire tonically and across a range of frequencies, it is critical to determine whether activation history modulates spike conduction failures across the range of frequencies where spiking activity has been observed. Interestingly, we observed that activity dependent depression of evoked responses was prominent at 5-20Hz at 22° while responses at 36° we're capable of following all frequencies and even led to post-train facilitation. This unexpected observation introduces the possibility that the SPNs blocked at higher T° represent a unique population with strong frequency dependent depression. Relating the present data to spike frequencies that have been recorded *in vivo,* supports the view that recruited axons are capable of encoding responses across a broad frequency range.

4.5.1 Effects of temperature

To determine the impact of T° on spike propagation in SPNs, we compared volleys at room and body T°. At 36°C, both fast- and slow-conducting SPN axons experienced a T°-sensitive conduction block, failing at rates between 24-50%. Given the high variability in axonal

recruitment observed in slow-conducting SPNs at 22°C, it is not surprising that these slow-conducting SPNs failed more frequently at 36°C compared to their faster-conducting counterparts. However, this observation was exclusive to IGN and not splanchnic axons. Thus, while the higher T°C promoted conduction block in all SPN axon populations, slower-conducting IGN axons were particularly susceptible. As the IGN contains branching axons, a putative mechanism is branch point failure.

4.5.1.1 Are branching axons uniquely prone to temperature-dependent changes in conduction?

To gain insight into the role axon branching has on temperature-sensitive conduction block, we collaborated with Harry Wu and Dr. Astrid Prinz (Biology Dept., Emory University) to develop a conductance-based multi-compartment model simulating an axonal branch point. This model featured a parent axon (P) branching into two daughter axons (D1 and D2) and incorporates three types of membrane currents: fast sodium (I_{Na}), delayed rectifier (I_{Kd}), and a leak current. The parameters for I_{Na} and I_{Kd} were adapted from an earlier model of a postganglionic neuron [211]. The model demonstrated that as temperature increases, there is a transition from reliable spike propagation in both D1 and D2, to failure in one of the branches, and eventually to failure in both branches (Figure 4.7). This model supported the proposition that branching points in axons in the IGN provide a unique site for warming-induced conduction failures.

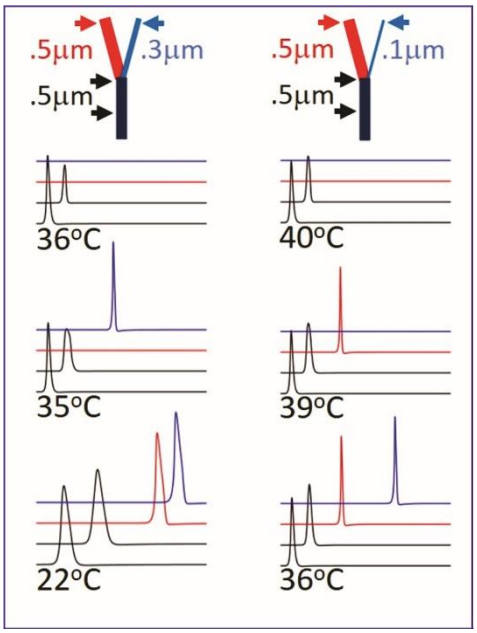

Figure 4.7. Influence of Temperature on branch point failure

Two model configurations (top) differ only in D2 diameter (blue). Voltage traces [1] show membrane potential at different temperatures for the locations indicated by arrows at the top. Both model versions show a transition from no failure to one branch failing, to both branches failing, as temperature increases. In the left model, the wider branch fails first while in the right model, the narrower branch fails first as temperature increases. [2]

4.5.1.2 Temperature-sensitive leak channels and spike fidelity

RNA sequencing shows that the two-pore-domain potassium (K_2P) channel TREK-1 (KCNK2), is present in thoracic SPNs [47]. TREK-1 channel activity increases with increasing T°, with peak thermal responsiveness from 32-37°C, with ~7-fold increase in current amplitude for every 10°C, indicating that physiological temperature variations can substantially influence its activity [212]. Increased TREK-1 channel activity may compromise spike conduction through two distinct mechanisms. (i) Hyperpolarization towards E_K would necessitate a larger depolarization for spike recruitment. (ii) An increased membrane conductance would reduce passive voltage amplitude and propagation space constant for regenerative spiking by downstream Na_V channels. As reported in chapter 5 below, there is electrophysiological and pharmacological evidence of TREK-1 channels in SPN axons.

4.5.1.3 TREK-1 channels and temperature dependent changes.

Thermoregulatory dysfunction as seen in states of hypo- or hyperthermia (32-40°C) is common in patients with spinal cord injury, and the presence of changes in TREK-1 activity in SPN axons may alter spike propagation [213-216]. Reduced TREK-1 activity during hypothermia may increase axonal excitability, possibly leading to the emergence of spontaneous spiking. Conversely, increased TREK-1 activity during hyperthermia, may decrease excitability. Increased SPN activity has been noted during hypothermia, but has been attributed to increased excitatory recruitment of spinal interneurons via muscle afferent activity [217]. Hyperthermia in rats has been shown to decrease sympathetic rhythm [218]. As even small changes above normal body temperature can compromise spike conduction [83], the SCI population that has a broad core temperature range, may be particularly vulnerable [213-216,219-221]. To test whether TREK-1 activation can block conduction in SPN axons, we apply TREK-1 agonist riluzole in Chapter 5 [222].

4.5.1.4 Changes in core body temperature may influence SPN recruitment.

The core body temperature range for humans and mice are similar. For humans, the normal range is 36.5-37.5° and in mice it is ~36-38° [223]. While it could be argued that recordings at room temperature are non-physiological, this is certainly not true for mice. Mice can enter a hypometabolic state known as torpor. Unlike homeotherms (humans, guinea pigs and rats), which maintain a relatively constant internal body temperature, heterotherms like mice can switch between maintaining a stable body temperature and allowing their body temperature to fluctuate with the ambient temperature [224 225]. When mouse torpor is stimulated by food deprivation and ambient temperature, core body temperature can reach 20°C. That SPN conduction undergoes more failures at 36°C than at 22°C may be physiologically important to

differences in autonomic signaling - including recruitment of additional functional populations - associated with torpor that are not active at 36°C. The differences may provide insight into functional populations of SPN axons required to exit torpor. While humans do not undergo torpor, insights gained from mice can be relevant to understanding how hypothermic conditions in humans (whether injury-induced or due to environmental exposure) modifies function of the sympathetic nervous system. Indeed, reduced temperatures that promote conduction across branch points may adaptively strengthen sympathetic drive in thoracic chain ganglia projections to cutaneous vasoconstrictors for heat retention and to brown adipose tissue (**BAT**) for heat generation. The thoracic paravertebral sympathetic ganglia in both human and mouse species are located within periaortic brown adipose tissue (**BAT**) that is capable of heat production through non-shivering thermogenesis [226-228]. Additional studies would benefit from more detailed analysis of the effects of smaller temperature changes on the spike conduction in functional subpopulations of thoracic SPNs.

4.5.2 Frequency dependent changes in amplitude of evoked responses

Our exploration into the frequency-dependent transmission in SPN axons is grounded in the context of existing literature, which shows that active SPNs typically fire at a rate of approximately 0.7Hz, with sympathetic nerve discharge (SND), such as in the splanchnic nerve, averaging around 1-2Hz (See Table 1.3). However, peak firing rates can escalate to as high as 20Hz, varying across different species [53 81 107 109 115 116 120 122 123 124 125 126 229]. In our studies, we examined the effects of 1 Hz single pulse and, 5-20Hz stimulus trains on SPN conduction. Our findings indicate that slow-conducting SPN axons exhibit fatigue at frequencies of 5Hz and above, with a notable maximal depression consistently occurring by the 6th pulse, regardless of the frequency intensity. This pattern was observed to take place approximately 1 second into the

5Hz train and 0.3 seconds into the 20Hz train. A critical aspect of our research was the comparison between the splanchnic and IGN responses. We noted two major differences: a more marked depression in the IGN SPNs by the end of the train pulse and a general inability of IGN SPN axons to recover after a conditioning train. Despite this frequency-dependent depression, it is noteworthy that in cases where responses did return to baseline, they consistently did so within a 90-second window, indicative of a shorter term plasticity instead of long-lasting changes in conduction properties. These insights contribute significantly to our understanding of SPN conduction under varied frequency conditions. However, there remain several gaps that future research could address. For instance, the specific mechanisms underpinning the observed fatigue and recovery patterns, particularly in relation to different SPN types, require further investigation. Additionally, the implications of these frequency-dependent changes in SPNs on overall sympathetic system function, especially under physiological and pathophysiological conditions, present an intriguing area for future exploration.

4.5.2.1 Branching axons are uniquely prone to activity-dependent changes in conduction.

Our research reveals that SPNs demonstrate a frequency-dependent decrease in the activity of slow-conducting populations, while fast-conducting SPNs display greater resilience to frequency trains. Furthermore, we observed that SPN axons within the IGN, which contain branching axons, exhibit a higher degree of signal depression compared to the unbranched SPN axons of the splanchnic nerve. Branching axons exhibit a unique susceptibility to activity-dependent conduction changes[73]. Before this study, the effects of frequency-dependent alterations in signal conduction in thoracic paravertebral SPN branching axons had not been thoroughly investigated.

Our findings indicate the mean diameter of SPN axons at the white commissure is approximately 0.64 µm. Given their small size, these axons are likely to experience substantial activity-

dependent hyperpolarization, along with slowing and blocking of conduction [70] [71]. Their thin diameter could render them especially vulnerable to Na^+ channel inactivation [149] and hyperpolarization controlled by a $[Na^+]i$ sensitive metabolic rheostat, as provided by the α3-Na^+/K^+ pump. As this neuronally expressed pump tracks activity history [189,190], it may play a significant role in regulating the dynamics of spike propagation failures in SPNs [86].

4.5.3 Optogenetic vs. electrical stimulation

We employed two distinct methods to recruit SPN axons in the T10 ventral root: optical recruitment of cholinergic axons and electrical stimulation. Strikingly different effects of T° and frequency were seen. Optically recruited axons were much more susceptible to failure. Results suggest the possibility that these stimuli target distinct SPN subpopulations, with optical stimulation more likely to recruit axons prone to frequency-dependent depression. Alternatively, the nature of the optical stimulus might introduce a time- and T°-sensitive alteration in the threshold intensity required for activation. It is possible that the 20ms pulse width used in optical stimulation could induce a prolonged depolarization in the axons, resulting in a sustained decrease in their excitability. Notably both electrical and optical recruitment, responses recovered to baseline values following stimulus train delivery after the 90s rest period provided between stimulus delivery paradigms. Overall, technical issues cannot fully account for the observed differences in electrical and optical responses seen between the splanchnic and interganglionic axons.

4.6 Conclusions

Utilizing an isolated *ex vivo* preparation with intact ventral roots and sympathetic chain, we investigated the effects of T° and activation history on the reliability of signal transmission along thoracic SPN axons. We observed that at room temperature, the slowest-conducting fibers

display the greatest variability in conduction, with heightened failures occurring in branching SPNs as temperatures increase. Furthermore, the slowest-conducting SPN axons are prone to frequency-dependent fatigue when stimulated at 5Hz and 20Hz. These results highlight the susceptibility of SPN axons, especially the slow-conducting and branching types, to high rates of failure under various thermal and frequency conditions. The effect on postganglionic neuron recruitment is still unclear. A decrease in the magnitude of population responses may be linked to diminished synaptic activity on postganglionic neurons. To fully understand the impact on postganglionic signaling, further investigation is required.

5 Modulation of Branch Point Failure

5.1 Abstract

Chapter 3 demonstrated that population-evoked SPN compound action potential responses arise from predominantly unmyelinated axons that propagate across a range of velocities with highest rates of inter-episode reliability seen in the slower conducting axons in both IGN and splanchnic nerves. Chapter 4 explored the effects of temperature (T°) and activation history on the magnitude of evoked responses, observing that increased T° (from 22-36°C) depressed responses - indicative of pronounced conduction failure – particularly in the slowest conducting IGN and splanchnic axons. The strong frequency-dependent depression of evoked response at 22°C was not observed in remaining axons recruited at 36°C.

This chapter posits that axonal conduction, especially in the slowest conducting axons, constitutes a critical site of neuromodulatory control of sympathetic output. Investigations assessed the role of $GABA_A$, serotonin, and acetylcholine receptors and and K^+ channels (via I_A and K_{leak}) in the modulation of SPN axonal conduction. Application of successively applied $GABA_AR$ antagonists led to selective depression of slower-conducting responses in the IGN nerve, consistent with preferential action on branching axons. Block of α5-$GABA_A$Rs with the inverse agonist L655,708 trended toward depression with subsequently applied picrotoxin then bicuculline having progressively larger and significant overall inhibitory actions. Acetylcholine (**ACh**) also preferentially reduced response amplitude in IGN slower-conducting axons, while serotonin reduced activity in slower-conducting axons from both IGN and splanchnic nerves.

Block of voltage-gated K^+ (K_v) channels with 4-aminopyridine (**4AP**) facilitated evoked faster- and slower-conducting responses in both IGN and splanchnic nerves while the K_v blocker tetraethylammonium (**TEA**) had no facilitatory effect, instead selectively depressing slower-

conducting IGN axons. The 4-AP induced facilitation was much greater in the slower-conducting axonal populations and could restore T°-dependent conduction block from previously non-responsive SPN axons.

As T°-dependent conduction block was associated with global DC shifts in recorded voltage consistent with membrane hyperpolarization, we explored the role of the T°-sensitive K_2P K_{leak} channel TREK-1 by application of agonists. Arachidonic acid selectively decreased the amplitude of slower-conducting IGN responses, while riluzole (after pre-incubation with 4-AP) caused a broader reduction in evoked responses.

Overall, results demonstrate that spike propagation in slower-conducting axonal populations is modifiable with $GABA_AR$ block, ACh, serotonin, TEA and arachidonic acid leading to depression while 4-AP was strongly facilitatory. Slower conducting axons within the IGN were identified as a uniquely sensitive group.

5.2 Introduction

Spinal cord sympathetic preganglionic neurons (SPNs) serve as the final integrated output from the CNS. SPNs project branching axons to provide divergent input to many postganglionic neurons across multiple ganglia of the paravertebral chain. Other SPNs project unbranching axons to prevertebral ganglia. Chapters 3 and 4 revealed that CAPs in SPNs encompass a spectrum of conduction velocities, with the highest variability between episodes observed in the slower-conducting unmyelinated axons. Notably, the greatest incidence of block was found in the axons presumed to be branching within the IGN, as opposed to the unbranching axons that make up the splanchnic nerve.

Conduction failures escalated with temperature, rising from 22°C to 36°C, and were influenced by frequency-dependent spike history. These failures were especially pronounced in the slowest-

conducting axons, particularly within the IGN. This chapter focuses on the neuromodulatory control of axon conduction across the same population of axons by putative receptor systems acting on $GABA_A$ receptors, serotonin and cholinergic receptors as well as on K_v K^+ channels controlling spike shape and the K_2P K^+ channels controlling membrane potential and leak conductance. Below, is an introduction to our understanding of these factors in relation to putative impact on axonal conduction. For this, adult mouse thoracic sympathetic chain ganglia were dissected, and synaptic transmission was blocked with hexamethonium, allowing us to record population conduction across different axon types under optical and electrical stimulation.

5.2.1 Modulation via $GABA_A$Rs

Initial research revealed that $GABA_A$R antagonists reduced the responses of SPN-evoked postganglionic neurons in paravertebral ganglia. However, the lack of GABAergic neurons [230-235] in sympathetic ganglia rendered the interpretation of these findings challenging. Because postganglionic neurons lack $GABA_A$Rs (as evidenced by recent RNA-sequencing data)[177], $GABA_A$R antagonist-modulated transmission must arise presynaptically. Although assumed to act on synaptic transmission, a possible role of these drugs on block of axonal conduction was not considered. Recent advancements in identifying and characterizing $GABA_A$R subunits have revealed that these receptors are also present in extra-synaptic locations, such as axonal branch points. Notably, these $GABA_A$Rs exhibit sensitivity to low concentrations of GABA and demonstrate a potential for constitutive activity[236]. These studies support the possibility of a role for $GABA_A$Rs in the modulation of SPN axonal conduction.

Intracellular somatic SPN recordings demonstrated membrane depolarization following block of $GABA_A$Rs with bicuculline and not gabazine, consistent with actions on extrasynaptic α_5-$GABA_A$Rs without expression of δ subunits (confirmed with PCR)[237]. The pharmacological

findings align with the presence of constitutively-active α5ɣ2-$GABA_A$Rs, which are primarily responsible for the tonic inhibition observed in the CNS[237-240]. Notably, this form of inhibition operates independently of action potentials.

Recent RNAseq data of adult mouse SPNs supports expression of α1-5, β1-3, ɣ1-3 but no expression of δ subunits [47]. Magnitude order of subunit expression is as follows: α2>α3>α1>α5>α4, β1=β3>β2, ɣ3>> ɣ2. Generally, α4-6, and δ subunits are found at extrasynaptic locations [241]. Overall, expression of extrasynaptic α5 and α4 subunits support the possibility of modulatory actions in SPN axons.

5.2.2 Modulation via A-current blockers

The functional role of K_v channels presents an intriguing aspect of axonal physiology. These channels are abundantly found in unmyelinated and demyelinated axons but are notably absent at the nodes of Ranvier in myelinated axons. In the latter, K_v channels are located beneath the myelin sheath but do not play a significant role in the repolarization phase of the action potential [242-244]. Contrasting this, in unmyelinated axons, K_v channels are observed to have a critical role in spike repolarization [242]. SPNs are largely unmyelinated [73]. Given their participation in spikes in unmyelinated axons, we assessed the role the K_v channel blockers 4-AP and TEA and demonstrated distinct facilitatory actions via 4-AP across fast- and slow-conducting axons. Given the observed reductions in evoked responses seen by prior spiking and increasing temperature (Chapter 4) and that various K_v channels are expressed in unmyelinated axons (see Table 1.5) we explored whether block of K_v channels could facilitate axonal recruitment and conduction, particularly at a higher temperature at which conduction block is considerable.

Like other neurons, SPNs possess a diverse array of voltage-gated K^+ (K_v) channels [47,153]. As ~99% of mouse SPN axons are unmyelinated [73], insight may be derived from investigations of

channels on unmyelinated axons. Other studies on unmyelinated axons have identified the involvement of various K_v channels, notably K_v1.1, 1.2, 1.4, 3.2, 3.4, 4.3& 7, as well as G protein-coupled inwardly-rectifying K^+ channel (GIRK), and the Ca^{2+}-activated K^+ channel (K_{ca}1.1) (see Chapter 1). Among these, selective RNA-sequencing on SPNs indicate high expression of K_v3.2, 4.3 & 7, GIRK, and K_{ca}1.1 channels [47]. Currently, the spatial distribution and specific role of these channels on SPN axon spiking behavior and modifiability remain uncharacterized. To begin this process, we explored the differential effects of the broad K_v channel blockers tetraethylammonium (TEA) and 4-aminopyridine (4-AP) on spike propagation in IGN and splanchnic nerve axonal populations separated by their conduction velocities. Emphasis was placed on block of A-type channels (K_A) known to be involved in spike repolarization [245]. Many K_A channels involved in axonal spike propagation are resistant to TEA [162] and 4-AP block of these channels can prolong action potentials to overcome conduction failure in unmyelinated axons [246].

5.2.3 Modulation via K^+ leak channels

Two-pore K^+ leak (K_2P) channels are widely expressed in neurons. Single nuclear RNA sequencing of SPNs shows expression of TREK-1 and TREK-2 K_2P channels, with TREK-1 expressed in subpopulations of thoracic SPNs and TREK-2 widely expressed in all SPNs [47]. TREK-1 channels also modulated by diverse signal transduction pathways including activation by arachidonic acid, and protein kinase G (PKG) and inhibition via PKA and PKC [247,248]. TREK-1 mediated currents are not inhibited by the traditional K_v channel blockers TEA and 4-AP. Riluzole activates both TREK-1 and TREK-2 channels [222,249]. Importantly, TREK-1 is activated gradually and reversibly in response to temperature increases (between 14-42°C) with a 10°C↑ causes ~7-fold↑ in current amplitude [212]. Such changes in response magnitude may lead to

significant axon membrane hyperpolarization and increased membrane leak conductance and consequently alter excitability, space constant (λ) and conduction velocity. As SPNs axons are largely unmyelinated, project long-distances, include branching axons, and are among those having the smallest known diameters [73], changes in TREK-1 activation may powerfully modulate axonal function.

5.2.4 Cholinergic and serotonergic modulation of SPN axons

As SPNs are cholinergic, modulation of synaptic transmission by presynaptic muscarinic acetylcholine receptors (**AChRs**) are expected. Previous studies focused on modulation of evoked synaptic response, and have not assessed possible modulation of spike conduction[250,251]. SPNs strongly express M2 and M3 muscarinic receptors [47]. In thoracic SPNs, there is also expression of α7 nicotinic AChRs [34,47]. In cervical sympathetic ganglia recordings with intact SPN axons, nicotine and the nAChR antagonist tubocurarine reduced the SPN compound action potential (CAP) by 25% and 14%, respectively [252], implicating their role in neuromodulation.

Several 5-HT receptor subtypes are found on SPNs. In adult mouse, a recent RNA-seq study identified expression of 5-$HT_{1F,}$ 5-HT_{2A}, 5-HT_{2C}, and 5-HT_7 [47] see https://seqseek.ninds.nih.gov/cholinergic/genes). Should 5-HT receptor expression occur along SPN axons, cellular signaling pathways downstream to receptor binding could influence spike conduction by modulation of channel activity. For example, 5-HT_{1F} G_i–coupled receptors would reduce expression of PKA and promote activation of K_{leak} channels in unmyelinated axons and reduce conduction. Likewise, activation of 5-HT_2 receptors which G_q-coupled activation of PKC or 5-HT_7 G_s–coupled receptors receptor activation of PKA could reduce K_{leak} to promote conduction in myelinated Aδ SPN fibers.

Overall, our exploration into neuromodulatory control on axonal conduction along SPNs seeks to uncover the intricate interplay between various neurotransmitter systems and ion channels. By dissecting the modulatory effects of $GABA_A$ receptors, serotonin, cholinergic receptors, and potassium channels on SPN axons, we hope to gain insight into complex mechanisms that govern neuronal excitability and signal propagation. Our findings will not only enhance the understanding of SPN axonal function but also pave the way for future research into the therapeutic modulation of sympathetic activity, offering new insights into the regulation of physiological responses across a spectrum of conditions.

5.3 Methods

5.3.1 Mice

Unless otherwise mentioned the experimental approach is similar to that undertaken in chapters 3 and 4 including use of ChAT-CHR2 mice.

5.3.2 Electrophysiology

Experiments were undertaken as described in previous chapters though some pharmacology was undertaken only using electrical stimulation (studies on $GABA_AR$ antagonists) and others only with optogenetic recruitment (5-HT application). The 5-HT experiments optogenetic recruitment of SPNs was undertaken via optical illumination of the ventral horn in an attached hemicord.

5.3.1 Analysis

For detailed methodology on CAP quantification see Section 3.3.2. When a single drug was added, paired t-tests were used to compare baseline to drug condition. When more than one drug was used before washout, repeated measures ANOVA was used to determine significant effects by comparing to baseline control values. This was complemented by Tukey's post hoc comparisons, applied as appropriate, to identify significant variations across different drug conditions. Values are represented as mean percent of baseline ± SEM.

Ideally, comparisons across preparations would involve recordings at the same site and use the same electrodes consistently. In experimental series in which such recordings were obtained, results were compared without any normalization procedure. In experimental series where variability in evoked responses across preparations was seen as large, a normalization procedure was used to weight individual experiment based on their baseline magnitude responses.

5.3.2 Pharmacology

Drugs, which were stored in 10 or 100mM stock solutions at −20◦C, were added to the reservoir of a perfusion bath (typically 100mL) with drug equilibration achieved via rapid recirculation. Drugs were applied by bath superfusion for between 5 and 30min until a maximum response was observed. Chemicals were obtained from Sigma Aldrich. L655,708, picrotoxin, bicuculline, arachidonic acid, riluzole and 4-AP were added in concentrations previously reported in rodent [253,254].

5.4 Results

In Chapter 4, we highlighted the pronounced effect of temperature on conduction block, especially in slower-conducting unmyelinated axons, as illustrated in Figure 4.5. Analysis of optically recruited SPN axons in Chapter 3 shows optical stimulation predominantly recruits slow-conducting unmyelinated SPN axons. At elevated temperatures, optically recruited responses in SPN axons were significantly reduced or entirely absent (data not shown). Hence pharmacological studies below undertaken at elevated temperatures only assessed electrically evoked responses unless otherwise stated.

5.4.1 SPN conduction block observed with broad-spectrum $GABA_AR$ antagonists

To investigate actions of modulators of $GABA_ARs$, we sequentially applied known $GABA_AR$ blockers to a bath held at 32°C (Figure 5.1 A-B). The α_5-$GABA_AR$ GABA binding site

antagonist (inverse agonist) L655,708 (20μM) did not affect SPN axons consistent with limited expression reported for α_5 in Alkaslasi et al [157] and Wang et al [255]. Subsequent application of the open channel non-competitive antagonist picrotoxin (50μM)[256] and competitive $GABA_AR$ antagonist bicuculline depressed slower-conducting IGN responses ($p<0.05$ and $p<0.01$ respectively, n=6, Figure 5.1 A, B). For slower-conducting IGN axons, there was a trend toward progressive reduction in response with each blocker applied. In comparison, splanchnic axons did not show a significant reduction in the presence of $GABA_AR$ blockers.

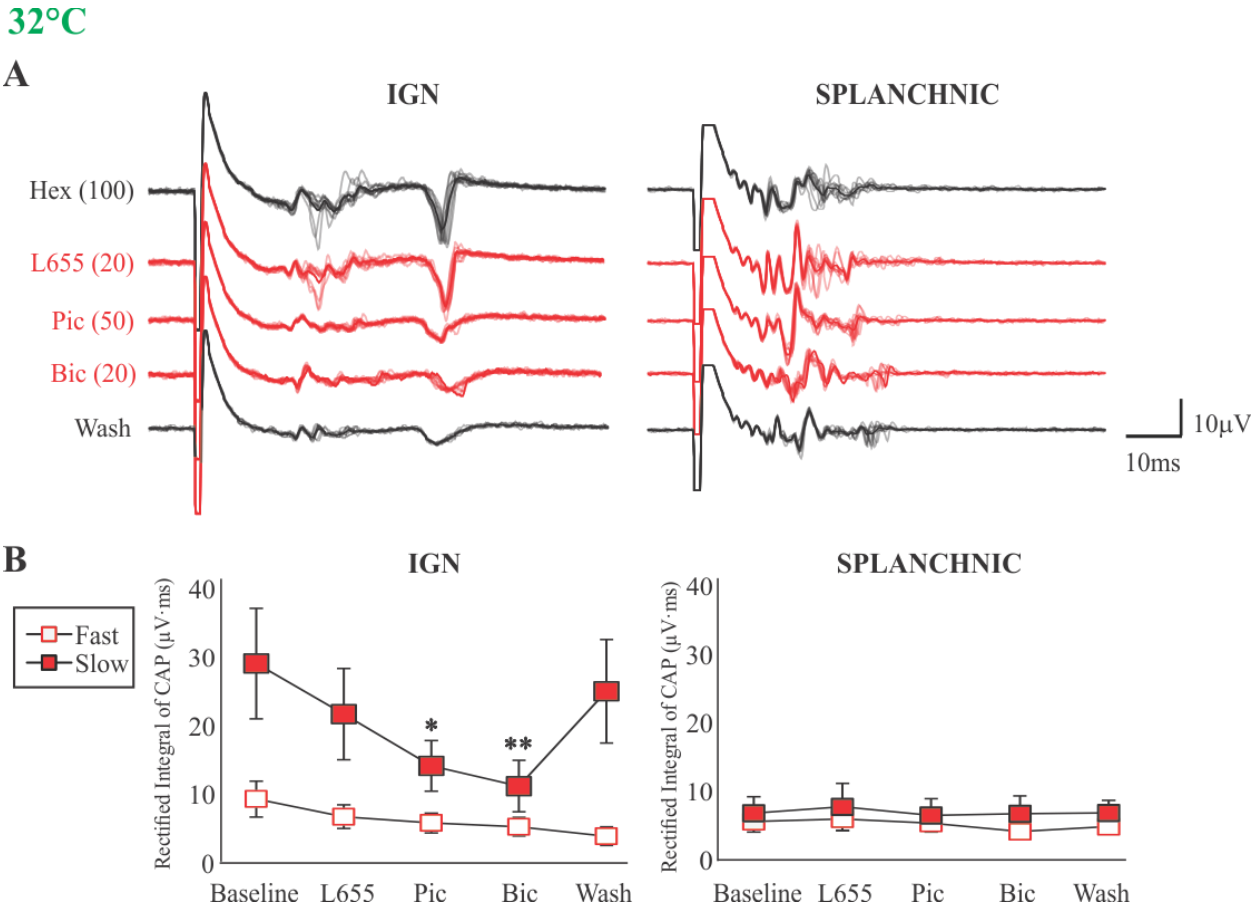

Figure 5.1 $GABA_AR$ antagonists increase conduction block in slow and branching SPN axons

[A] Shown is a typical raw trace of evoked responses, elicited through supramaximal stimulation using 200 μA/500 μs electrical impulses. The traces have been high-pass filtered at 100 Hz. Displayed here are 10 superimposed episodes for each drug condition, with their averages

emphasized for clarity. **[B]** Comparative analysis of $GABA_A$ modulators: rectified integrals of the evoked response for each fiber type during each drug condition were averaged. Significant block was seen following application of picrotoxin (50µM, $p<0.05$) and bicuculline (10µM, $p<0.01$) for IGN. Statistical tests were undertaken using repeated measures ANOVA and Bonferroni t-test for all pairwise multiple comparisons (n=6; *, $p<0.05$; **, $p<0.01$; error bars are SEM).

5.4.2 Pharmacological block of voltage-gated K^+ channels.

5.4.2.1 Optically recruited SPN axons show a greater facilitation following application of 4-aminopyridine (4-AP).

The shape and propagation of action potentials in neurons are significantly influenced by various post-spike voltage-gated K^+ conductances. Among these, the K_A family of fast K^+ channels play a critical role in reducing spike duration through the acceleration of spike repolarization. Application a broad-spectrum voltage-gated K^+ channel blocker 4-AP (50 µM) blocks various K_A channels. In compound action potential (**CAP**) population recordings of unmyelinated axons in the cerebellum and hippocampus, 4-AP leads to increases in both CAP amplitude and duration [257].

To explore the role of voltage-gated K^+ channels in SPN spike propagation, we assessed dose-dependent changes in conduction by 4-AP at cumulative doses of 1, 5, 10, 50, and 100µM. We observed dose-dependent facilitatory actions that largely leveled off at 50µM (Figure 5.2A). As this dose is consistent with prior work using 4-AP for non-specific blockade of K_A channels, this dose was used for subsequent studies on effects of spike conduction or recruitment.

Experiments were conducted at 32°C. At this temperature the fastest-conducting myelinated axons in splanchnic could not be quantified due to its overlap with stimulus artifact. Raw traces show application of 4-AP (50µM) increased the area of the CAP. Increases in the electrically evoked CAP responses were seen in all nerves except for the fast-conducting SPN axons. The

CAP for T12 slower-conducting SPNs was facilitated by 83.8% while splanchnic slow conducting axons were facilitated by 384.9% ($p<0.05$ and $p<0.01$ respectively, n=6, Figure 5.2 C). The CAP of electrically evoked faster-conducting unmyelinated SPN axons increased by 85.5% ($p<0.05$, n=6). Compared to the facilitation seen in the faster-conducting axons, response facilitation was much more pronounced in slower conducting axons except for those recruited electrically in the IGN (Figure 5.2C).

Optically recruited SPNs exhibited a remarkably higher degree of 4-AP induced facilitation compared to electrically recruited SPNs, with an average ninefold increase. To evaluate the statistical significance of these findings, we employed t-tests across different stimulation modalities. The results showed that, on average, 4-AP enhanced the response of faster-conducting IGN SPNs by 37.6% with electrical recruitment, whereas this increase soared to 326% with optical recruitment ($p<0.05$). In the case of splanchnic faster-conducting SPNs, a similar trend was observed: there was an 85.5% mean increase in response to electrical recruitment, contrasting sharply with an 818.5% mean increase for optical recruitment ($p<0.05$). Additionally, we noted significant differences in the slower-conducting SPNs of the splanchnic nerve, where the response increased by 384.9% with electrical recruitment and a much more pronounced 3260.5% with optical recruitment ($p<0.05$). In comparison, slower-conducting IGN axons did not show statistically significant differences in the degree of facilitation between optical and electrical stimulation. This may be attributed to a Type II error arising from small sample sizes and high variability within the data.

The much greater 4-AP induced increase in evoked responses optically is consistent with their preferential temperature dependent conduction failures shown in Chapter 3. This preferential sensitivity of optically evoked SPN axon populations to temperature-dependent depression and

subsequent facilitation by 4-AP supports the presence of axonal populations whose conduction can be prevented via activation of voltage-gated K^+ channels (see Figure 5.2A). This finding underscores the significant role of post-spike voltage-gated K^+ channels in modulating axonal conduction.

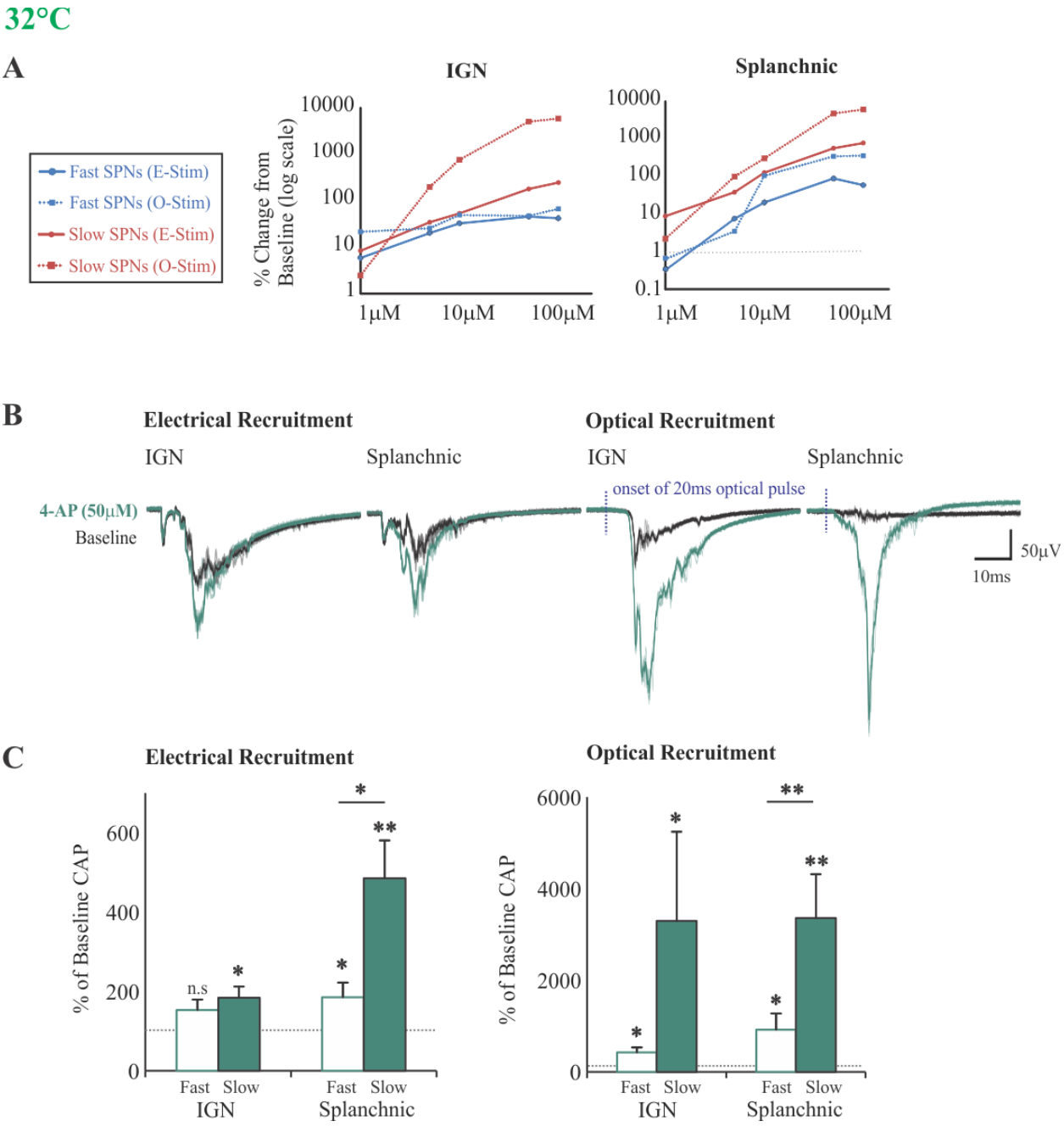

Figure 5.2 4-AP preferentially increases SPN conduction of slow-conducting SPNs

[A] Application of 4-AP increases the SPN recruitment overall, however greater actions are seen in slow-conducting SPNs, particularly those recruited optically. Similar response amplification is seen in IGN and splanchnic nerves. 4-AP response begins to plateau at a 50µM dose. (n=2). **[B]** Shown are typical raw traces of evoked responses, elicited through supramaximal stimulation using 200 µA/500 µs electrical impulses and 6.6mW/µm^2 20ms optical impulses. The traces have been high-pass filtered at 25 Hz. Note the downward increase in amplitude following 4-AP. **[C]** Quantification of the 4-AP response is plotted for fast and slow conducting SPNs. Paired t-tests were conducted to assess significance of amplitude of evoked responses between baseline and their percent increase following application of 4-AP (n=6; *, $p<0.05$; **, $p<0.01$; error bars are SEM). Asterisks above bars represent significantly different increase recruitment of slower over faster conducting axons.

5.4.2.2 Differential actions of 4-AP and tetraethylammonium (TEA)

The nonspecific voltage-gated K^+ channel blocker TEA has a similar pharmacological profile to 4-AP[258]. Like 4-AP, TEA reduced conduction failures in unmyelinated cerebellar granule axons, likely by an increased spike duration [83]. We examine the effects of TEA (1 mM) on evoked responses at 32°C. In contrast to expectations of a dramatic facilitation as seen with 4-AP, TEA depressed the amplitude of slower-conducting axons of the IGN by 81.1% ($p<0.01$) and had no effect on response amplitude of faster-conducting IGN axons or on faster- or slower-conducting splanchnic axons (Figure 5.3). In comparison, subsequent application of 4-AP invariably led to significantly increased response amplitude in all populations relative to that seen in the presence of TEA (Figure 5.3A&B).

To determine if preincubation with TEA enhances the effects of 4-AP, we compared two experimental groups. In the first group, TEA was preincubated before the addition of 4-AP, as indicated by the data in Figure 5.3. The second group was treated solely with 4-AP, with results presented in Figure 5.2. Using an independent two-sample T-test, we found that the facilitative effect of 4-AP was generally consistent across various populations, regardless of whether TEA was present. However, a notable exception was observed in the optically evoked, slow-

conducting splanchnic SPNs, where in the presence of TEA, 4-AP was less facilitatory ($p < 0.05$). These results suggest that generally, TEA and 4-AP do not have a synergistic effect.

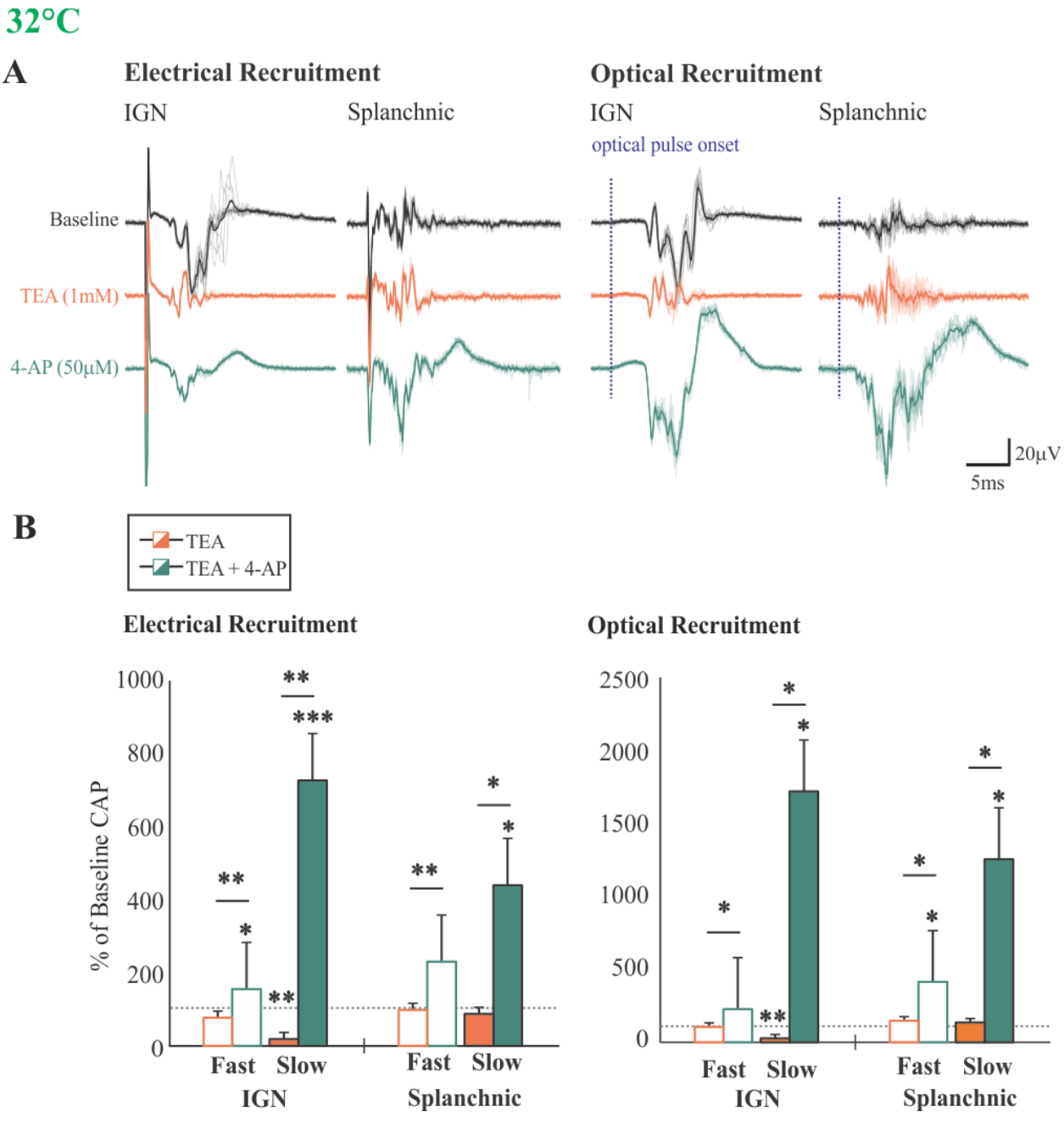

Figure 5.3 Differential actions of K+ channel blockers TEA and 4-AP

[A] Shown are typical raw traces of evoked responses, elicited through supramaximal stimulation using 200 µA/500 µs electrical impulses and 6.6mW/µm^2 20ms optical impulses. The traces have been high-pass filtered at 100 Hz. **[B]**. Quantification of the evoked responses for each drug treatment is plotted for fast and slow conducting SPNs. 4-AP response was significant for all fiber types compared to hexamethonium baselines except for fast-conducting splanchnic axons. TEA exhibited a significant decrease from baseline in electrically and optically recruited slow-conducting IGN axons ($p<0.01$) but was otherwise no different from baseline. In all cases, the 4-AP response was significantly greater than the TEA response. Experiments were conducted at 32° C. Repeated measures ANOVA were employed to determine the significance of drug application effects, followed by a posthoc T-test for a comparative analysis between TEA and 4-AP. (n=4; *, $p<0.05$; **, $p<0.01$; ***, $p<0.001$; error bars are SEM).

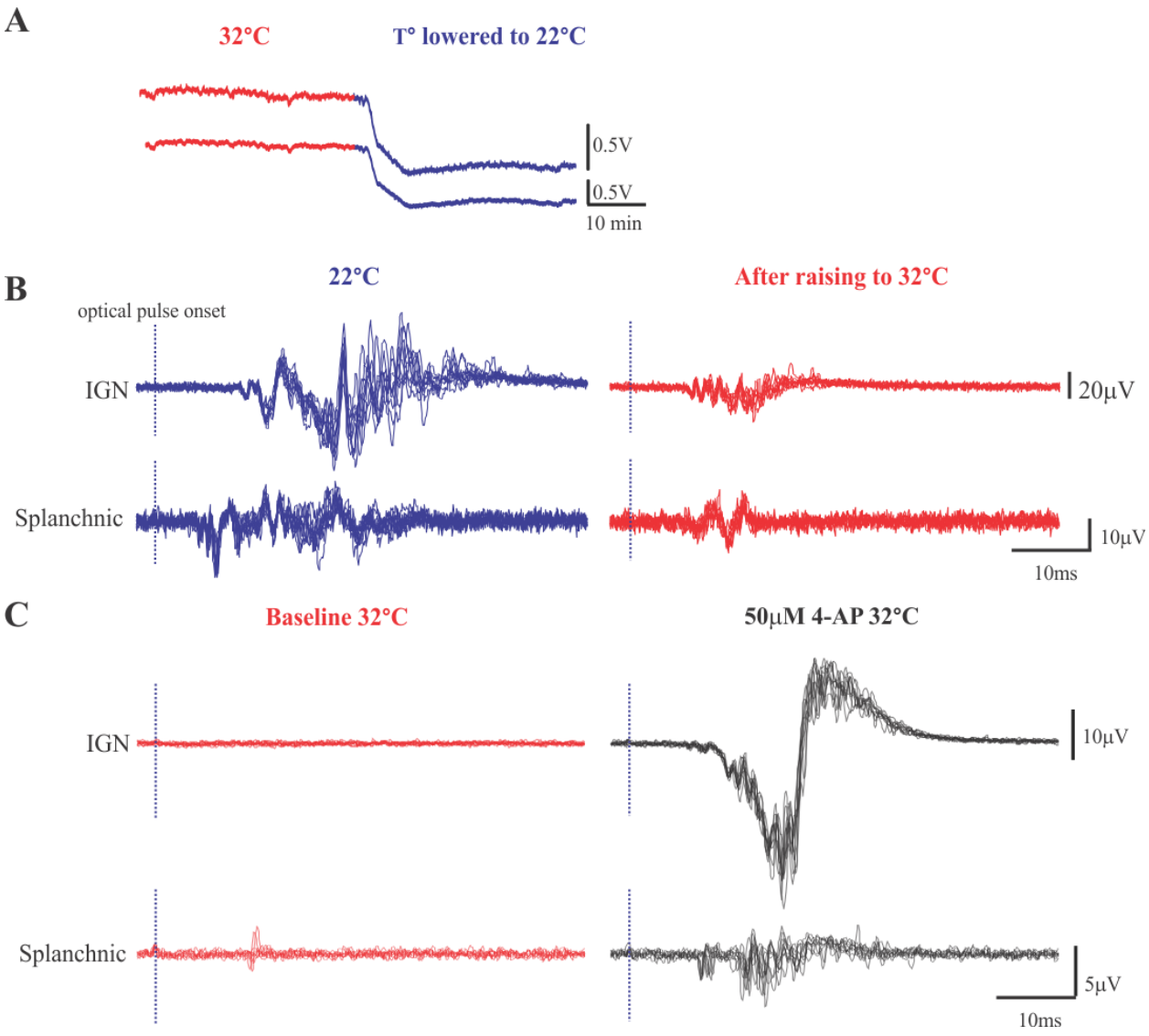

Figure 5.4 4-AP restores temperature-sensitive conduction block of optically recruited SPN axons

[A] This figure demonstrates a consistent negative-going depolarization in IGN and splanchnic recordings in one animal which was observed across 6/6 animals tested (not shown). The depicted DC shift suggests that an increase in temperature is likely to produce a hyperpolarizing effect. **[B]** Shown is an example of temperature-dependent conduction block in optically recruited SPN axons within IGN and splanchnic nerves. This panel displays ten overlaid episodes of evoked responses triggered by optical stimulation at 32°C and 22°C, showcasing how higher temperature prompts conduction failure. Shown are typical raw traces of evoked responses, elicited through supramaximal stimulation using 200 µA/500 µs electrical impulses and 6.6mW/µm^2 20ms optical impulses **[C]** Restoration of axonal conduction at 32°C in the presence of 4-AP. In a separate mouse without optically-recruited response at 32°C, application of 4-AP restored conduction in many SPN axons. The dotted line at beginning of raw recordings reflects timing of optical illumination.

5.4.3 Role of K_2P leak channels in the temperature-dependent in block of spike conduction.

5.4.3.1 DC shifts are associated with changes in temperature consistent with activation of a K+ leak conductance

Although we could not directly record axonal membrane potential, we undertook DC recordings whose extracellular negative or positive shifts in polarity should reflect depolarizing or hyperpolarizing shifts in membrane potential, respectively. We observed consistent parallel temperature-dependent changes in polarity in both IGN and splanchnic recordings. Lowering temperature from 32°C to 22°C produced a negative DC shift reflective of membrane depolarization (**Figure 5.4A**). Conversely, elevating temperature has the opposite positive DC shift in polarity (not shown). We found that positive shifts in DC polarity from 22°C to 32°C were associated with conduction block of optogenetically evoked responses in recordings from IGN and splanchnic nerves (**Figure 5.4B**); see also **Figure 5.4.A**. As the splanchnic nerve contains only SPN axons, we interpret the DC polarizing actions in the IGN, which also contains postganglionic axons, to also involve actions on SPN axons.

5.4.3.2 4-AP can surmount loss of temperature increase-induced conduction block

We tested whether 4-AP could surmount the temperature increase-induced conduction block, presumed due to K_A block-induced increases in spike width and height, particularly in optically recruited SPN axons, which are highly susceptible to temperature-dependent conduction block. Application of 4-AP successfully restored conduction in cases where optically-recruited responses were either minimally observable (n=5/6) or completely absent (n=1/6) in the IGN (**Figure 5.4B**).

5.4.3.3 Potassium leak channel activators riluzole and arachidonic acid block axon conduction

Increasing temperature may lead to membrane hyperpolarization and increase in membrane leak conductance due to activation of temperature sensitive two-pore K^+ leak (**K_2P**) channels and consequently play a significant role in limiting the conduction of spikes.

TREK-1 channel currents are not inhibited by the traditional voltage gated K^+ channel blockers TEA and 4-AP [248], while the polyunsaturated fatty acid arachidonic acid (**AA**) and riluzole can activate TREK-1 channels [212,222].

As riluzole activates K_A currents, we implemented a preincubation step with 4-AP to effectively inhibit A-currents before applying varying concentrations of riluzole (0.5-50μM)[249] to better focus riluzole actions on K^+_{leak} channels. Regarding electrically-evoked responses, Riluzole preferentially decreased activity in slower-conducting IGN axons (73.1±4.4% reduction; $p<0.05$). For splanchnic, decreases were seen in both faster- and slower-conducting populations (40.9±4.4%; $p<0.01$ and 56.6±5.6%; $p<0.01$, reductions respectively). Regarding optically evoked responses, decreases were seen in both faster- and slower-conducting IGN populations (75.9±9.4%; $p<0.01$ and 57.9±16.5%;$p<0.05$ reductions respectively) while only slower-conducting SPNs showed a reduction (45.2±12.8%; $p<0.05$).

In one experiment, pre-application of riluzole (50μM) significantly reduced electrically evoked responses and completely abolished those that were optically recruited (Figure 5.5C) while subsequent administration of 4-AP (50μM) not only increased the electrical responses but also revived and intensified the optically-evoked response. However, these responses were accompanied by a noticeable decrease in conduction velocity, consistent with expected actions on K^+_{leak} channels in decreasing membrane resistivity.

The findings indicate a distinct difference in how electrically-evoked and optically-recruited SPNs respond to riluzole treatment. Specifically, only the slower-conducting SPNs in the IGN showed a significant reduction in response when electrically evoked, highlighting a possible difference in sensitivity or density of leak potassium channels in these neurons. Moreover, optically-recruited SPNs, regardless of their conduction speed or nerve type (IGN or splanchnic), exhibited a marked decrease in their evoked responses. This suggests a more uniform or widespread effect of riluzole on these neurons.

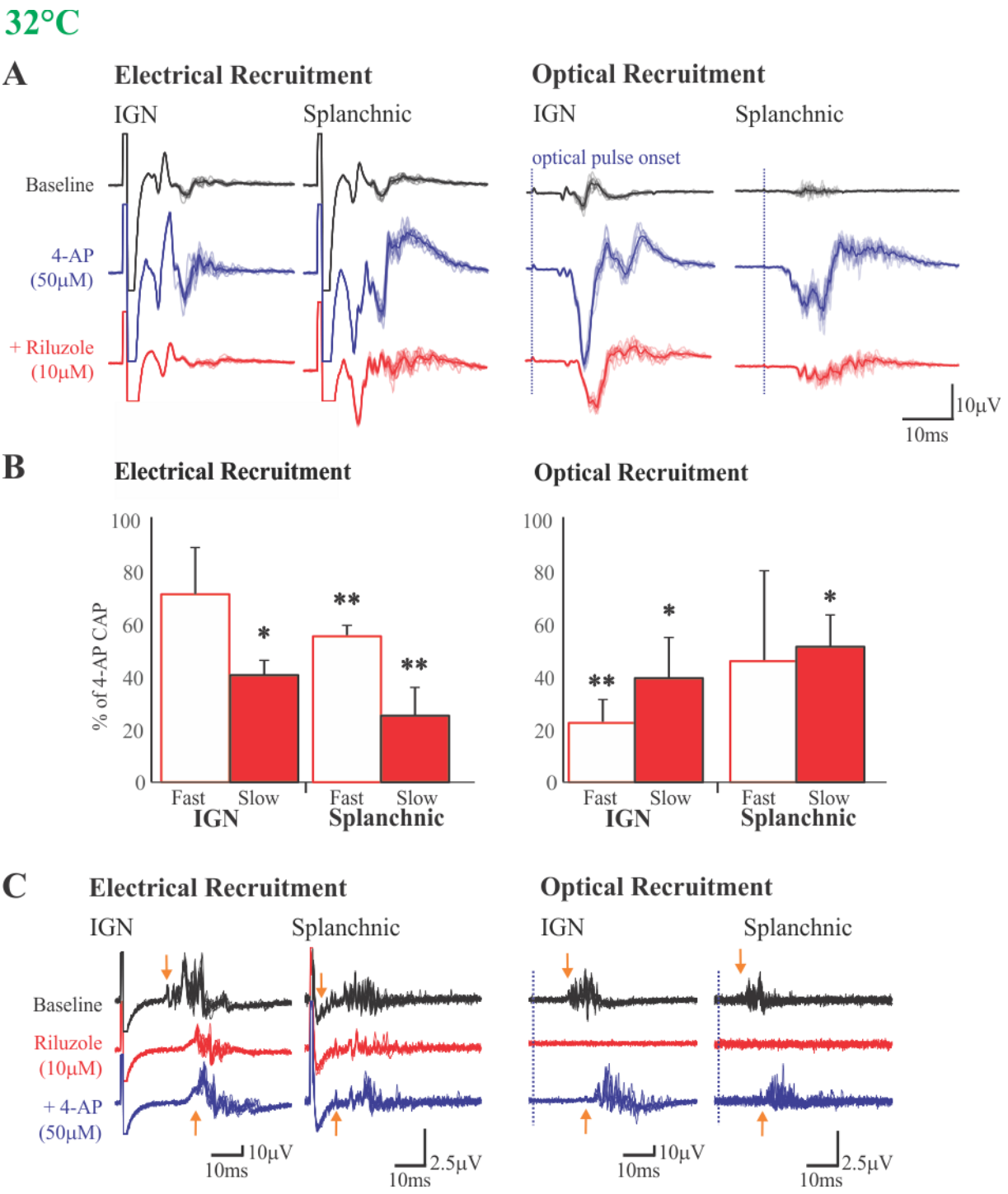

Figure 5.5 Effect of riluzole subsequent to K+ channel block with 4-AP

[A] Shown are typical evoked responses in SPNs, triggered by supramaximal stimulation via 200 μA/500 μs electrical and 6.6mW/mm^2 20ms optical impulses. These traces have been high-pass filtered at 100 Hz to illustrate the effects of 4-AP and riluzole. **[B]** The graph shows the influence of riluzole (concentration range 0.5-50μM) on the rectified integral of the maximal CAP induced

by 4-AP in electrically evoked slow-conducting IGN axons (and all optically-evoked SPN populations. Statistical analysis was conducted using paired t-tests to determine the significance of riluzole's effect on 4-AP induced conduction enhancement in SPNs (n=3; *, $p<0.05$; error bars are SEM). **[C]** Riluzole was administered before the application of 4-AP which reduced electrically evoked CAP while eliminating the optically evoked CAP. However, the subsequent introduction of 4-AP resulted in an increase in electrically evoked SPNs and successfully restored the optically evoked SPNs (n=1). The orange arrow highlights delay of CAP onset even after restoration.

Arachidonic acid (10µM) led to a reduction in the amplitude of slow conducting IGN responses elicited electrically (46.9% reduction; $p<0.001$), as demonstrated in Figure 5.6B. Interestingly, a similar trend was observed in optically recruited SPN axons (42.9% reduction $p<0.01$), marking a divergence from the results seen with riluzole. The observed discrepancies in the effects of arachidonic acid and riluzole on optically recruited SPNs could potentially be ascribed to the pre-incubation with 4-AP in the riluzole experiment. As illustrated in Figure 5.3, 4-AP exerts a significant impact on optically recruited SPNs. Therefore, the presence of 4-AP might have amplified the effectiveness of riluzole, leading to more pronounced results in these neurons.

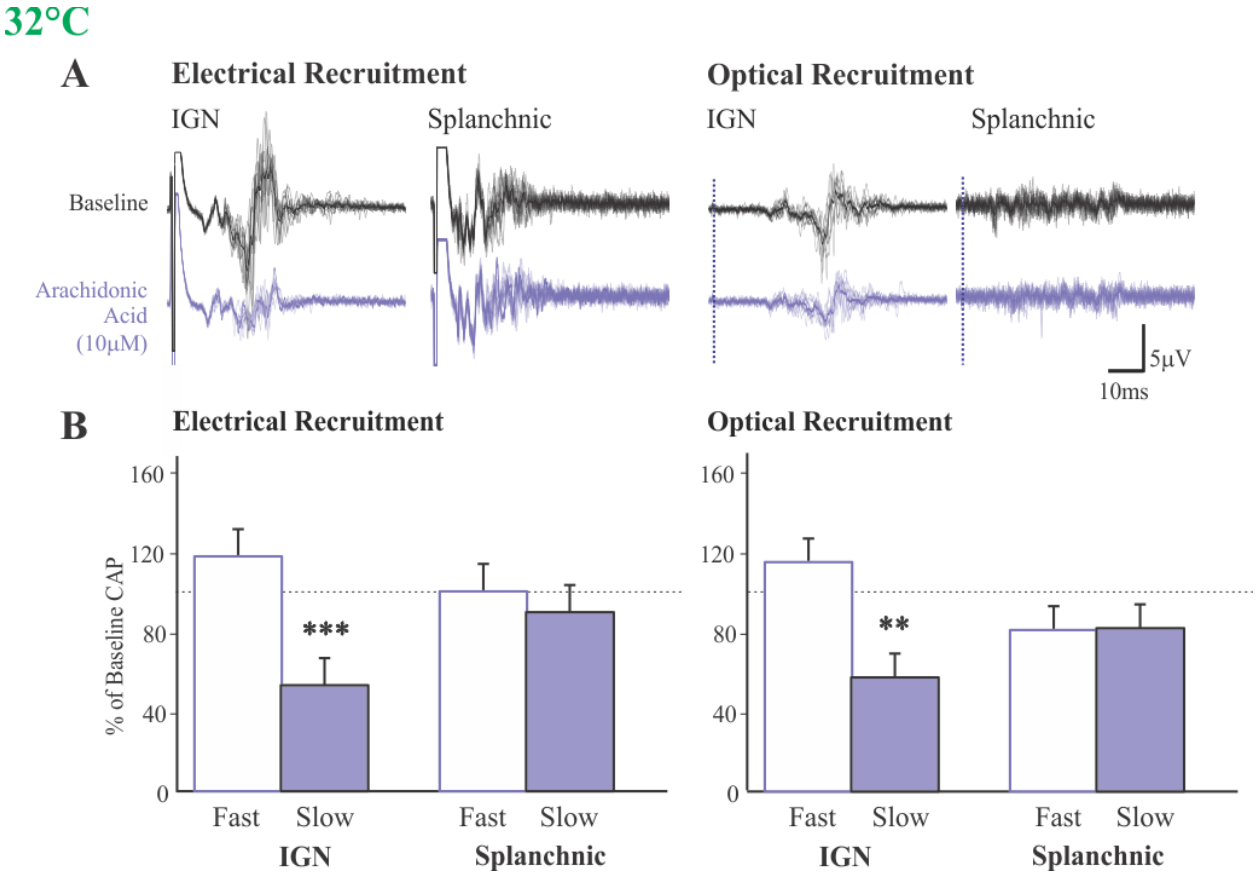

Figure 5.6 Arachidonic acid contributes to blocking slow-conducting SPN fibers recruited optically and electrically

[A] Displayed are typical evoked responses in SPNs, triggered by supramaximal stimulation via 200 µA/500 µs electrical impulses and 6.6mW/µm^2 20ms optical impulses optical impulses. These traces have been high-pass filtered at 100 Hz. **[B]** The graph shows partial block by arachidonic acid (10µM) on the rectified integral of slow-conducting IGN axons by electrical and optical stimulation. The experiments were performed at a controlled temperature of 32°C. Statistical analysis was conducted using paired t-tests to determine the significance (n=5; **, p<0.01; ***, p<0.001; error bars represent SEM).

5.4.4 Modulation via 5-HT

In our experiments conducted at 22°C, 5-HT (50µM) revealed distinct responses between IGN and splanchnic axons. Slower-conducting evoked responses in IGN and splanchnic were depressed (49±6.9%; p<0.05 and 56±8.2%; p<0.05 reduction, respectively; Figure 5.7B). This

differential effect suggests a potential variation in the distribution or function of 5-HT receptors across these neurons, although the conclusions are limited by the underpowered IGN data.

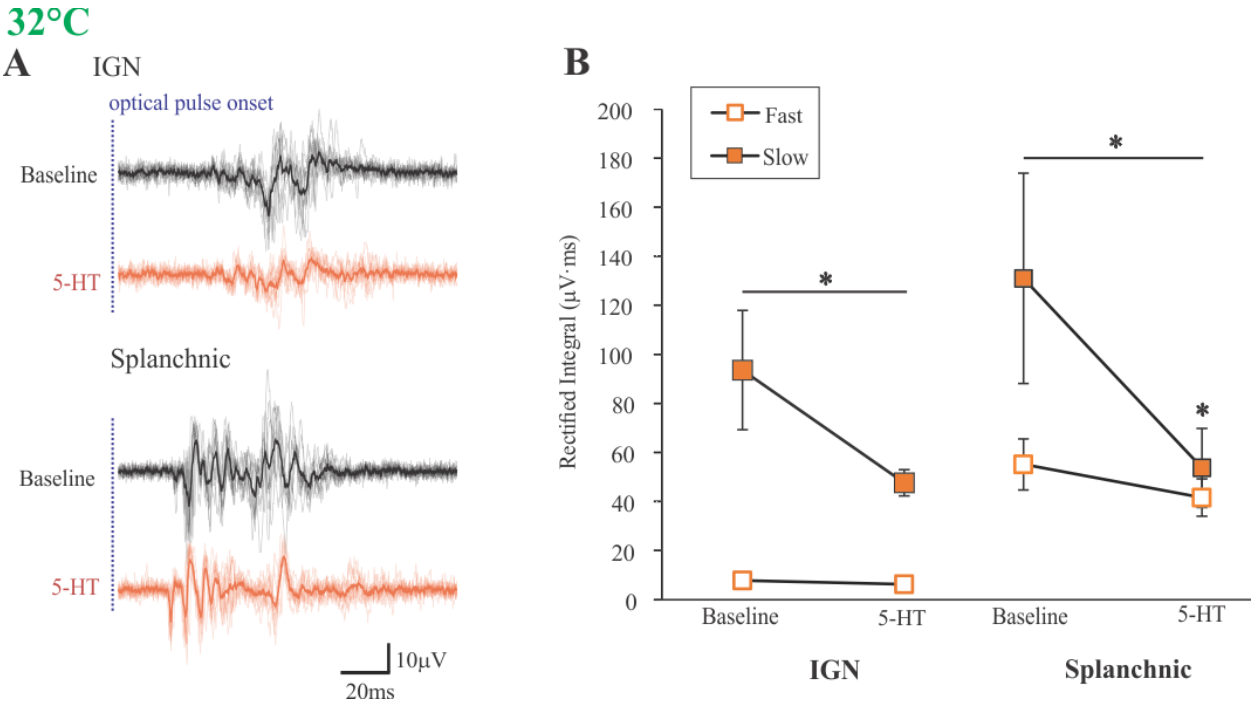

Figure 5.7 5-HT actions on spike conduction in SPN axons

[A] Displayed are typical evoked responses in SPNs, triggered by supramaximal stimulation via 200 µA/500 µs electrical impulses and 6.6mW/µm2 20ms optical impulses. These traces have been high-pass filtered at 100 Hz. 5-HT induced block can be seen in orange. **[B]** Shown is the impact of 5-HT (50µM) on SPN conduction. To account for inter-animal variability in modulation we assessed differences in rectified integrals of CAP and found rectified integrals (µV·ms) of CAP to be reduced with application of 5HT in slow conducting IGN SPNs, slow conducting splanchnic SPNs. Statistical analysis was conducted using paired t-tests (n=7; *, $p<0.05$). Error bars represent SEM.

5.4.1 Presynaptic nicotinic acetylcholine receptors may be a site for SPN axon modulation.

Following the blockade of ganglionic transmission with hexamethonium, we specifically assessed the cholinergic actions on presynaptic SPN axons by applying neostigmine and acetylcholine (ACh). The cholinesterase neostigmine (20µM) was used to prevent ACh degradation. Changes in evoked responses in the presence of neostigmine alone would be interpreted as due to increasing endogenously released ACh. Subsequently applied ACh

(100μM) would be expected to have actions on receptors in relation to the dose applied. An example of evoked responses is shown in Figure 5.8A. Negative DC shifts were seen in 4/6 experiments in both the IGN and splanchnic nerves following the application of neostigmine and ACh (Figure 5.3 B_1). In all of these experiments (6/6), both IGN and splanchnic nerves exhibited an increase background spontaneous spiking activity after the application of neostigmine and ACh, consistent with the DC-shift being due to membrane depolarization (Figure 5.3 B_2). Remarkably, ACh preferentially and strongly blocked conduction in the slower-conducting IGN axons (to 12% of control, $p<0.05$; Figure 5.8C). Note that spiking activity in the IGN could reflect increased activity in presynaptic SPN axons and/or postganglionic axons while that seen in the splanchnic nerve represents selective activity in preganglionic SPN axons.

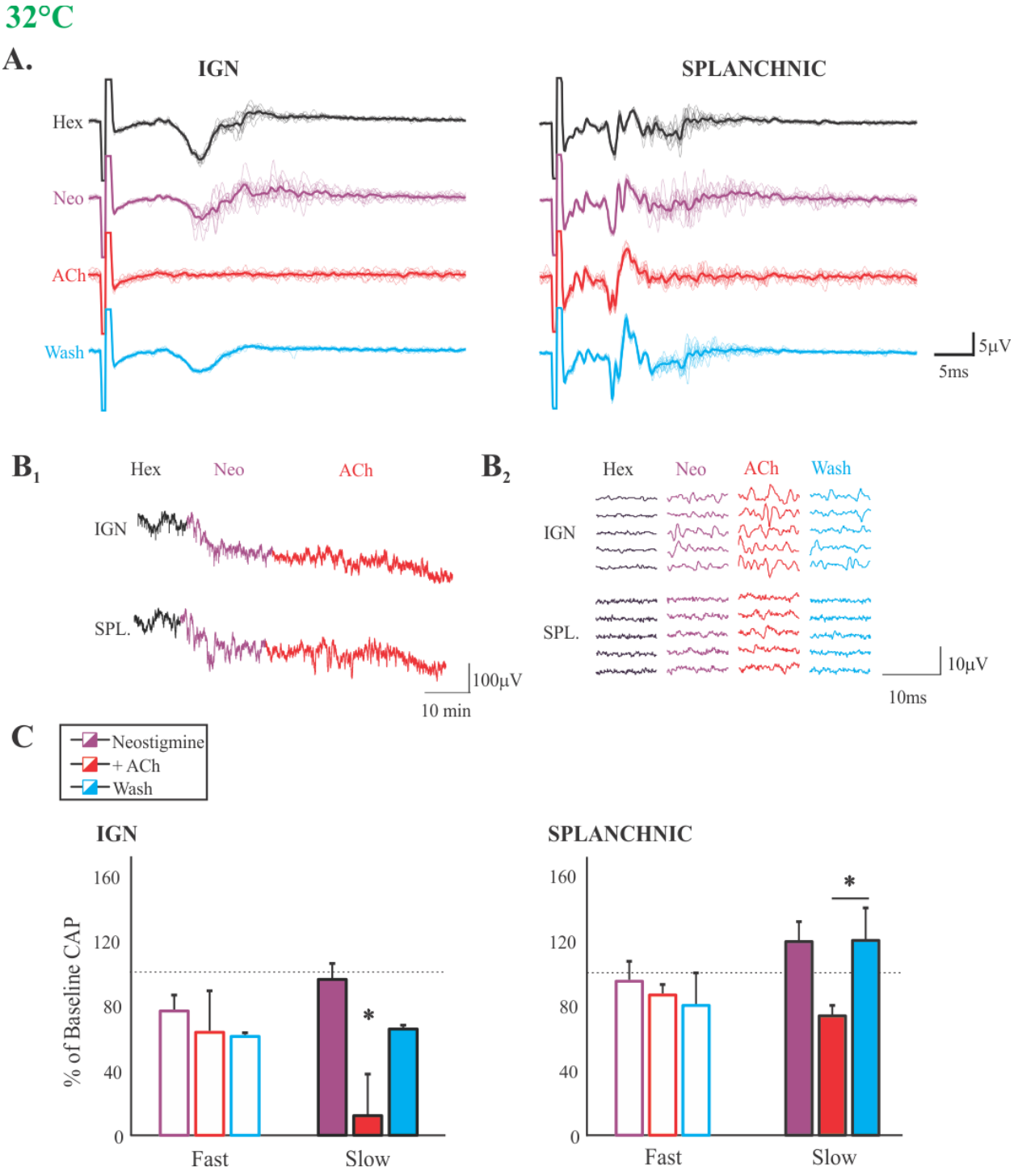

Figure 5.8 Evidence of presynaptic cholinergic modulation

(A) Representative raw traces of electrically-evoked responses in IGN and splanchnic SPN axons, the effects of the cholinesterase inhibitor neostigmine (20 µM) and ACh (100 µM) application, and subsequent washout of applied drugs. Each trace is evoked by a 200 µA/500 µs electrical stimulus and has been high-pass filtered at 100 Hz for clarity. In all panels, drug

applications are denoted by a change in the color of the trace. **[B_1]** Example DC recordings showing clear increases in negativity following application of neostigmine and ACh. Clear negative DC shifts in IGN and splanchnic nerves were seen in 4 out of 6 experiments. Extracellular DC shifts after applied neostigmine and Ach reflect membrane depolarization. Recordings were undertaken coincident with stimulation of the ventral root every minute. **[B_2]** Shown in an example of emergent spontaneous activity (particularly in IGN recordings) after applied neostigmine and Ach seen during DC shifts (demonstrated by a series of 5 stacked epochs taken 1 minute apart). Emergent spontaneous activity was seen in 6/6 preparations. **[C]** Cholinergic actions were selectively associated with a significant amplitude reduction (by 88 ±3.6%) in IGN slow conducting axons subsequent to applied ACh. Statistical tests were undertaken using repeated measures ANOVA (n=6; *, $p<0.05$; error bars are SEM).

5.5 Discussion

5.5.1 Overview of Key Findings

Previous chapters have established that SPN axons, particularly the unmyelinated ones, exhibit significant time-dependent variations in evoked conduction, with a higher failure rate in spike conduction observed in IGN (branching) axons compared to splanchnic (unbranching) ones. These failures were found to be sensitive to both stimulation frequency and temperature, with elevated temperatures or repetitive stimulation leading to increased failure rates in the slowest conducting SPN axons.

The work in this chapter further demonstrates the modifiability of SPN axonal conduction by changes in activation of K^+ channels and neurotransmitter systems as summarized below. (1) The $GABA_AR$ antagonists picrotoxin and bicuculline reduced evoked responses in IGN (branching) axons. (2) The voltage-gated K^+ channel blockers 4-AP and TEA had profoundly different actions on evoked responses: 4-AP greatly facilitated evoked responses in slower-conducting axons while TEA depressed responses. (3) We observed that the reduction in evoked response with ↑T° was associated with changes in DC polarization consistent with membrane hyperpolarization. As TREK-1 K_2P leak channels are activated by ↑T°, the TREK-1 channel activators riluzole and arachidonic acid (AA) were applied and reduced recruitment of slower-conducting responses. That riluzole also reduced axonal recruitment in all other optically evoked

responses may be related to additional actions of riluzole elsewhere [259]. (4) Applied 5-HT or ACh (in neostigmine) reduced response amplitude in IGN slower-conducting axons. Further studies are required to identify the presynaptic receptors involved in this depolarization. Nevertheless, the results do show SPN axonal conduction is sensitive to changes in both serotonergic and cholinergic modulatory events.

The consistent reduction in IGN slower-conducting branching axons as opposed to the non-branching axons in the splanchnic nerve, supports a selective modulation of these paravertebral axons. That IGN slower-conducting axons are also preferentially diminished by ↑T° (Chapter 4) may indicate that TREK-1 expression is more common in these axons, as TREK-1 expression is found in specific subpopulations of thoracic SPNs[47].

Integrated the present studies with those in chapters 3 and 4, our findings demonstrate that individual SPN axons spike propagation is not unfailing but rather highly susceptible to conduction failures, with reliability under the control of various factors including temperature, spike history, $GABA_A$Rs, voltage-gated potassium channels, K_2P leak channels, and neuromodulatory transmitters.

5.5.2 Modulation via GABAARs

5.5.2.1 GABAergic modulation of SPN axonal conduction

Using $GABA_A$R antagonists, this work identified a role for SPN axonal $GABA_A$Rs in promoting spike conduction. The present observations are consistent with earlier observations of reduced recruitment of postganglionic neurons by $GABA_A$R antagonists [232 233,235,260]. The fact effect sizes were more pronounced in slow-conducting axons within the IGN suggests that these neurotransmitters primarily affect conduction in branching axons, supporting the notion that axonal branch points are a site of spike conduction control. At 32°C, picrotoxin and bicuculline

selectively depressed the evoked CAP in slow-conducting IGN axons. Extrasynaptic α_5-$GABA_AR$s can be preferentially localized at axonal branch points, with tonic activity that promotes conduction across branch points [236,261]. SPNs extrasynaptic constitutively active α_5-$GABA_AR$s [47,237], but whether their expression was localized to SPN branch points was not explored. We observed a trend for reduced conduction following block of α_5-$GABA_AR$s with the inverse agonist L655,708, but significance was achieved only with subsequent application of broader acting $GABA_AR$ antagonists. Further investigation into the effects on α5-$GABA_AR$s at lower temperatures is warranted given the observed temperature-dependent loss of slower conducting IGN axons.

$GABA_AR$ effects are dependent on membrane E_{Cl}, which, based on the relative activity of transporters may be depolarizing or hyperpolarizing. There is limited evidence of KCC2 expression in axons [262] which would suggest that E_{Cl} would be at a more hyperpolarizing value. Nevertheless, our results indicate that E_{Cl} is more depolarized than resting membrane potential in contrast to results suggesting activity of $GABA_AR$ is hyperpolarizing [233,234,263]. There is also evidence that $GABA_AR$s is depolarizing [264]. Hyperpolarizing or depolarizing effects of $GABA_AR$ activation may relate to changes in resting membrane potential under different conditions (e.g. modulation of K_2P leak conductance). While it is possible that other transporters are involved in Cl^- transport, that $GABA_AR$ antagonists reduced conduction in only putatively branching axons, suggests that their tonic activity is depolarizing and operating mechanistically like that seen in myelinated sensory axons.

The observation that $GABA_AR$ blockers exert effects supports tonic $GABA_AR$ activity promoted spike propagation. Tonic activity would require the presence of endogenously synthesized GABA or the presence of $GABA_AR$s with constitutive activity. Regarding possible sources of

endogenous GABA, there is evidence of GABA synthesis in rat sympathetic ganglia [265] and an RNAseq study identifies the GABA-synthesis enzyme GAD65 expression in a distinct subpopulation of SPNs [47]. Additionally, the interstitial fluid bathing SPN axons has access to the circulatory system with plasma GABA levels higher than in the CNS and under dietary influences [266,267]. Conversely, the inference regarding constitutive activity stems from the fact that postganglionic neurons in the paravertebral chain ganglia, traversed by SPN axons, are not GABAergic [177]. α5ɣ2-containingt $GABA_A$Rs display constitutive activity in the central nervous system [268] [238-240,269]. Extrasynaptic α_5-containing $GABA_A$ receptors are implicated [191,236,270,271] with constitutive activity of $GABA_A$Rs at axonal branch points shown to be a nodal site for conduction control in somatosensory systems [207,236,271,272]. As SPNs have low expression of constitutively-active α_5-$GABA_A$Rs [273] [47], localization at axonal branch points may similarly control divergence and hence response amplification to postganglionic neurons.

Modulation via presynaptic axonal $GABA_A$Rs would provide an unrecognized mechanism for control of response amplification and spatial spread in the sympathetic paravertebral system. Importantly, control is at a CNS-PNS interface site with access to humoral factors that have known actions on α_5-$GABA_A$Rs [274-278]. Future studies should test modulation across the physiological range of firing frequencies, show an absence of sensitive to the synaptic $GABA_A$R blocker gabazine, and look at the effects of $GABA_A$R agonists. A study on the effects of allosteric modulators is also warranted. For example, the stress-induced 3α-reduced neuroactive steroids are potent positive allosteric modulators of α5-$GABA_A$Rs [274,279,280].

5.5.3 Modulation via 4-AP and TEA

5.5.3.1 Increased conduction following 4-AP application can provide mechanistic insight into modulation of SPN gain via block of K_A

We tested the actions of the Kv channel blocker 4-AP in SPN axons. A previous study on dorsal root afferents found that 4-AP specifically affected unmyelinated C-fibers, where it notably prolonged spike duration in single fiber recordings. Furthermore, when observing population CAPs, 4-AP could significantly increase CAP amplitude [246]. 4-AP was also able to reverse temperature-dependent conduction block non-myelinated rat spinal roots [243,246].

We found that 4-AP increased evoked responses in slower-conducting in axons in both IGN and splanchnic nerves and also restored temperature dependent loss of axonal conduction. Optically-evoked 4-AP response facilitation was far greater than electrical. This disparity in responses may be attributed to the differential recruitment of SPN populations with differing K^+ channel subtypes and expression densities.

4-AP but not TEA has known actions on the voltage-gated K_A channels of the K_v3 and K_v4 family [281]. If this is the site of 4-AP actions, the results demonstrate that block of these channels results in a significant increase in preganglionic drive. This finding has potential implications for controlling SPN output strength, particularly in cases where K^+ channel expression is altered. For example, alterations in voltage-gated potassium currents have been associated with hyperexcitability in primary afferents in spinal cord injury models [282,283]. Future experiments should use Phrixotoxin-1 (1-10 μM, Tocris) to selectively block Kv4.2/Kv4.3 potassium channels [284].

It has been reported that 4-AP but not TEA promotes presynaptic recruitment of N-type $Ca_v2.2$ channels via actions on the β3 subunit [285]. As voltage-gated Ca^{2+} (Ca_v) channels are expressed in unmyelinated axons [155] it is possible that 4-AP recruited Ca_v channels. SPNs have strong expression of $Ca_v2.2$ (CACNA1b) but expression of the β3 subunit (CACNb3) is limited to 2 of 15 thoracic SPN subpopulations [47]. 4-AP actions on Ca_v channels should broaden spikes and could support the substantial negative shift in the recorded responses. To determine whether negative deflections induced by 4-AP are Ca_v mediated, it will be necessary to conduct studies involving the blockade of these channels. Regardless, the recruitment of axons by 4-AP, which were previously inhibited at higher temperatures, along with the identification of new unit recruitment at lower doses of 4-AP before the onset of larger negative events, reinforces the role of K_A channels in modulating spike conduction.

Finally, the facilitation induced by 4-AP was consistently observed in both splanchnic and IGN CAPs, suggesting that 4-AP-sensitive potassium channels play a crucial role in unmyelinated axons. This effect appears to be non-discriminatory with respect to whether these axons are branching or non-branching, indicating a broad functional relevance of these channels in various types of unmyelinated axons.

Our observed 4-AP actions may be important clinically as therapeutics currently used to promote conduction in demyelinated large axons (fampridine; 4-AP) [286] may also increase magnitude of SPN actions onto postganglionic neurons. Such increases would be consistent with induced hypertensive crisis associated with afferent -induced autonomic dysreflexia.

5.5.3.2 Differential actions of TEA and 4-AP

Both TEA and 4-AP are known to enhance action potential amplitude in demyelinated and unmyelinated axons [83,243,246]. Like 4-AP, though less consistent in its effect, TEA can promote conduction caused by temperature block in nonmyelinated fibers [243]. At 32°C, 1 mM of TEA, produced no significant changes in amplitude across most populations, except for depression in slow-conducting axons of the IGN under both electrical and optical stimulation. Given that 4-AP and TEA are blockers at many common voltage-gated K^+ channels the lack of facilitatory effect by TEA may be related to dose applied. It has been noted that concentrations of up to 50mM are required to achieve a facilitatory effect, whereas our experiments employed only a 1mM concentration [243].

TEA has previously been reported as a blocker of ganglionic transmission [287] and presumed to be via postsynaptic depolarization block of spiking [288] where block of multiple voltage-gated K^+ channels leads to a progressive depolarization with subsequent maintained inactivation of voltage-gated Na^+ channels. It is therefore possible that depressant actions of TEA on slow IGN axons may be via inadequate block of synaptic transmission with hexamethonium (100µM) in this subpopulation of axons. Alternately, and arguably more likely, TEA-induced depression in slow-conducting IGN axons could be via selective depolarization block of these preganglionic axons.

We compared the pharmacological actions across the family of voltage-gated K^+ (**K_v**) channels (https://www.guidetopharmacology.org/) with sensitivity to block by 4-AP and TEA. Given the doses applied, observed 4-AP effects are likely attributed to the selective pharmacological actions of 4-AP on $K_v4.2$ and/or $K_v4.3$ channels. These K_A channels are highly expressed in

SPNs [47] and Kv4.3 has been shown to be expressed in unmyelinated axons[167]. Accordingly, these channels likely play a crucial role in modulating propagation failure along axonal spikes. Physiological or pharmacological mechanisms controlling their activity could allow significant control of their divergent actions onto postganglionic neurons with subsequent impact on response magnitude in innervated effector sites.

5.5.4 Modulation via Potassium Leak Channels

As shown in Chapter 4 (Figure 4.5) there was a pronounced conduction block in slower-conducting unmyelinated SPNs at 36° compared to 22°. That optical stimulation preferentially recruited the slowest-conducting axons (Chapter 3) aligns with our observation that optically recruited responses in SPN axons were significantly diminished or entirely absent at 36°.

Notably, a decrease in temperature led to a depolarizing negative DC shift (Figure 5.2A), or conversely, an increase in temperature leads to a hyperpolarizing DC shift. This was paralleled by findings that higher temperatures promote conduction block in SPN axons within both IGN and splanchnic nerves (refer to Figures 4.1 and 5.2A2).

Building on these insights, we explored whether the associated temperature-dependent reduction in evoked responses was due to activation of the temperature-sensitive two-pore K^+ leak (K_2P) channel TREK-1. TREK-1 channels are highly expressed in SPNs [47] and show a 20 fold increase in activity when temperature rises from 22-42°C [289,290]. We focused on testing the effects of the TREK-1 channel activator riluzole, and the polyunsaturated fatty acid positive modulator arachidonic acid [212,222].

Our findings revealed preferential depression of the slower-conducting responses following application of riluzole or arachidonic acid in IGN, with riluzole also depressing responses in the

splanchnic nerve. Before applying riluzole, we preincubated the bath with 4-AP to inhibit the voltage-gated K^+ channel (K_V) channels $K_v4.2$ and $K_v4.3$, which are also reportedly inhibited by riluzole [291] [292]. The TREK-1 mediated currents are not inhibited by the traditional (K_v) blockers TEA and 4-AP [248].

While riluzole also inhibits persistent sodium (Na^+) currents and $GABA_ARs$[293-295], which could explain the observed effects, the similar outcomes achieved with arachidonic acid suggest the involvement of K2P TREK-1 channel activation. Riluzole induces a negative shift in the I_H current, and axons express both HCN1 and HCN2 channels[296]. This alteration should not affect the threshold for initiating spikes or the recruitment of action potentials, but it may modify the properties of repetitive firing. Notably though, riluzole responses were stronger and broader and clearly associated with a slowed CV (figure 5.5) (n=3). Slowing of CV would be consistent with the increased membrane leak associated with activation of K_2P channels. In comparison, slowing of CV with arachidonic acid was less obvious. It is possible that higher doses of arachidonic acid than that chosen (10 μM) based on other *in vitro* studies [297] may have led to stronger modulatory actions.

Notably, the effects of riluzole may provide insight into a unique role for TREK-1 channels as being important for defining temperature thresholds and temperature ranges as previously demonstrated in nociceptors [298]. The role of TREK-1 as a temperature sensor is further supported by a lack of 164hermos-sensitive TRP channels at this temperature range [47].

Interestingly, TREK-1 channels are physiologically modulated through transduction pathways. These channels are notably activated by polyunsaturated fatty acids and various anesthetics, highlighting their responsiveness to diverse molecular signals [299,300]. Conversely, these channels are inhibited by the NO/cGMP/PKG, Gs/cAMP/PKA and the Gq/PLC/DAG/PKC signaling

pathways [247,248]. That TREK-1 channels are subject to negative regulation by G_S and G_q G protein-coupled receptors, support modulatory control via PGE2, serotonin 5-$HT_{2\&7}$ receptors and muscarinic $M_{1,3,5}$ receptors [301,302].

5.5.1 Monoaminergic Modulation

Recent RNA-seq database analysis has identified the presence of 5-HT_{1F}, 5-HT_{2A}, 5-HT_{2C}, and 5-HT_7 receptors in SPNs [47]. In our studies at 22°C, 5-HT (50µM) preferentially depressed slower conducting responses in both IGN and splanchnic nerve. Modulatory responses support the presence of 5-HT receptors on SPN axons. To our knowledge there are no neuronal sources associated with 5-HT release [177,303], meaning that either 5-HT arises from nonneuronal sources and/or these receptors are constitutively active. Regarding non-neuronal sources, all 5-HT is circulated via blood platelets and plasma which may act on SPN axonally distributed 5-HT receptors. In comparison, there is considerable evidence of constitutive activity of 5-HT_2 receptors, [304]. Future studies using selective 5-HT_2 inverse agonists like SB206553 or cyproheptadine would provide evidence of their constitutive activity.

Additional pharmacology assessing the presence of other expressed 5-HT receptors would also provide important information on the mechanism of serotonergic modulation. 5-HT G-protein-coupled actions on TREK-1 channels may be one mechanisms of their neuromodulation in evoked responses. As 5-HT_2 receptors are G_q-coupled, they would be expected to inhibit TREK-1 channels. 5-HT_7 G_s-coupled receptors would be expected to act similarly. In comparison G_i-coupled 5-HT_{1F} receptors may support TREK-1 channel activation. That the present series was undertaken at room temperature may have prevented any modulation via this pathway.

5-HT_7 receptors have been implicated in the modulation of K^+ channels such that activation can lead to hyperpolarization of the cell membrane, possibly through the opening of potassium

channels [284]. Aside from 5-$HT_{2A/C}$ G_q activation of protein kinase C, consequent activation of phospholipase C-induced production of IP3 leads to an increase Ca^{2+} release from IP3-sensitive stores and may be implicated in inhibiting $GABA_AR$ activity [305,306]. 5-HT_{1F} receptors are coupled to G_i/G_o proteins, leading to the inhibition of adenylyl cyclase and a decrease in cAMP level. While not directly known for modulating potassium channels, the signaling pathway through G_i/G_o proteins can indirectly influence potassium channel activity.

To support the notion that serotonin (5-HT) modulate spike conduction, evidence is needed to demonstrate the localization of receptors along the axons. Additionally, it must be shown that neurotransmitters are present in concentrations high enough to activate these receptors or that the receptors themselves exhibit constitutive activity.

5.5.2 Cholinergic Modulation of SPN Axons

Following the blockade of ganglionic transmission using hexamethonium, we assessed presynaptic cholinergic modulatory actions following application of ACh in the presence of the cholinesterase inhibitor neostigmine. ACh led DC shifts consistent with greater depolarization and increased spontaneous activity in both nerves. ACh also preferentially reduced evoked responses in IGN slow conducting axons. The identity of the ACh receptors responsible for observed actions may be either nicotinic or muscarinic. Additional studies using receptor selective agonists and antagonists are required to identify the cholinergic receptor(s) involved. Potential targets are muscarinic M_3 receptors that are expressed in SPNs along with nicotinic receptors containing (in descending order of expression) α7, β2 α4, α1, α10 and α9 subunits [47].

Aside from local diffusion following release from presynaptic terminals, ACh effects could also arise from non-vesicular release[307]. Given that SPN axons are exposed to the circulatory system, fluctuations in circulatory ACh levels could influence axonal receptors, thereby globally

modulating sympathetic axonal excitability[308]. Furthermore, the synthesis of ACh by non-neuronal cells in vascular endothelial tissues, combined with the presence of soluble choline acetyltransferase (ChAT) in the plasma, may regulate ACh levels to exert effects in a paracrine manner[309].

5.5.3 Comparative Analysis of Modulatory Effects

When comparing modulatory effects, it becomes evident that slow-conducting axons demonstrate a heightened sensitivity to modulation. This observation aligns well with the patterns we noted regarding temperature and frequency perturbations, as discussed in the previous chapter. Furthermore, differential actions were seen between optically recruited and electrically recruited SPNs.

Interestingly, our analysis revealed that the distinctions between IGN SPNs and splanchnic SPNs were not as straightforward as anticipated, showing variability depending on the modulation strategy employed. For instance, we observed that $GABA_AR$ antagonists and ACh preferentially depressed population responses in slower conducting IGN axons, implying a selective localization of $GABA_AR$ and modulatory cholinergic receptors on slower conducting IGN axons. In comparison, 5HT (applied at 22° compared to 32° in experiments above) selectively depressed population responses in the slower-conducting axons in both the IGN and splanchnic nerves. Meanwhile, K_v block and K_2P activation had more widespread effects on population responses indicative of more widespread expression of these channels. Facilitation of conduction through K_v block was the most profound and widespread.

In conclusion, studies focusing on the recruitment or inhibition of channels and receptors, which are presumably expressed in SPN axons, demonstrate the potential to regulate population-evoked responses. The slower conducting axons have greater capacity for modulation of conduction with

greatest actions in the IGN, presumably indicating that conduction along their branching axons is a key site of regulation. The heightened sensitivity of slower-conducting axons to various modulators, alongside the differential responses based on recruitment method and nerve type, points to a nuanced landscape of neural modulation. In particular, the distinct control of IGN slower-conducting axons by $GABA_A$Rs and cholinergic agents, highlights this population as functionally distinct with regards to conduction control. These findings not only enhance our understanding of neuronal modulation but also pave the way for more targeted investigations into the functional roles of these diverse neuronal pathways.

5.5.4 Implications for Neurophysiological Understanding

In this chapter, we provide a conceptually novel mechanism of CNS-PNS gain control in a little explored but physiologically critical area in vertebrate neuroscience: the CNS sympathetic output stage. Prior to this study little was known about SPN conduction along the axon proper.

We have firmly established that controlling conduction along SPN multisegmented axonal branches is not just an overlooked aspect but a vital, physiologically modifiable presynaptic feature in the regulation of sympathetic output. Our *in vitro* studies, focusing on evoked responses of SPN axons can be effectively modulated.

We have conclusively demonstrated that conduction failures across SPN branching and unbranching axons is a physiologically phenomenon and is subject to modulation. This discovery is not just of academic interest but holds substantial clinical implications. Our findings establish foundational mechanisms that are directly pertinent to spinal cord injury (SCI) and autonomic disorders. This paves the way for future research to validate these mechanisms *in vivo* and to explore their potential therapeutic applications. Our work, thus, marks a significant milestone in

neurophysiological research, offering new avenues for understanding and manipulating sympathetic output in both health and disease.

6 Summary and General Discussion

This thesis explored the complex mechanisms governing spike propagation in spinal cord sympathetic preganglionic neurons (SPNs), which act as the final integrated output from the CNS to postganglionic neurons in both paravertebral and prevertebral ganglia. To investigate these neurons, an *ex vivo* approach was developed using adult mouse thoracic sympathetic chain ganglia. These ganglia were dissected to maintain *in situ* continuity with ventral roots, and synaptic transmission was blocked to focus on SPN axonal responses. The study used both optical and electrical stimulation to recruit SPN axons in ChAT-CHR2 adult mice, recording population responses in branching axons across the IGN and in unbranching axons in the splanchnic nerve that project to prevertebral ganglia. The responses were categorized into faster- and slower-conducting subpopulations, and anterograde labeling provided insights into the axonal branching of SPNs.

The research revealed that SPN axonal volleys exhibit a range of conduction velocities, all of which were consistent with unmyelinated axons in the IGN and lightly myelinated and unmyelinated in the splanchnic nerve. Slower-conducting axons in both IGN and splanchnic nerves had the highest variability in population response profile. These axons experienced frequency-dependent depression of evoked responses, with pronounced conduction failures in the slowest conducting axons. Further, the study found that the slowest-conducting axons were susceptible to modulation by $GABA_AR$ block, 5-HT and ACh receptor activation, and pharmacological interventions affecting K_V (putatively K_A) and K2P K_{leak} channels. A summary of key findings is provided in Figure 6.1.

Overall, unmyelinated axons from CNS preganglionic neurons in autonomic circuits had high spike propagation failure rates. This previously unrecognized feature and that conduction failure

magnitude was under modulatory control together demonstrate that conduction is a key feature of output control beyond the CNS-driven recruitment of SPN spiking within the spinal cord. Given the range of conduction failures seen, particularly in the slowest conducting unmyelinated axons, we hypothesize that the encoding of sympathetic drive is optimized for low-frequency information transfer of population-encoded responses to minimize metabolic costs, consistent with the 'law of diminishing returns' [86].

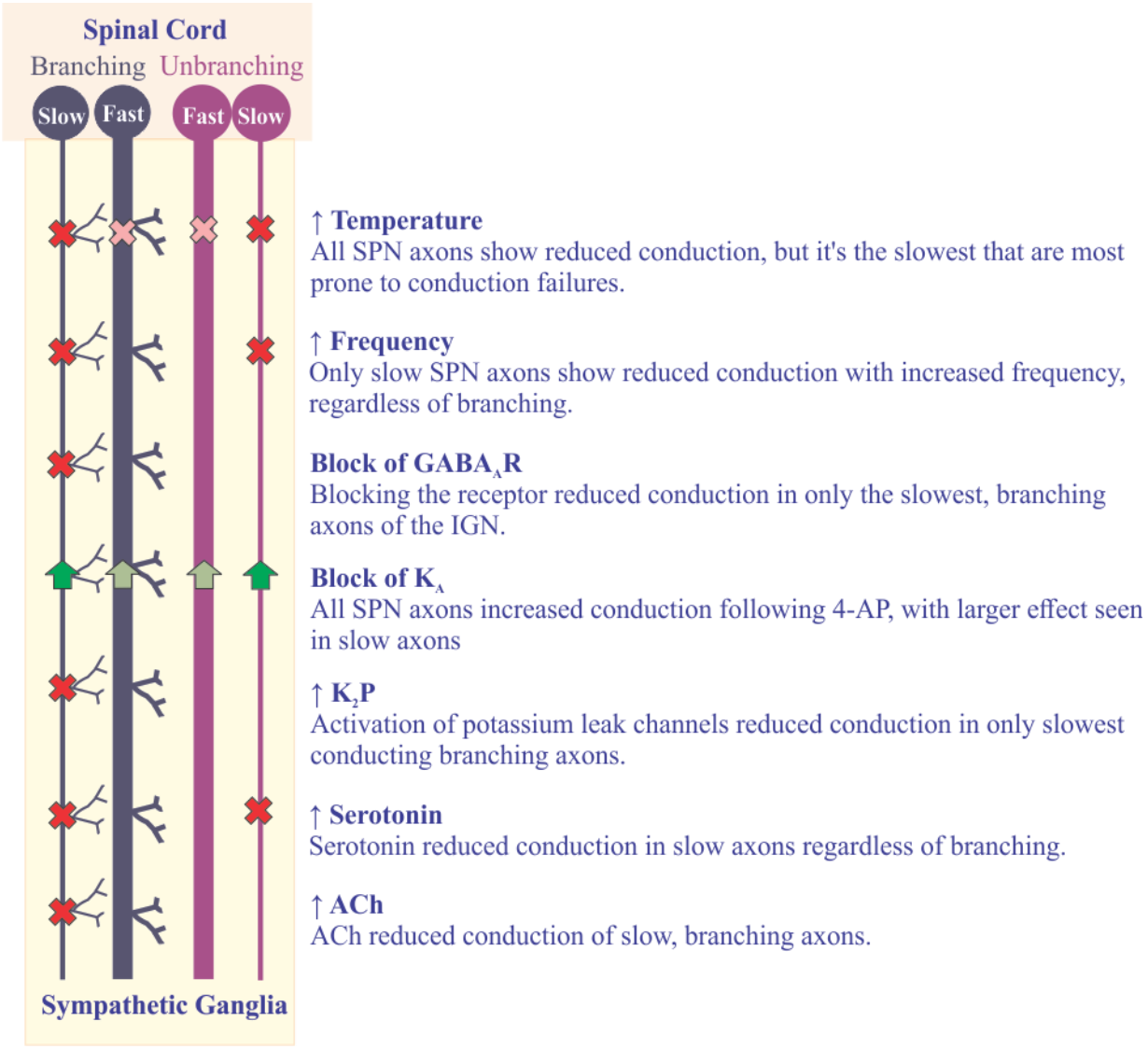

Figure 6.1 Summary of Key Findings

This schematic illustrates how various factors influence the conduction in SPN axons, based on findings from this thesis. It includes four types of axons: fast and slow branching axons, along with fast and slow unbranching axons. A green arrow indicates an improved evoked response in the SPN volley, signaling either enhanced conduction efficiency or the involvement of additional SPN axons, with a darker green shade denoting a stronger response. Conversely, a red "X" marks the presence of conduction failure, where a darker red signifies a more significant block.

6.1 Conduction failure behavior in sympathetic preganglionic axons

For SPN paravertebral axons with broad multisegmental divergent projections, it is easy to consider regulation of propagation distance by conduction failure as a mechanism to control receptive field size of postsynaptic postganglionic neurons targets. As such this enables SPN axons to provide powerful modulatory control of sympathetic output strength [271]. This phenomenon may act as a behavioral state-dependent gating mechanism, with differing levels of spike propagation under different physiological conditions, spike propagation can be promoted or depressed.

Failures in conduction could be triggered by a variety of factors, including activation history, neuroactive factors in circulation, or changes in channel function. This selective inhibition would effectively reduce the excitatory input to the postganglionic neurons, thereby modulating the overall sympathetic tone. The rationale behind this could be twofold: to prevent overstimulation of target organs and tissues, ensuring a balanced autonomic response, and to conserve energy by reducing unnecessary neurotransmitter release and axonal firing. This process might be particularly important in maintaining homeostasis, where the precise regulation of sympathetic activity is crucial for organismal health and adaptive responses to environmental changes.

6.2 Modulation via factors in circulation

In our research, we have successfully demonstrated that preganglionic conduction can be modulated by circulating factors such as 5-HT and GABA. The reduction of SPN spike

propagation by 5-HT suggests its physiological role in decreasing sympathetic drive. It is well documented in the literature that 5-HT levels rise after meals and shortly after darkness sets in, highlighting its regulatory impact on sympathetic activity in response to nutritional and circadian cues[310]. Regarding GABAA receptor modulators, this thesis did not investigate the effects of neurosteroids on $GABA_A$ receptors directly. However, it is plausible that circulating neurosteroids may act on SPN spike conduction[311-313]. GABA may act as an excitatory agent, amplifying SPN responsiveness and elevating sympathetic activity. This heightened activity is crucial during emergency situations or conditions requiring increased physiological performance. The application of the neurosteroid pregnanolone, which serves as a positive allosteric modulator for $GABA_A$ receptors, can illustrate this effect.

6.3 Thermo-dysfunction

In individuals with spinal cord injury (SCI), who frequently suffer from thermoregulatory dysfunction, understanding the relationship between body temperature and conduction in SPNs is crucial. SCI disrupts sympathetic autonomic control, leading to impaired regulation of blood flow and body temperature, making individuals susceptible to both hypothermia and hyperthermia[213,214 213,214]. Research has indicated that deviations from normal body temperature can significantly affect spike conduction in neural pathways [83], posing a particular risk for those with SCI. Interestingly, in the context of thermoregulatory dysfunction, lower body temperatures (hypothermia) might lead to increased conduction at SPN branch points, potentially resulting in excessive sympathetic output. This could manifest as overcompensation in physiological responses, such as increased blood vessel constriction, which might further challenge, or adaptively augment the body's ability to maintain a stable temperature. Conversely, elevated body temperatures (hyperthermia) could lead to decreased conduction in these axons,

diminishing the sympathetic response when it might be needed to dissipate heat via sweating, by may adaptively augment heat dissipation by maximizing vasodilation. Future research focusing on the effects of temperature changes on conduction, particularly at branch points or along unmyelinated axons in SPNs within the 33-39°C range -reflecting hypo- or hyperthermia conditions post-SCI - will be informative and clinically-relevant. For example, pharmacologic control of K_V and K_2P leak channels could be an effective strategy to modulate output strength by alterations in preganglionic conduction.

In conclusion, our research sheds light on the intricate mechanisms modulating SPN axon activity, paving the way for a deeper understanding of neuronal communication and potential therapeutic targets.

7 References

1 Rezajooi, K. *et al.* NG2 proteoglycan expression in the peripheral nervous system: upregulation following injury and comparison with CNS lesions. *Molecular and cellular neurosciences* **25**, 572-584, doi:10.1016/j.mcn.2003.10.009 (2004).

2 Wu, H.-F. *et al.* Norepinephrine transporter defects lead to sympathetic hyperactivity in Familial Dysautonomia models. *Nat Commun* **13**, 7032 (2022).

3 McLachlan, E. M. Transmission of signals through sympathetic ganglia--modulation, integration or simply distribution? *Acta physiologica Scandinavica* **177**, 227-235, doi:10.1046/j.1365-201X.2003.01075.x (2003).

4 Wehrwein, E. A., Orer, H. S. & Barman, S. M. Overview of the Anatomy, Physiology, and Pharmacology of the Autonomic Nervous System. *Comprehensive Physiology*, doi:doi:10.1002/cphy.c150037 (2016).

5 Langley, J. N. *The autonomic nervous system*. (W. Heffer, 1921).

6 Janig, W. *The Integrative Action of the Autonomic Nervous System*. (Cambridge University Press, 2006).

7 Bartness, T. J., Vaughan, C. H. & Song, C. K. Sympathetic and sensory innervation of brown adipose tissue. *International journal of obesity (2005)* **34 Suppl 1**, S36-42, doi:10.1038/ijo.2010.182 (2010).

8 Vaughan, C. H., Zarebidaki, E., Ehlen, J. C. & Bartness, T. J. Analysis and measurement of the sympathetic and sensory innervation of white and brown adipose tissue. *Methods in enzymology* **537**, 199-225, doi:10.1016/B978-0-12-411619-1.00011-2 (2014).

9 Espinosa-Medina, I. *et al.* The sacral autonomic outflow is sympathetic. *Science (New York, N.Y.)* **354**, 893-897, doi:10.1126/science.aah5454 (2016).

10 Guyenet, P. G. The sympathetic control of blood pressure. *Nat Rev Neurosci.* **7**, 335-346. (2006).

11 Shafton, A. D., Oldfield, B. J. & McAllen, R. M. CRF-like immunoreactivity selectively labels preganglionic sudomotor neurons in cat. *Brain research* **599**, 253-260, doi:10.1016/0006-8993(92)90399-t (1992).

12 Nagashima, K., Nakai, S., Tanaka, M. & Kanosue, K. Neuronal circuitries involved in thermoregulation. *Autonomic neuroscience : basic & clinical* **85**, 18-25, doi:10.1016/s1566-0702(00)00216-2 (2000).

13 Janig, W. & McLachlan, E. M. Identification of distinct topographical distributions of lumbar sympathetic and sensory neurons projecting to end organs with different functions in the cat. *The Journal of comparative neurology* **246**, 104-112, doi:10.1002/cne.902460107 (1986).

14 Gibbins, I. Functional organization of autonomic neural pathways. *Organogenesis* **9**, 169-175, doi:10.4161/org.25126 (2013).

15 Janig, W. & Habler, H. J. Neurophysiological analysis of target-related sympathetic pathways--from animal to human: similarities and differences. *Acta physiologica Scandinavica* **177**, 255-274, doi:10.1046/j.1365-201X.2003.01088.x (2003).

16 Zimmerman, A. L., Sawchuk, M. & Hochman, S. Monoaminergic modulation of spinal viscero-sympathetic function in the neonatal mouse thoracic spinal cord. *PloS one* **7**, e47213, doi:10.1371/journal.pone.0047213 (2012).

17 Martin, L. J. *et al.* The mitochondrial permeability transition pore in motor neurons: involvement in the pathobiology of ALS mice. *Experimental neurology* **218**, 333-346, doi:10.1016/j.expneurol.2009.02.015 (2009).

18 Cabot, J. B., Alessi, V., Carroll, J. & Ligorio, M. Spinal cord lamina V and lamina VII interneuronal projections to sympathetic preganglionic neurons. *The Journal of comparative neurology* **347**, 515-530, doi:10.1002/cne.903470404 (1994).

19 Deuchars, S. A. Multi-tasking in the spinal cord--do 'sympathetic' interneurones work harder than we give them credit for? *The Journal of physiology* **580**, 723-729, doi:10.1113/jphysiol.2007.129429 (2007).

20 Deuchars, S. A. & Lall, V. K. Sympathetic preganglionic neurons: properties and inputs. *Comprehensive Physiology* **5**, 829-869, doi:10.1002/cphy.c140020 (2015).

21 Donoghue, S., Felder, R. B., Jordan, D. & Spyer, K. M. The central projections of carotid baroreceptors and chemoreceptors in the cat: a neurophysiological study. *The Journal of physiology* **347**, 397-409, doi:10.1113/jphysiol.1984.sp015072 (1984).

22 Petras, J. M. & Faden, A. I. The origin of sympathetic preganglionic neurons in the dog. *Brain research* **144**, 353-357, doi:10.1016/0006-8993(78)90160-9 (1978).

23 Rando, T. A., Bowers, C. W. & Zigmond, R. E. Localization of neurons in the rat spinal cord which project to the superior cervical ganglion. *The Journal of comparative neurology* **196**, 73-83, doi:10.1002/cne.901960107 (1981).

24 Hall, J. E. & Hall, M. E. *Guyton and Hall textbook of medical physiology e-Book*. (Elsevier Health Sciences, 2020).

25 Lichtman, J. W., Purves, D. & Yip, J. W. Innervation of sympathetic neurones in the guinea-pig thoracic chain. *J Physiol.* **298**, 285-299. (1980).

26 Nja, A. & Purves, D. Specific innervation of guinea-pig superior cervical ganglion cells by preganglionic fibres arising from different levels of the spinal cord. *The Journal of physiology* **264**, 565-583 (1977).

27 Lichtman, J. W., Purves, D. & Yip, J. W. On the purpose of selective innervation of guinea-pig superior cervical ganglion cells. *J Physiol.* **292**, 69-84. (1979).

28 Sah, P. & McLachlan, E. M. Membrane properties and synaptic potentials in rat sympathetic preganglionic neurons studied in horizontal spinal cord slices in vitro. *Journal of the autonomic nervous system* **53**, 1-15 (1995).

29 Anderson, C. R., McLachlan, E. M. & Srb-Christie, O. Distribution of sympathetic preganglionic neurons and monoaminergic nerve terminals in the spinal cord of the rat. *The Journal of comparative neurology* **283**, 269-284, doi:10.1002/cne.902830208 (1989).

30 Rubin, E. Development of the rat superior cervical ganglion: ingrowth of preganglionic axons. *The Journal of Neuroscience* **5**, 685, doi:10.1523/JNEUROSCI.05-03-00685.1985 (1985).

31 Forehand, C., Ezerman, E., Rubin, E. & Glover, J. Segmental patterning of rat and chicken sympathetic preganglionic neurons: correlation between soma position and axon projection pathway. *The Journal of Neuroscience* **14**, 231-241, doi:10.1523/jneurosci.14-01-00231.1994 (1994).

32 Feldberg, W. & Gaddum, J. H. The chemical transmitter at synapses in a sympathetic ganglion. *The Journal of physiology* **81**, 305-319, doi:10.1113/jphysiol.1934.sp003137 (1934).

33 Munhoz, C. D. *et al.* Stress-induced neuroinflammation: mechanisms and new pharmacological targets. *Brazilian journal of medical and biological research = Revista*

brasileira de pesquisas medicas e biologicas / Sociedade Brasileira de Biofisica ... [et al.] **41**, 1037-1046 (2008).

34 Skok, V. I. Nicotinic acetylcholine receptors in autonomic ganglia. *Auton Neurosci.* **97**, 1-11. (2002).

35 Del Signore, A., Gotti, C., Rizzo, A., Moretti, M. & Paggi, P. Nicotinic acetylcholine receptor subtypes in the rat sympathetic ganglion: pharmacological characterization, subcellular distribution and effect of pre- and postganglionic nerve crush. *Journal of neuropathology and experimental neurology* **63**, 138-150, doi:10.1093/jnen/63.2.138 (2004).

36 McKinnon, M. *Characterization of Thoracic Sympathetic Postganglionic Neurons* Emory University School of Medicine, (2019).

37 Jänig, W. in *The Integrative Action of the Autonomic Nervous System: Neurobiology of Homeostasis* (ed Wilfrid Jänig) 167-199 (Cambridge University Press, 2022).

38 Laskey, W. & Polosa, C. Characteristics of the sympathetic preganglionic neuron and its synaptic input. *Progress in neurobiology* **31**, 47-84 (1988).

39 Wang, S. *et al.* Ablation of TRPV1+ afferent terminals by capsaicin mediates long-lasting analgesia for trigeminal neuropathic pain. *eneuro*, ENEURO.0118-0120., doi:10.1523/eneuro.0118-20.2020 (2020).

40 Baldwin, C., Sasek, C. A. & Zigmond, R. E. Evidence that some preganglionic sympathetic neurons in the rat contain vasoactive intestinal peptide- or peptide histidine isoleucine amide-like immunoreactivities. *Neuroscience* **40**, 175-184, doi:10.1016/0306-4522(91)90183-o (1991).

41 Yamamoto, K., Senba, E., Matsunaga, T. & Tohyama, M. Calcitonin gene-related peptide containing sympathetic preganglionic and sensory neurons projecting to the superior cervical ganglion of the rat. *Brain research* **487**, 158-164, doi:10.1016/0006-8993(89)90952-9 (1989).

42 Dun, N. J., Dun, S. L. & Hwang, L. L. Nociceptin-like immunoreactivity in autonomic nuclei of the rat spinal cord. *Neuroscience letters* **234**, 95-98, doi:10.1016/s0304-3940(97)00666-6 (1997).

43 Dun, S. L., Chianca, D. A., Jr., Dun, N. J., Yang, J. & Chang, J. K. Differential expression of cocaine- and amphetamine-regulated transcript-immunoreactivity in the rat spinal preganglionic nuclei. *Neuroscience letters* **294**, 143-146 (2000).

44 Gonsalvez, D. G., Kerman, I. A., McAllen, R. M. & Anderson, C. R. Chemical coding for cardiovascular sympathetic preganglionic neurons in rats. *The Journal of neuroscience : the official journal of the Society for Neuroscience* **30**, 11781-11791, doi:10.1523/JNEUROSCI.0796-10.2010 (2010).

45 Dun, N. J. *et al.* Nitric oxide synthase immunoreactivity in the rat, mouse, cat and squirrel monkey spinal cord. *Neuroscience* **54**, 845-857 (1993).

46 Blum, J. A. *et al.* Single-cell transcriptomic analysis of the adult mouse spinal cord reveals molecular diversity of autonomic and skeletal motor neurons. *Nature neuroscience*, doi:10.1038/s41593-020-00795-0 (2021).

47 Alkaslasi, M. R. *et al.* Single nucleus RNA-sequencing defines unexpected diversity of cholinergic neuron types in the adult mouse spinal cord. *Nat Commun* **12**, 2471, doi:10.1038/s41467-021-22691-2 (2021).

48 Skok, V. I. & Ivanov, A. Y. What is the ongoing activity of sympathetic neurons? *Journal of the autonomic nervous system* **7**, 263-270, doi:https://doi.org/10.1016/0165-1838(83)90079-6 (1983).

49 Hirst, G. D. & McLachlan, E. M. Development of dendritic calcium currents in ganglion cells of the rat lower lumbar sympathetic chain. *The Journal of physiology* **377**, 349-368 (1986).

50 Janig, W. & McLachlan, E. M. Characteristics of function-specific pathways in the sympathetic nervous system. *Trends in neurosciences* **15**, 475-481 (1992).

51 Karila, P. & Horn, J. P. Secondary nicotinic synapses on sympathetic B neurons and their putative role in ganglionic amplification of activity. *Journal of Neuroscience* **20**, 908-918 (2000).

52 Jänig, W. in *Autonomic ganglia* 349-395 (Harwood Academic Publishers, 1995).

53 Bratton, B., Davies, P., Janig, W. & McAllen, R. Ganglionic transmission in a vasomotor pathway studied in vivo. *J Physiol.* **588**, 1647-1659. doi: 1610.1113/jphysiol.2009.185025. Epub 182010 Mar 185022. (2010).

54 Blackman, J. G. & Purves, R. D. Intracellular recordings from ganglia of the thoracic sympathetic chain of the guinea-pig. *J Physiol.* **203**, 173-198. (1969).

55 Gibbins, I. L., Jobling, P., Messenger, J. P., Teo, E. H. & Morris, J. L. Neuronal morphology and the synaptic organisation of sympathetic ganglia. *Journal of the autonomic nervous system* **81**, 104-109 (2000).

56 Janig, W. in *The Integrative Action of the Autonomic Nervous System: Neurobiology of Homeostasis* (ed Wilfrid Jänig) i-i (Cambridge University Press, 2022).

57 Boyd, H. D., McLachlan, E. M., Keast, J. R. & Inokuchi, H. Three electrophysiological classes of guinea pig sympathetic postganglionic neurone have distinct morphologies. *The Journal of comparative neurology* **369**, 372-387, doi:10.1002/(SICI)1096-9861(19960603)369:3<372::AID-CNE4>3.0.CO;2-2 (1996).

58 Gibbins, I. L., Jobling, P., Teo, E. H., Matthew, S. E. & Morris, J. L. Heterogeneous expression of SNAP-25 and synaptic vesicle proteins by central and peripheral inputs to sympathetic neurons. *The Journal of comparative neurology* **459**, 25-43, doi:10.1002/cne.10527 (2003).

59 Gibbins, I. L. & Morris, J. L. Structure of peripheral synapses: autonomic ganglia. *Cell and tissue research* **326**, 205-220, doi:10.1007/s00441-006-0233-1 (2006).

60 McLachlan, E. M., Davies, P. J., Häbler, H. J. & Jamieson, J. On-going and reflex synaptic events in rat superior cervical ganglion cells. *The Journal of physiology* **501 (Pt 1)**, 165-181, doi:10.1111/j.1469-7793.1997.165bo.x (1997).

61 Rimmer, K. & Horn, J. P. Weak and straddling secondary nicotinic synapses can drive firing in rat sympathetic neurons and thereby contribute to ganglionic amplification. *Frontiers in neurology* **1**, 130, doi:10.3389/fneur.2010.00130 (2010).

62 Zhu, Z. R. *et al.* Conduction failures in rabbit saphenous nerve unmyelinated fibers. *Neurosignals* **17**, 181-195, doi:10.1159/000209279 (2009).

63 Westerfield, M., Joyner, R. W. & Moore, J. W. Temperature-sensitive conduction failure at axon branch points. *Journal of neurophysiology* **41**, 1-8, doi:10.1152/jn.1978.41.1.1 (1978).

64 Purves, D. & Lichtman, J. W. Geometrical differences among homologous neurons in mammals. *Science (New York, N.Y.)* **228**, 298-302 (1985).

65 Langley, J. N. On axon-reflexes in the pre-ganglionic fibres of the sympathetic system. *The Journal of physiology* **25**, 364-398, doi:10.1113/jphysiol.1900.sp000803 (1900).

66 Purves, D., Rubin, E., Snider, W. & Lichtman, J. Relation of animal size to convergence, divergence, and neuronal number in peripheral sympathetic pathways. *The Journal of Neuroscience* **6**, 158-163, doi:10.1523/jneurosci.06-01-00158.1986 (1986).

67 Bucher, D. & Goaillard, J. M. Beyond faithful conduction: short-term dynamics, neuromodulation, and long-term regulation of spike propagation in the axon. *Progress in neurobiology* **94**, 307-346, doi:10.1016/j.pneurobio.2011.06.001 (2011).

68 Debanne, D. Information processing in the axon. *Nature Reviews Neuroscience* **5**, 304-316, doi:10.1038/nrn1397 (2004).

69 Swadlow, H., Kocsis, J. & Waxman, S. Modulation of Impulse Conduction Along the Axonal Tree. *Annual Review of Biophysics and Bioengineering* **9**, 143-179, doi:10.1146/annurev.bb.09.060180.001043 (1980).

70 Donadio, V. & Liguori, R. Microneurographic recording from unmyelinated nerve fibers in neurological disorders: An update. *Clinical Neurophysiology* **126**, 437-445, doi:https://doi.org/10.1016/j.clinph.2014.10.009 (2015).

71 Serra, J., Campero, M., Ochoa, J. & Bostock, H. Activity-dependent slowing of conduction differentiates functional subtypes of C fibres innervating human skin. *The Journal of physiology* **515 (Pt 3)**, 799-811 (1999).

72 Debanne, D., Campanac, E., Bialowas, A., Carlier, E. & Alcaraz, G. Axon physiology. *Physiological reviews* **91**, 555-602, doi:10.1152/physrev.00048.2009 (2011).

73 Lewis, J. C. & Burton, P. R. Ultrastructural studies of the superior cervical trunk of the mouse: Distribution, cytochemistry and stability of fibrous elements in preganglionic

fibers. *Journal of Comparative Neurology* **171**, 605-618, doi:10.1002/cne.901710411 (1977).

74 Ebbesson, S. O. E. A quantitative study of human superior cervical sympathetic ganglia. *The Anatomical record* **146**, 353-356, doi:https://doi.org/10.1002/ar.1091460408 (1963).

75 Low, P. A., Dyck, P. J. J. J. o. N. & Neurology, E. Splanchnic preganglionic neurons in man: III. Morphometry of Myelinated Fibers of Rami Communicantes. *Journal of Neuropathology & Experimental Neurology* **37**, 734-740 (1978).

76 Gasser, H. S. The classification of nerve fibers. (1941).

77 Pinto, V., Szucs, P., Derkach, V. A. & Safronov, B. V. Monosynaptic convergence of C- and Adelta-afferent fibres from different segmental dorsal roots on to single substantia gelatinosa neurones in the rat spinal cord. *The Journal of physiology* **586**, 4165-4177, doi:10.1113/jphysiol.2008.154898 (2008).

78 Llewellyn-Smith, I. J., Pilowsky, P., Minson, J. B. & Chalmers, J. Synapses on axons of sympathetic preganglionic neurons in rat and rabbit thoracic spinal cord. *The Journal of comparative neurology* **354**, 193-208, doi:10.1002/cne.903540204 (1995).

79 Blackman, J. G., Crowcroft, P. J., Devine, C. E., Holman, M. E. & Yonemura, K. Transmission from pregnanglionic fibres in the hypogastric nerve to peripheral ganglia of male guinea-pigs. *The Journal of physiology* **201**, 723-743 (1969).

80 Cassell, J. F. & McLachlan, E. M. The effect of a transient outward current (IA) on synaptic potentials in sympathetic ganglion cells of the guinea-pig. *J Physiol.* **374**, 273-288. (1986).

81 Gilbey, M. P., Peterson, D. F. & Coote, J. H. Some characteristics of sympathetic preganglionic neurones in the rat. *Brain research* **241**, 43-48 (1982).

82 Jobling, P. & Gibbins, I. L. Electrophysiological and morphological diversity of mouse sympathetic neurons. *Journal of neurophysiology* **82**, 2747-2764 (1999).

83 Pekala, D., Szkudlarek, H. & Raastad, M. Typical gray matter axons in mammalian brain fail to conduct action potentials faithfully at fever-like temperatures. *Physiological Reports* **4**, e12981, doi:10.14814/phy2.12981 (2016).

84 Perge, J. A., Koch, K., Miller, R., Sterling, P. & Balasubramanian, V. How the Optic Nerve Allocates Space, Energy Capacity, and Information. **29**, 7917-7928, doi:10.1523/JNEUROSCI.5200-08.2009 %J The Journal of Neuroscience (2009).

85 Hursh, J. B. Conduction velocity and diameter of nerve fibers. *American Journal of Physiology* **127**, 131-139 (1939).

86 Perge, J. A., Niven, J. E., Mugnaini, E., Balasubramanian, V. & Sterling, P. Why Do Axons Differ in Caliber? *The Journal of Neuroscience* **32**, 626-638, doi:10.1523/jneurosci.4254-11.2012 (2012).

87 Low, P. A. & Dyck, P. J. J. A. N. Splanchnic preganglionic neurons in man: II. Morphometry of myelinated fibers of T7 ventral spinal root. *Acta neuropath. (Berl.)* **40**, 219-225 (1977).

88 Clifton, G. L., Coggeshall, R. E., Vance, W. H. & Willis, W. D. Receptive fields of unmyelinated ventral root afferent fibres in the cat. *The Journal of physiology* **256**, 573-600 (1976).

89 Rubin, E. Development of the rat superior cervical ganglion: ganglion cell maturation. *The Journal of Neuroscience* **5**, 673, doi:10.1523/JNEUROSCI.05-03-00673.1985 (1985).

90 Schafer, T., Schwab, M. E. & Thoenen, H. Increased formation of preganglionic synapses and axons due to a retrograde trans-synaptic action of nerve growth factor in the rat sympathetic nervous system. *The Journal of neuroscience : the official journal of the Society for Neuroscience* **3**, 1501-1510 (1983).

91 Goldstein, S. S. & Rall, W. Changes of action potential shape and velocity for changing core conductor geometry. *Biophysical journal* **14**, 731-757, doi:10.1016/s0006-3495(74)85947-3 (1974).

92 Levy, R. A. Presynaptic control of input to the central nervous system *Canadian Journal of Physiology and Pharmacology* **58**, 751-766 (1980).

93 Jaffey, D. M., McAdams, J., Baronowsky, E. A., Black, D. & Powley, T. L. Vagal preganglionic axons arborize in the myenteric plexus into two types: nitrergic and non-nitrergic postganglionic motor pools? *American Journal of Physiology-Regulatory, Integrative and Comparative Physiology* **324**, R305-R316 (2023).

94 Mirgorodsky, V. N. & Skok, V. I. Intracellular potentials recorded from a tonically active mammalian sympathetic ganglion. *Brain research* **15**, 570-572, doi:10.1016/0006-8993(69)90187-5 (1969).

95 Mannard, A. & Polosa, C. Analysis of background firing of single sympathetic preganglionic neurons of cat cervical nerve. *Journal of neurophysiology* **36**, 398-408, doi:10.1152/jn.1973.36.3.398 (1973).

96 Bronk, D., Lewy, F. & Larrabee, M. The hypothalamic control of sympathetic rhythms. *American Journal of Physiology* (1936).

97 Gernandt, B. & Zotterman, Y. The Effect of Respiratory Changes upon the Spontaneous Injury Discharge of Afferent Mammalian and Human Nerve Fibres. *Acta physiologica Scandinavica* **11**, 248-259 (1946).

98 Kahn, N. & Mills, E. Centrally evoked sympathetic discharge: a functional study of medullary vasomotor areas. *The Journal of physiology* **191**, 339-352 (1967).

99 Kaneko, Y., McCubbin, J. W. & Page, I. H. Central inhibition of vasomotor activity by guanethidine. *Journal of Pharmacology and Experimental Therapeutics* **135**, 21-24 (1962).

100 Hagbarth, K. E. & Vallbo, Å. Pulse and respiratory grouping of sympathetic impulses in human muscle nerves. *Acta physiologica Scandinavica* **74**, 96-108 (1968).

101 Widdicombe, J. Action potentials in parasympathetic and sympathetic efferent fibres to the trachea and lungs of dogs and cats. *The Journal of physiology* **186**, 56-88 (1966).

102 Adrian, E., Bronk, D. W. & Phillips, G. Discharges in mammalian sympathetic nerves. *The Journal of physiology* **74**, 115 (1932).

103 Polosa, C., Rosenberg, P., Mannard, A., Wolkove, N. & Wyszogrodski, I. Oscillatory behavior of the sympathetic system induced by picrotoxin. *Canadian journal of physiology and pharmacology* **47**, 815-826 (1969).

104 Cohen, M. I. & Gootman, P. M. Periodicities in efferent discharge of splanchnic nerve of the cat. *American Journal of Physiology-Legacy Content* **218**, 1092-1101 (1970).

105 McCall, R. B. & Gebber, G. L. Brain stem and spinal synchronization of sympathetic nervous discharge. *Brain research* **89**, 139-143, doi:https://doi.org/10.1016/0006-8993(75)90141-9 (1975).

106 Su, C. K., Cheng, Y. W. & Lin, S. Biophysical and histological determinants underlying natural firing behaviors of splanchnic sympathetic preganglionic neurons in neonatal rats. *Neuroscience* **150**, 926-937, doi:https://doi.org/10.1016/j.neuroscience.2007.10.011 (2007).

107 Stalbovskiy, A. O., Briant, L. J., Paton, J. F. & Pickering, A. E. Mapping the cellular electrophysiology of rat sympathetic preganglionic neurones to their roles in cardiorespiratory reflex integration: a whole cell recording study in situ. *The Journal of physiology* **592**, 2215-2236, doi:10.1113/jphysiol.2014.270769 (2014).

108 Dembowsky, K., Czachurski, J. & Seller, H. Morphology of sympathetic preganglionic neurons in the thoracic spinal cord of the cat: an intracellular horseradish peroxidase study. *The Journal of comparative neurology* **238**, 453-465, doi:10.1002/cne.902380409 (1985).

109 Dembowsky, K., Czachurski, J. & Seller, H. An intracellular study of the synaptic input to sympathetic preganglionic neurones of the third thoracic segment of the cat. *Journal of the autonomic nervous system* **13**, 201-244, doi:https://doi.org/10.1016/0165-1838(85)90012-8 (1985).

110 Gilbey, M. P., Numao, Y. & Spyer, K. M. Discharge patterns of cervical sympathetic preganglionic neurones related to central respiratory drive in the rat. **378**, 253-265, doi:10.1113/jphysiol.1986.sp016218 (1986).

111 Boczek-Funcke, A. *et al.* Classification of preganglionic neurones projecting into the cat cervical sympathetic trunk. *The Journal of physiology* **453**, 319-339, doi:10.1113/jphysiol.1992.sp019231 (1992).

112 Dembowsky, K., Czachurski, J. & Seller, H. Three types of sympathetic preganglionic neurones with different electrophysiological properties are identified by intracellular recordings in the cat. *Pflugers Archiv : European journal of physiology* **406**, 112-120, doi:10.1007/bf00586671 (1986).

113 Spanswick, D. & Logan, S. D. Sympathetic preganglionic neurones in neonatal rat spinal cord in vitro: electrophysiological characteristics and the effects of selective excitatory amino acid receptor agonists. *Brain research* **525**, 181-188 (1990).

114 Pickering, A. E., Spanswick, D. & Logan, S. D. Whole-cell recordings from sympathetic preganglionic neurons in rat spinal cord slices. *Neuroscience letters* **130**, 237-242 (1991).

115 Lewis, D. I. & Coote, J. H. Electrophysiological characteristics of vasomotor preganglionic neurons and related neurons in the thoracic spinal cord of the rat: An intracellular study in vivo. *Neuroscience* **152**, 534-546, doi:https://doi.org/10.1016/j.neuroscience.2007.10.022 (2008).

116 Inokuchi, H. *et al.* Membrane properties and dendritic arborization of the intermediolateral nucleus neurons in the guinea-pig thoracic spinal cord in vitro. *Journal of the autonomic nervous system* **43**, 97-106 (1993).

117 Gladwell, S. J. & Coote, J. H. Fast excitatory post synaptic potentials and their response to catecholaminergic antagonists in rat sympathetic preganglionic neurones in vitro. *Neuroscience letters* **268**, 89-92 (1999).

118 Coote, J. H. & Westbury, D. R. Intracellular recordings from sympathetic preganglionic neurones. *Neuroscience letters* **15**, 171-175, doi:https://doi.org/10.1016/0304-3940(79)96108-1 (1979).

119 Wilson, J. M., Coderre, E., Renaud, L. P. & Spanswick, D. Active and passive membrane properties of rat sympathetic preganglionic neurones innervating the adrenal medulla. *The Journal of physiology* **545**, 945-960 (2002).

120 Zimmerman, A., Bai, L. & Ginty, D. D. The gentle touch receptors of mammalian skin. *Science (New York, N.Y.)* **346**, 950-954, doi:10.1126/science.1254229 (2014).

121 Zimmermann, J. B. & Jackson, A. Closed-loop control of spinal cord stimulation to restore hand function after paralysis. *Frontiers in neuroscience* **8**, 87, doi:10.3389/fnins.2014.00087 (2014).

122 Gladwell, S. J. & Coote, J. H. Evidence that the firing pattern of sympathetic preganglionic neurones is determined by an interaction between amines and an excitatory amino acid. *Neurosci Lett.* **268**, 89-92. (1999).

123 Minoura, Y., Onimaru, H., Iigaya, K. & Kobayashi, Y. Modulation of sympathetic preganglionic neuron activity via adrenergic receptors. *Hypertension Research* **41**, 499-505, doi:10.1038/s41440-018-0049-x (2018).

124 Sacchi, O. & Perri, V. Quantal release of acetylcholine from the nerve endings of the guinea-pig superior cervical ganglion. *Pflugers Archiv : European journal of physiology* **329**, 207-219, doi:10.1007/bf00586615 (1971).

125 Bennett, M. R. & McLachlan, E. M. An electrophysiological analysis of the synthesis of acetylcholine in preganglionic nerve terminals. *The Journal of physiology* **221**, 669-682, doi:10.1113/jphysiol.1972.sp009775 (1972).

126 Macefield, V. G. On the number of preganglionic neurons driving human postganglionic sympathetic neurons: a comparison of modeling and empirical data. *Frontiers in neuroscience* **5**, 132, doi:10.3389/fnins.2011.00132 (2011).

127 Polosa, C., Yoshimura, M. & Nishi, S. Electrophysiological Properties of Sympathetic Preganglionic Neurons. *Annual review of physiology* **50**, 541-551, doi:10.1146/annurev.ph.50.030188.002545 (1988).

128 Wyszogrodski, I. & Polosa, C. The inhibition of sympathetic preganglionic neurons by somatic afferents. *Canadian journal of physiology and pharmacology* **51**, 29-38, doi:10.1139/y73-005 (1973).

129 Rohlicek, C. V. & Polosa, C. Neural effects of systemic hypoxia and hypercapnia on hindlimb vascular resistance in acute spinal cats. *Pflügers Archiv European Journal of Physiology* **406**, 392-396 (1986).

130 Pickering, A. E., Spanswick, D. & Logan, S. D. 5-Hydoxytryptamine evokes depolarizations and membrane potential oscillations in rat sympathetic preganglionic neurones. *The Journal of physiology* **480 (Pt 1)**, 109-121 (1994).

131 Marina, N., Taheri, M. & Gilbey, M. P. Generation of a physiological sympathetic motor rhythm in the rat following spinal application of 5-HT. *The Journal of physiology* **571**, 441-450, doi:10.1113/jphysiol.2005.100677 (2006).

132 Larrabee, M. G. & Bronk, D. W. Prolonged facilitation of synaptic excitation in sympathetic ganglia. *Journal of neurophysiology* **10**, 139-154, doi:10.1152/jn.1947.10.2.139 (1947).

133 Job, C. & Lundberg, A. On the significance of post- and pre-synaptic events for facilitation and inhibition in the sympathetic ganglion of the cat. *Acta physiologica Scandinavica* **28**, 14-28, doi:10.1111/j.1748-1716.1953.tb00956.x (1953).

134 Morita, K., North, R. A. & Tokimasa, T. Muscarinic presynaptic inhibition of synaptic transmission in myenteric plexus of guinea-pig ileum. *The Journal of physiology* **333**, 141-149, doi:10.1113/jphysiol.1982.sp014444 (1982).

135 McLachlan, E. M. An analysis of the release of acetylcholine from preganglionic nerve terminals. *J Physiol.* **245**, 447-466. (1975).

136 Bachoo, M. & Polosa, C. The pattern of sympathetic neurone activity during expiration in the cat. *The Journal of physiology* **378**, 375-390 (1986).

137 Bronk, D. & Pumphrey, E. Response of a Sympathetic Ganglion to High Frequency Stimulation. *Proceedings of the Society for Experimental Biology and Medicine* **32**, 1661-1663 (1935).

138 Bourdois, P., McCandless, D. & MacIntosh, F. A prolonged after-effect of intense synaptic activity on acetylcholine in a sympathetic ganglion. *Canadian journal of physiology and pharmacology* **53**, 155-165 (1975).

139 Alkadhi, K. A. & McIsaac, R. J. Non-nicotinic transmission during ganglionic block with chlorisondamine and nicotine. *European journal of pharmacology* **24**, 78-85 (1973).

140 Bullock, T. H. Facilitation of conduction rate in nerve fibres. *The Journal of physiology* **114**, 89 (1951).

141 Waxman, S. G. & Swadlow, H. A. The conduction properties of axons in central white matter. *Progress in neurobiology* **8**, 297-324 (1977).

142 Barron, D. H. & Matthews, B. H. C. Intermittent conduction in the spinal cord. *The Journal of physiology* **85**, 73-103, doi:10.1113/jphysiol.1935.sp003303 (1935).

143 Krnjević, K. & Miledi, R. Presynaptic failure of neuromuscular propagation in rats. *The Journal of physiology* **149**, 1 (1959).

144 Grossman, Y., Parnas, I. & Spira, M. E. Differential conduction block in branches of a bifurcating axon. *The Journal of physiology* **295**, 283-305, doi:10.1113/jphysiol.1979.sp012969 (1979).

145 Aston-Jones, G., Segal, M. & Bloom, F. E. Brain aminergic axons exhibit marked variability in conduction velocity. *Brain research* **195**, 215-222 (1980).

146 Wessendorf, M. W., Proudfit, H. K. & Anderson, E. G. The identification of serotonergic neurons in the nucleus raphe magnus by conduction velocity. *Brain research* **214**, 168-173 (1981).

147 Gee, M. D., Lynn, B. & Cotsell, B. Activity-dependent slowing of conduction velocity provides a method for identifying different functional classes of C-fibre in the rat saphenous nerve. *Neuroscience* **73**, 667-675, doi:10.1016/0306-4522(96)00070-x (1996).

148 Obreja, O. *et al.* Patterns of activity-dependent conduction velocity changes differentiate classes of unmyelinated mechano-insensitive afferents including cold nociceptors, in pig and in human. *Pain.* **148**, 59-69. doi: 10.1016/j.pain.2009.1010.1006. Epub 2009 Nov 1013. (2010).

149 De Col, R., Messlinger, K. & Carr, R. W. Conduction velocity is regulated by sodium channel inactivation in unmyelinated axons innervating the rat cranial meninges. *The Journal of physiology* **586**, 1089-1103, doi:10.1113/jphysiol.2007.145383 (2008).

150 Brown, D. & Selyanko, A. Membrane currents underlying the cholinergic slow excitatory post‐synaptic potential in the rat sympathetic ganglion. *The Journal of physiology* **365**, 365-387 (1985).

151 McFARLANE, S. & Cooper, E. Postnatal development of voltage-gated K currents on rat sympathetic neurons. *Journal of neurophysiology* **67**, 1291-1300 (1992).

152 Bordey, A., Feltz, P. & Trouslard, J. Kinetics of A-currents in sympathetic preganglionic neurones and glial cells. *Neuroreport* **7**, 37-40 (1995).

153 Miyazaki, T., Dun, N. J., Kobayashi, H. & Tosaka, T. Voltage-dependent potassium currents of sympathetic preganglionic neurons in neonatal rat spinal cord thin slices. *Brain research* **743**, 1-10 (1996).

154 Belluzzi, O. & Sacchi, O. A quantitative description of the sodium current in the rat sympathetic neurone. *The Journal of physiology* **380**, 275-291, doi:https://doi.org/10.1113/jphysiol.1986.sp016285 (1986).

155 Vacher, H., Mohapatra, D. P. & Trimmer, J. S. Localization and targeting of voltage-dependent ion channels in mammalian central neurons. *Physiological reviews* **88**, 1407-1447, doi:10.1152/physrev.00002.2008 (2008).

156 Sotnikova, T. D. *et al.* The dopamine metabolite 3-methoxytyramine is a neuromodulator. *PLoS One.* **5**, e13452. doi: 13410.11371/journal.pone.0013452. (2010).

157 2021, F.-S.-s.

158 Boiko, T. *et al.* Compact myelin dictates the differential targeting of two sodium channel isoforms in the same axon. *Neuron* **30**, 91-104, doi:10.1016/s0896-6273(01)00265-3 (2001).

159 Trimmer, J. S. Subcellular localization of K+ channels in mammalian brain neurons: remarkable precision in the midst of extraordinary complexity. *Neuron* **85**, 238-256, doi:10.1016/j.neuron.2014.12.042 (2015).

160 Van Wart, A., Trimmer, J. S. & Matthews, G. Polarized distribution of ion channels within microdomains of the axon initial segment. *The Journal of comparative neurology* **500**, 339-352, doi:10.1002/cne.21173 (2007).

161 Cooper, E. C., Milroy, A., Jan, Y. N., Jan, L. Y. & Lowenstein, D. H. Presynaptic localization of Kv1.4-containing A-type potassium channels near excitatory synapses in the hippocampus. *The Journal of neuroscience : the official journal of the Society for Neuroscience* **18**, 965-974, doi:10.1523/jneurosci.18-03-00965.1998 (1998).

162 Jerng, H. H., Pfaffinger, P. J. & Covarrubias, M. Molecular physiology and modulation of somatodendritic A-type potassium channels. *Molecular and cellular neurosciences* **27**, 343-369, doi:10.1016/j.mcn.2004.06.011 (2004).

163 Trimmer, J. S. & Rhodes, K. J. Localization of voltage-gated ion channels in mammalian brain. *Annual review of physiology* **66**, 477-519, doi:10.1146/annurev.physiol.66.032102.113328 (2004).

164 Devaux, J. *et al.* Kv3.1b is a novel component of CNS nodes. *The Journal of neuroscience : the official journal of the Society for Neuroscience* **23**, 4509-4518, doi:10.1523/jneurosci.23-11-04509.2003 (2003).

165 Laube, G. *et al.* Ultrastructural localization of Shaker-related potassium channel subunits and synapse-associated protein 90 to septate-like junctions in rat cerebellar Pinceaux. *Brain research. Molecular brain research* **42**, 51-61, doi:10.1016/s0169-328x(96)00120-9 (1996).

166 Chien, L. Y., Cheng, J. K., Chu, D., Cheng, C. F. & Tsaur, M. L. Reduced expression of A-type potassium channels in primary sensory neurons induces mechanical hypersensitivity. *The Journal of neuroscience : the official journal of the Society for Neuroscience* **27**, 9855-9865, doi:10.1523/JNEUROSCI.0604-07.2007 (2007).

167 Buniel, M., Glazebrook, P. A., Ramirez-Navarro, A. & Kunze, D. L. Distribution of voltage-gated potassium and hyperpolarization-activated channels in sensory afferent

fibers in the rat carotid body. *The Journal of comparative neurology* **510**, 367-377, doi:10.1002/cne.21796 (2008).

168 Vervaeke, K., Gu, N., Agdestein, C., Hu, H. & Storm, J. F. Kv7/KCNQ/M-channels in rat glutamatergic hippocampal axons and their role in regulation of excitability and transmitter release. *The Journal of physiology* **576**, 235-256, doi:10.1113/jphysiol.2006.111336 (2006).

169 Devaux, J. J., Kleopa, K. A., Cooper, E. C. & Scherer, S. S. KCNQ2 is a nodal K+ channel. *The Journal of neuroscience : the official journal of the Society for Neuroscience* **24**, 1236-1244, doi:10.1523/jneurosci.4512-03.2004 (2004).

170 Callewaert, G., Eilers, J. & Konnerth, A. Axonal calcium entry during fast 'sodium' action potentials in rat cerebellar Purkinje neurones. *The Journal of physiology* **495**, 641-647, doi:10.1113/jphysiol.1996.sp021622 (1996).

171 Bielefeldt, K. & Jackson, M. B. A calcium-activated potassium channel causes frequency-dependent action-potential failures in a mammalian nerve terminal. *Journal of neurophysiology* **70**, 284-298, doi:10.1152/jn.1993.70.1.284 (1993).

172 Lev-Ram, V. & Grinvald, A. Activity-dependent calcium transients in central nervous system myelinated axons revealed by the calcium indicator Fura-2. *Biophysical journal* **52**, 571-576, doi:10.1016/s0006-3495(87)83246-0 (1987).

173 Grafe, P., Quasthoff, S., Grosskreutz, J. & Alzheimer, C. Function of the hyperpolarization-activated inward rectification in nonmyelinated peripheral rat and human axons. *Journal of neurophysiology* **77**, 421-426 (1997).

174 Elliott, P., Marsh, S. J. & Brown, D. A. Inhibition of Ca-spikes in rat preganglionic cervical sympathetic nerves by sympathomimetic amines. *British journal of pharmacology* **96**, 65-76 (1989).

175 Blum, J. A. *et al.* Single-cell transcriptomic analysis of the adult mouse spinal cord. *bioRxiv*, 2020.2003.2016.992958, doi:10.1101/2020.03.16.992958 (2020).

176 Halder, M., McKinnon, M. L., Li, Y., Wenner, P. & Hochman, S. Isolation and Electrophysiology of Murine Sympathetic Postganglionic Neurons in the Thoracic Paravertebral Ganglia. *Bio-protocol* **11**, e4189, doi:10.21769/BioProtoc.4189 (2021).

177 Furlan, A. *et al.* Visceral motor neuron diversity delineates a cellular basis for nipple- and pilo-erection muscle control. *Nature neuroscience* **19**, 1331-1340, doi:10.1038/nn.4376 (2016).

178 Eccles, J. C. The action potential of the superior cervical ganglion. *The Journal of physiology* **85**, 179-206 172 (1935).

179 Erulkar, S. D. & Woodward, J. K. Intracellular recording from mammalian superior cervical ganglion in situ. *Journal of Physiology* **199**, 189-203, doi:10.1113/jphysiol.1968.sp008648 (1968).

180 Murray, J. G. & Thompson, J. W. Two types of synaptic selectivity and their interrelation during sprouting in the guinea-pig superior cervical ganglion. *J Physiol.* **135**, 133-162. (1957).

181 Cassell, J. F., Clark, A. L. & McLachlan, E. M. Characteristics of phasic and tonic sympathetic ganglion cells of the guinea-pig. *The Journal of physiology* **372**, 457-483 (1986).

182 Li, C. & Horn, J. P. Physiological classification of sympathetic neurons in the rat superior cervical ganglion. *Journal of neurophysiology* **95**, 187-195, doi:10.1152/jn.00779.2005 (2006).

183 Springer, M. G., Kullmann, P. H. & Horn, J. P. Virtual leak channels modulate firing dynamics and synaptic integration in rat sympathetic neurons: implications for ganglionic transmission in vivo. *The Journal of physiology* **593**, 803-823, doi:10.1113/jphysiol.2014.284125 (2015).

184 Staley, K. J., Otis, T. S. & Mody, I. Membrane properties of dentate gyrus granule cells: comparison of sharp microelectrode and whole-cell recordings. *Journal of neurophysiology* **67**, 1346-1358 (1992).

185 Rall, W. Core Conductor Theory and Cable Properties of Neurons. *Comprehensive Physiology*, doi:doi:10.1002/cphy.cp010103 (2011).

186 devices, M. Clampex 10.2 Tutorial.

187 Rubin, E. & Purves, D. Segmental organization of sympathetic preganglionic neurons in the mammalian spinal cord. *The Journal of comparative neurology* **192**, 163-174, doi:10.1002/cne.901920111 (1980).

188 Llewellyn, M. E., Thompson, K. R., Deisseroth, K. & Delp, S. L. Orderly recruitment of motor units under optical control in vivo. *Nature medicine* **16**, 1161-1165, doi:10.1038/nm.2228 (2010).

189 Zhang, H. Y. & Sillar, K. T. Short-term memory of motor network performance via activity-dependent potentiation of Na+/K+ pump function. *Current biology : CB* **22**, 526-531, doi:10.1016/j.cub.2012.01.058 (2012).

190 Dobretsov, M. & Stimers, J. R. Neuronal function and alpha3 isoform of the Na/K-ATPase. *Front Biosci* **10**, 2373-2396 (2005).

191 Hari, K. *et al.* GABA facilitates spike propagation through branch points of sensory axons in the spinal cord. *Nature neuroscience*, doi:10.1038/s41593-022-01162-x (2022).

192 Vyklicky, L. *et al.* Primary afferent depolarization and changes in extracellular potassium concentration induced by L-glutamate and L-proline in the isolated spinal cord of the frog. *Brain research* **117**, 153-156 (1976).

193 Shreckengost, J., Calvo, J., Quevedo, J. & Hochman, S. Bicuculline-sensitive primary afferent depolarization remains after greatly restricting synaptic transmission in the mammalian spinal cord. *The Journal of neuroscience : the official journal of the Society for Neuroscience* **30**, 5283-5288, doi:10.1523/jneurosci.3873-09.2010 (2010).

194 Cattaneo, A. & Capsoni, S. Painless Nerve Growth Factor: A TrkA biased agonist mediating a broad neuroprotection via its actions on microglia cells. *Pharmacological Research* **139**, 17-25, doi:https://doi.org/10.1016/j.phrs.2018.10.028 (2019).

195 Wang, F. B., Holst, M. C. & Powley, T. L. The ratio of pre- to postganglionic neurons and related issues in the autonomic nervous system. *Brain Res Brain Res Rev.* **21**, 93-115. (1995).

196 Cajal, S. R. y. *Cajal's Degeneration and Regeneration of the Nervous System*. (Oxford University Press, 1991).

197 Pinto, V., Szucs, P., Lima, D. & Safronov, B. V. Multisegmental Aδ- and C-Fiber Input to Neurons in Lamina I and the Lateral Spinal Nucleus. *The Journal of Neuroscience* **30**, 2384, doi:10.1523/JNEUROSCI.3445-09.2010 (2010).

198 Hodgkin, A. L. & Katz, B. The effect of temperature on the electrical activity of the giant axon of the squid. *The Journal of physiology* **109**, 240-249, doi:10.1113/jphysiol.1949.sp004388 (1949).

199 Arlow, R. L., Foutz, T. J. & McIntyre, C. C. Theoretical principles underlying optical stimulation of myelinated axons expressing channelrhodopsin-2. *Neuroscience* **248**, 541-551, doi:10.1016/j.neuroscience.2013.06.031 (2013).

200 Rattay, F. The basic mechanism for the electrical stimulation of the nervous system. *Neuroscience* **89**, 335-346 (1999).

201 Bostock, H., Sherratt, R. M. & Sears, T. A. Overcoming conduction failure in demyelinated nerve fibres by prolonging action potentials. *Nature* **274**, 385-387, doi:10.1038/274385a0 (1978).

202 Purves, D. & Lichtman, J. W. Elimination of synapses in the developing nervous system. *Science (New York, N.Y.)* **210**, 153, doi:10.1126/science.7414326 (1980).

203 Renganathan, M., Cummins, T. R. & Waxman, S. G. Nitric oxide blocks fast, slow, and persistent Na+ channels in C-type DRG neurons by S-nitrosylation. *Journal of neurophysiology* **87**, 761-775 (2002).

204 Rama, S., Zbili, M. & Debanne, D. Signal propagation along the axon. *Current opinion in neurobiology* **51**, 37-44, doi:https://doi.org/10.1016/j.conb.2018.02.017 (2018).

205 McAllen, R. M., Allen, A. M. & Bratton, B. O. A neglected 'accessory' vasomotor pathway: implications for blood pressure control. *Clinical and experimental pharmacology & physiology* **32**, 473-477, doi:10.1111/j.1440-1681.2005.04214.x (2005).

206 Mason, D. F. Depolarizing action of neostigmine at an autonomic ganglion. *British journal of pharmacology and chemotherapy* **18**, 572-587 (1962).

207 Wall, P. D. Control of impulse conduction in long range branches of afferents by increases and decreases of primary afferent depolarization in the rat. *The European journal of neuroscience* **6**, 1136-1142 (1994).

208 Stegeman, D. F. & De Weerd, J. P. C. Modelling compound action potentials of peripheral nerves in situ. II. A study of the influence of temperature. *Electroencephalography and clinical neurophysiology* **54**, 516-529, doi:https://doi.org/10.1016/0013-4694(82)90037-2 (1982).

209 Zhang, Y., Bucher, D. & Nadim, F. Ionic mechanisms underlying history-dependence of conduction delay in an unmyelinated axon. *eLife* **6**, e25382, doi:10.7554/eLife.25382 (2017).

210 Jänig, W. in *The Integrative Action of the Autonomic Nervous System: Neurobiology of Homeostasis* (ed Wilfrid Jänig) 397-402 (Cambridge University Press, 2022).

211 McKinnon, M. L. *et al.* Dramatically Amplified Thoracic Sympathetic Postganglionic Excitability and Integrative Capacity Revealed with Whole-Cell Patch-Clamp Recordings. *eNeuro* **6**, ENEURO.0433-0418.2019, doi:10.1523/ENEURO.0433-18.2019 (2019).

212 Maingret, F. *et al.* TREK-1 is a heat-activated background K+ channel. *The EMBO journal* **19**, 2483-2491, doi:https://doi.org/10.1093/emboj/19.11.2483 (2000).

213 Handrakis, J. P. *et al.* Effect of Mild Cold Exposure on Cognition in Persons with Tetraplegia. *Journal of neurotrauma* **32**, 1168-1175, doi:10.1089/neu.2014.3719 (2015).

214 Khan, S., Plummer, M., Martinez-Arizala, A. & Banovac, K. Hypothermia in patients with chronic spinal cord injury. *The journal of spinal cord medicine* **30**, 27-30 (2007).

215 Cabanac, M. & Massonnet, B. Thermoregulatory responses as a function of core temperature in humans. *The Journal of physiology* **265**, 587-596 (1977).

216 Attia, M. & Engel, P. Thermoregulatory set point in patients with spinal cord injuries (spinal man). *Paraplegia* **21**, 233-248, doi:10.1038/sc.1983.37 (1983).

217 Suda, I., Koizumi, K. & Brooks, C. M. Analysis of Effects of Hypothermia on Central Nervous System Responses. *American Journal of Physiology-Legacy Content* **189**, 373-380, doi:10.1152/ajplegacy.1957.189.2.373 (1957).

218 Johnson, C. D. & Gilbey, M. P. On the dominant rhythm in the discharges of single postganglionic sympathetic neurones innervating the rat tail artery. *The Journal of physiology* **497**, 241-259, doi:https://doi.org/10.1113/jphysiol.1996.sp021764 (1996).

219 Sminia, P., Zee, J. V. D., Wondergem, J. & Haveman, J. Effect of hyperthermia on the central nervous system: A review. *International Journal of Hyperthermia* **10**, 1-30, doi:10.3109/02656739409009328 (1994).

220 Bischoff, F. Conditions required to produce a prolonged hypothermia in the mouse. *Cancer research* **2**, 370-371 (1942).

221 Dietrich, W. D. & Bramlett, H. M. in *Progress in brain research* Vol. 162 (ed Hari Shanker Sharma) 201-217 (Elsevier, 2007).

222 Cadaveira-Mosquera, A., Ribeiro, S. J., Reboreda, A., Pérez, M. & Lamas, J. A. Activation of TREK Currents by the Neuroprotective Agent Riluzole in Mouse Sympathetic Neurons. *The Journal of Neuroscience* **31**, 1375-1385, doi:10.1523/jneurosci.2791-10.2011 (2011).

223 Reitman, M. L. Of mice and men - environmental temperature, body temperature, and treatment of obesity. *FEBS letters* **592**, 2098-2107, doi:10.1002/1873-3468.13070 (2018).

224 Hrvatin, S. *et al.* Neurons that regulate mouse torpor. *Nature* **583**, 115-121, doi:10.1038/s41586-020-2387-5 (2020).

225 Geiser, F. Metabolic rate and body temperature reduction during hibernation and daily torpor. *Annual review of physiology* **66**, 239-274, doi:10.1146/annurev.physiol.66.032102.115105 (2004).

226 Madden, C. J. & Morrison, S. F. A high-fat diet impairs cooling-evoked brown adipose tissue activation via a vagal afferent mechanism. *American journal of physiology. Endocrinology and metabolism* **311**, E287-292, doi:10.1152/ajpendo.00081.2016 (2016).

227 Enerbäck, S. The origins of brown adipose tissue. *The New England journal of medicine* **360**, 2021-2023, doi:10.1056/NEJMcibr0809610 (2009).

228 Francois, M. *et al.* Sympathetic innervation of the interscapular brown adipose tissue in mouse. *Annals of the New York Academy of Sciences* **1454**, 3-13, doi:10.1111/nyas.14119 (2019).

229 Janig, W., Krauspe, R. & Wiedersatz, G. Transmission of impulses from pre- to postganglionic vasoconstrictor and sudomotor neurons. *Journal of the autonomic nervous system* **6**, 95-106 (1982).

230 Farkas, Z., Kása, P., Balcar, V. J., Joó, F. & Wolff, J. R. Type A and B gaba receptors mediate inhibition of acetylcholine release from cholinergic nerve terminals in the superior cervical ganglion of rat. *Neurochemistry international* **8**, 565-572, doi:https://doi.org/10.1016/0197-0186(86)90193-2 (1986).

231 Kása, P., Dobó, E. & Wolff, J. R. 83-93 (Springer Berlin Heidelberg).

232 BOWERY, N. G. & BROWN, D. A. DEPOLARIZING ACTIONS OF γ-AMINOBUTYRIC ACID AND RELATED COMPOUNDS ON RAT SUPERIOR

CERVICAL GANGLIA IN VITRO. *British journal of pharmacology* **50**, 205-218, doi:10.1111/j.1476-5381.1974.tb08563.x (1974).

233 DE GROAT, W. C. The actions of γ-Aminobtjtyric acid and related amino acids on mammalian autonomic ganglia. *Journal of Pharmacology and Experimental Therapeutics* **172**, 384-396 (1970).

234 Adams, P. R. & Brown, D. A. Action of -aminobutyric acid (GABA) on rat sympathetic ganglion cells. *British journal of pharmacology* **47**, 639P-640P (1973).

235 Galvan, M., Grafe, P. & ten Bruggencate, G. Presynaptic actions of 4-Aminopyridine and γ-aminobutyric acid on rat sympathetic ganglia in vitro. *Naunyn-Schmiedeberg's archives of pharmacology* **314**, 141-147, doi:10.1007/BF00504530 (1980).

236 Lucas-Osma, A. M. *et al.* Extrasynaptic ∝5GABAA receptors on proprioceptive afferents produce a tonic depolarization that modulates sodium channel function in the rat spinal cord. *Journal of neurophysiology*, doi:10.1152/jn.00499.2018 (2018).

237 Wang, L., Spary, E., Deuchars, J. & Deuchars, S. A. Tonic GABAergic Inhibition of Sympathetic Preganglionic Neurons: A Novel Substrate for Sympathetic Control. *The Journal of Neuroscience* **28**, 12445-12452, doi:10.1523/jneurosci.2951-08.2008 (2008).

238 McCartney, M. R., Deeb, T. Z., Henderson, T. N. & Hales, T. G. Tonically Active GABA_A Receptors in Hippocampal Pyramidal Neurons Exhibit Constitutive GABA-Independent Gating. *Molecular pharmacology* **71**, 539, doi:10.1124/mol.106.028597 (2007).

239 O'Neill, N. & Sylantyev, S. The Functional Role of Spontaneously Opening GABAA Receptors in Neural Transmission. *Frontiers in molecular neuroscience* **12**, doi:10.3389/fnmol.2019.00072 (2019).

240 Pirker, S., Schwarzer, C., Wieselthaler, A., Sieghart, W. & Sperk, G. GABA(A) receptors: immunocytochemical distribution of 13 subunits in the adult rat brain. *Neuroscience* **101**, 815-850, doi:10.1016/s0306-4522(00)00442-5 (2000).

241 Walton, J. C., McNeill, J. K. t., Oliver, K. A. & Albers, H. E. Temporal Regulation of GABA(A) Receptor Subunit Expression: Role in Synaptic and Extrasynaptic Communication in the Suprachiasmatic Nucleus. *eNeuro* **4**, doi:10.1523/eneuro.0352-16.2017 (2017).

242 Preston, R. J., Waxman, S. G. & Kocsis, J. D. Effects of 4-aminopyridine on rapidly and slowly conducting axons of rat corpus callosum. *Experimental neurology* **79**, 808-820, doi:10.1016/0014-4886(83)90044-4 (1983).

243 Bostock, H., Sears, T. A. & Sherratt, R. M. The effects of 4-aminopyridine and tetraethylammonium ions on normal and demyelinated mammalian nerve fibres. *The Journal of physiology* **313**, 301-315, doi:10.1113/jphysiol.1981.sp013666 (1981).

244 Chiu, S. Y. & Ritchie, J. M. Potassium channels in nodal and internodal axonal membrane of mammalian myelinated fibres. *Nature* **284**, 170-171, doi:10.1038/284170a0 (1980).

245 Pathak, D., Guan, D. & Foehring, R. C. Roles of specific Kv channel types in repolarization of the action potential in genetically identified subclasses of pyramidal neurons in mouse neocortex. *Journal of neurophysiology* **115**, 2317-2329, doi:10.1152/jn.01028.2015 (2016).

246 Sherratt, R. M., Bostock, H. & Sears, T. A. Effects of 4-aminopyridine on normal and demyelinated mammalian nerve fibres. *Nature* **283**, 570-572, doi:10.1038/283570a0 (1980).

247 Sandoz, G. *et al.* AKAP150, a switch to convert mechano-, pH- and arachidonic acid-sensitive TREK K(+) channels into open leak channels. *The EMBO journal* **25**, 5864-5872, doi:10.1038/sj.emboj.7601437 (2006).

248 Enyedi, P. & Czirják, G. Molecular background of leak K+ currents: two-pore domain potassium channels. *Physiological reviews* **90**, 559-605, doi:10.1152/physrev.00029.2009 (2010).

249 Duprat, F. *et al.* The neuroprotective agent riluzole activates the two P domain K(+) channels TREK-1 and TRAAK. *Molecular pharmacology* **57**, 906-912 (2000).

250 North, R. A. in *Handbook of Physiology, The Nervous System, Intrinsic Regulatory Systems of the Brain* (ed Floyd E. Bloom) 115-153 (Oxford University Press, 1986).

251 Keast, J. R., Kawatani, M. & De Groat, W. C. Sympathetic modulation of cholinergic transmission in cat vesical ganglia is mediated by alpha 1- and alpha 2-adrenoceptors. *The American journal of physiology* **258**, R44-50, doi:10.1152/ajpregu.1990.258.1.R44 (1990).

252 Quilliam, J. P. & Shand, D. G. THE SELECTIVITY OF DRUGS BLOCKING GANGLIONIC TRANSMISSION IN THE RAT. *British journal of pharmacology and chemotherapy* **23**, 273-284 (1964).

253 Alkadhi, K. A. Rhythmic Discharge Induced by Temperature Variation and Drugs in Isolated Sympathetic Ganglia. *Clinical and Experimental Hypertension* **30**, 497-510, doi:10.1080/10641960802251867 (2008).

254 Ivanov, A. & Zilberter, Y. Critical state of energy metabolism in brain slices: the principal role of oxygen delivery and energy substrates in shaping neuronal activity. *Frontiers in neuroenergetics* **3**, 9, doi:10.3389/fnene.2011.00009 (2011).

255 Prinz AA (2008). Plasticity and stability in neuronal and network dynamics. In: Soltesz I, S. K., eds. Computational Neuroscience in Epilepsy, Elsevier.

256 Newland, C. F. & Cull-Candy, S. G. On the mechanism of action of picrotoxin on GABA receptor channels in dissociated sympathetic neurones of the rat. *The Journal of physiology* **447**, 191-213, doi:10.1113/jphysiol.1992.sp018998 (1992).

257 Palani, D., Pekala, D., Baginskas, A., Szkudlarek, H. & Raastad, M. Action potentials recorded from bundles of very thin, gray matter axons in rat cerebellar slices using a grease-gap method. *Journal of neuroscience methods* **208**, 119-127, doi:10.1016/j.jneumeth.2012.05.005 (2012).

258 Kirchhoff, C., Leah, J. D., Jung, S. & Reeh, P. W. Excitation of cutaneous sensory nerve endings in the rat by 4-aminopyridine and tetraethylammonium. *Journal of neurophysiology* **67**, 125-131, doi:10.1152/jn.1992.67.1.125 (1992).

259 Doble, A. The pharmacology and mechanism of action of riluzole. *Neurology* **47**, S233-241, doi:10.1212/wnl.47.6_suppl_4.233s (1996).

260 Brown, D. A. & Marsh, S. Axonal GABA-receptors in mammalian peripheral nerve trunks. *Brain Res.* **156**, 187-191. (1978).

261 Hari, K. *et al.* Nodal GABA facilitates axon spike transmission in the spinal cord. *bioRxiv*, 2021.2001.2020.427494, doi:10.1101/2021.01.20.427494 (2021).

262 Williams, J. R., Sharp, J. W., Kumari, V. G., Wilson, M. & Payne, J. A. The neuron-specific K-Cl cotransporter, KCC2. Antibody development and initial characterization of the protein. *The Journal of biological chemistry* **274**, 12656-12664, doi:10.1074/jbc.274.18.12656 (1999).

263 Adams, P. R. & Brown, D. A. Actions of gamma-aminobutyric acid on sympathetic ganglion cells. *The Journal of physiology* **250**, 85-120 (1975).

264 Barolet, A. W., Li, A., Liske, S. & Morris, M. E. Antagonist actions of bicuculline methiodide and picrotoxin on extrasynaptic gamma-aminobutyric acid receptors. *Can J Physiol Pharmacol.* **63**, 1465-1470. (1985).

265 Häppölä, O., Päivärinta, H., Soinila, S., Wu, J. Y. & Panula, P. Localization of L-glutamate decarboxylase and GABA transaminase immunoreactivity in the sympathetic ganglia of the rat. *Neuroscience* **21**, 271-281, doi:10.1016/0306-4522(87)90338-1 (1987).

266 Löscher, W. GABA in plasma and cerebrospinal fluid of different species. Effects of gamma-acetylenic GABA, gamma-vinyl GABA and sodium valproate. *Journal of neurochemistry* **32**, 1587-1591, doi:10.1111/j.1471-4159.1979.tb11104.x (1979).

267 de Bie, T. H., Balvers, M. G. J., de Vos, R. C. H., Witkamp, R. F. & Jongsma, M. A. The influence of a tomato food matrix on the bioavailability and plasma kinetics of oral gamma-aminobutyric acid (GABA) and its precursor glutamate in healthy men. *Food & Function* **13**, 8399-8410, doi:10.1039/D2FO01358D (2022).

268 FINAL, H.-P. C. P. D.-.-. Hochman-Prinz CRCNS Project Description 10-29-15 FINAL. (2015).

269 Wang, G. & Thompson, S. M. Maladaptive homeostatic plasticity in a rodent model of central pain syndrome: thalamic hyperexcitability after spinothalamic tract lesions. *The Journal of neuroscience : the official journal of the Society for Neuroscience* **28**, 11959-11969 (2008).

270 Trigo, F. F., Marty, A. & Stell, B. M. Axonal GABAA receptors. *The European journal of neuroscience* **28**, 841-848, doi:10.1111/j.1460-9568.2008.06404.x (2008).

271 Wall, P. D. Do nerve impulses penetrate terminal arborizations? A pre-presynaptic control mechanism. *Trends in neurosciences* **18**, 99-103 (1995).

272 Wall, P. D. & McMahon, S. B. Long range afferents in rat spinal cord. III. Failure of impulse transmission in axons and relief of the failure after rhizotomy of dorsal roots. *Philosophical transactions of the Royal Society of London. Series B, Biological sciences* **343**, 211-223, doi:10.1098/rstb.1994.0022 (1994).

273 Deuchars, S. A., Milligan, C. J., Stornetta, R. L. & Deuchars, J. GABAergic neurons in the central region of the spinal cord: a novel substrate for sympathetic inhibition. *The Journal of neuroscience : the official journal of the Society for Neuroscience* **25**, 1063-1070, doi:10.1523/jneurosci.3740-04.2005 (2005).

274 Gunn, B., Brown, A., Lambert, J. & Belelli, D. Neurosteroids and GABAA Receptor Interactions: A Focus on Stress. *Frontiers in neuroscience* **5**, doi:10.3389/fnins.2011.00131 (2011).

275 Lambert, J. J., Belelli, D., Peden, D. R., Vardy, A. W. & Peters, J. A. Neurosteroid modulation of GABAA receptors. *Progress in neurobiology* **71**, 67-80, doi:https://doi.org/10.1016/j.pneurobio.2003.09.001 (2003).

276 Belelli, D., Casula, A., Ling, A. & Lambert, J. J. The influence of subunit composition on the interaction of neurosteroids with GABAA receptors. *Neuropharmacology* **43**, 651-661, doi:https://doi.org/10.1016/S0028-3908(02)00172-7 (2002).

277 Belelli, D. & Lambert, J. J. Neurosteroids: endogenous regulators of the GABAA receptor. *Nature Reviews Neuroscience* **6**, 565-575, doi:10.1038/nrn1703 (2005).

278 Crowley, T., Cryan, J. F., Downer, E. J. & O'Leary, O. F. Inhibiting neuroinflammation: The role and therapeutic potential of GABA in neuro-immune interactions. *Brain,*

behavior, and immunity **54**, 260-277, doi:https://doi.org/10.1016/j.bbi.2016.02.001 (2016).

279 Alexander, S. P. H. *et al.* THE CONCISE GUIDE TO PHARMACOLOGY 2019/20: Ion channels. *British journal of pharmacology* **176**, S142-S228, doi:10.1111/bph.14749 (2019).

280 Eser, D. *et al.* Panic Induction with Cholecystokinin-Tetrapeptide (CCK-4) Increases Plasma Concentrations of the Neuroactive Steroid 3 α, 5 α Tetrahydrodeoxycorticosterone (3 α, 5 α-THDOC) in Healthy Volunteers. *Neuropsychopharmacology : official publication of the American College of Neuropsychopharmacology* **30**, 192-195 (2005).

281 Harding, S. D. *et al.* The IUPHAR/BPS guide to PHARMACOLOGY in 2022: curating pharmacology for COVID-19, malaria and antibacterials. *Nucleic acids research* **50**, D1282-D1294, doi:10.1093/nar/gkab1010 (2022).

282 Muqeem, T., Ghosh, B., Pinto, V., Lepore, A. C. & Covarrubias, M. Regulation of Nociceptive Glutamatergic Signaling by Presynaptic Kv3.4 Channels in the Rat Spinal Dorsal Horn. *The Journal of Neuroscience* **38**, 3729, doi:10.1523/JNEUROSCI.3212-17.2018 (2018).

283 Ritter, D. M. *et al.* Dysregulation of Kv3.4 channels in dorsal root ganglia following spinal cord injury. *The Journal of neuroscience : the official journal of the Society for Neuroscience* **35**, 1260-1273, doi:10.1523/JNEUROSCI.1594-14.2015 (2015).

284 Siwiec, M., Kusek, M., Sowa, J. E., Tokarski, K. & Hess, G. 5-HT(7) receptors increase the excitability of hippocampal CA1 pyramidal neurons by inhibiting the A-type

potassium current. *Neuropharmacology* **177**, 108248, doi:10.1016/j.neuropharm.2020.108248 (2020).

285 Wu, Z. Z., Li, D. P., Chen, S. R. & Pan, H. L. Aminopyridines potentiate synaptic and neuromuscular transmission by targeting the voltage-activated calcium channel beta subunit. *The Journal of biological chemistry* **284**, 36453-36461, doi:10.1074/jbc.M109.075523 (2009).

286 Paredes-Cruz, M. *et al.* Functional improvement in individuals with chronic spinal cord injury treated with 4-aminopyridine: A systematic review. *Frontiers in neurology* **13**, 1034730, doi:10.3389/fneur.2022.1034730 (2022).

287 Shand, D. G. THE MODE OF ACTION OF DRUGS BLOCKING GANGLIONIC TRANSMISSION IN THE RAT. *British journal of pharmacology and chemotherapy* **24**, 89-97 (1965).

288 Paton, W. D. & Perry, W. L. The relationship between depolarization and block in the cat's superior cervical ganglion. *The Journal of physiology* **119**, 43-57, doi:10.1113/jphysiol.1953.sp004827 (1953).

289 Maingret, F., Patel, A. J., Lesage, F., Lazdunski, M. & Honoré, E. Mechano- or acid stimulation, two interactive modes of activation of the TREK-1 potassium channel. *The Journal of biological chemistry* **274**, 26691-26696, doi:10.1074/jbc.274.38.26691 (1999).

290 Chemin, J. *et al.* A phospholipid sensor controls mechanogating of the K+ channel TREK-1. *The EMBO journal* **24**, 44-53, doi:10.1038/sj.emboj.7600494 (2005).

291 Ahn, S. N., Guu, J. J., Tobin, A. J., Edgerton, V. R. & Tillakaratne, N. J. Use of c-fos to identify activity-dependent spinal neurons after stepping in intact adult rats. *Spinal cord* **44**, 547-559, doi:10.1038/sj.sc.3101862 (2006).

292 Sankaranarayanan, A. *et al.* Naphtho[1,2-d]thiazol-2-ylamine (SKA-31), a new activator of KCa2 and KCa3.1 potassium channels, potentiates the endothelium-derived hyperpolarizing factor response and lowers blood pressure. *Molecular pharmacology* **75**, 281-295, doi:10.1124/mol.108.051425 (2009).

293 Frizzo, M. E. The Effect of Glutamatergic Modulators on Extracellular Glutamate: How Does this Information Contribute to the Discovery of Novel Antidepressants? *Current Therapeutic Research* **91**, 25-32, doi:https://doi.org/10.1016/j.curtheres.2019.100566 (2019).

294 Debono, M.-W., Le Guern, J., Canton, T., Doble, A. & Pradier, L. Inhibition by riluzole of electrophysiological responses mediated by rat kainate and NMDA receptors expressed in Xenopus oocytes. *European journal of pharmacology* **235**, 283-289, doi:https://doi.org/10.1016/0014-2999(93)90147-A (1993).

295 He, Y. *et al.* Neuroprotective agent riluzole potentiates postsynaptic GABAA receptor function. *Neuropharmacology* **42**, 199-209, doi:https://doi.org/10.1016/S0028-3908(01)00175-7 (2002).

296 Bellingham, M. C. Pre- and postsynaptic mechanisms underlying inhibition of hypoglossal motor neuron excitability by riluzole. *Journal of neurophysiology* **110**, 1047-1061, doi:10.1152/jn.00587.2012 (2013).

297 Fink, M. *et al.* A neuronal two P domain K+ channel stimulated by arachidonic acid and polyunsaturated fatty acids. *The EMBO journal* **17**, 3297-3308, doi:10.1093/emboj/17.12.3297 (1998).

298 Noël, J. *et al.* The mechano-activated K+ channels TRAAK and TREK-1 control both warm and cold perception. *The EMBO journal* **28**, 1308-1318, doi:10.1038/emboj.2009.57 (2009).

299 Patel, A. J. *et al.* A mammalian two pore domain mechano-gated S-like K+ channel. *The EMBO journal* **17**, 4283-4290, doi:10.1093/emboj/17.15.4283 (1998).

300 Patel, A. J. & Honore, E. Properties and modulation of mammalian 2P domain K+ channels. *Trends in neurosciences* **24**, 339-346 (2001).

301 Chemin, J. *et al.* Mechanisms underlying excitatory effects of group I metabotropic glutamate receptors via inhibition of 2P domain K+ channels. *The EMBO journal* **22**, 5403-5411, doi:10.1093/emboj/cdg528 (2003).

302 Murbartián, J., Lei, Q., Sando, J. J. & Bayliss, D. A. Sequential phosphorylation mediates receptor- and kinase-induced inhibition of TREK-1 background potassium channels. *The Journal of biological chemistry* **280**, 30175-30184, doi:10.1074/jbc.M503862200 (2005).

303 Rippe, B., Allison, R. C., Parker, J. C. & Taylor, A. E. Effects of histamine, serotonin, and norepinephrine on circulation of dog lungs. *Journal of applied physiology: respiratory, environmental and exercise physiology* **57**, 223-232, doi:10.1152/jappl.1984.57.1.223 (1984).

304 Murray, M., Fischer, I., Smeraski, C., Tessler, A. & Giszter, S. Towards a definition of recovery of function. *Journal of neurotrauma* **21**, 405-413, doi:10.1089/089771504323004557 (2004).

305 Feng, J., Cai, X., Zhao, J. & Yan, Z. Serotonin receptors modulate GABAA receptor channels through activation of anchored protein kinase C in prefrontal cortical neurons. *Journal of Neuroscience* **21**, 6502-6511 (2001).

306 Wang, H. *et al.* 5-HT2 receptors mediate functional modulation of GABAa receptors and inhibitory synaptic transmissions in human iPS-derived neurons. *Scientific reports* **6**, 20033, doi:10.1038/srep20033 (2016).

307 Abramochkin, D. V. *et al.* Non-quantal release of acetylcholine from parasympathetic nerve terminals in the right atrium of rats. *Experimental physiology* **95**, 265-273, doi:10.1113/expphysiol.2009.050302 (2010).

308 Vijayaraghavan, S. *et al.* Regulated Extracellular Choline Acetyltransferase Activity- The Plausible Missing Link of the Distant Action of Acetylcholine in the Cholinergic Anti-Inflammatory Pathway. *PloS one* **8**, e65936, doi:10.1371/journal.pone.0065936 (2013).

309 Kawashima, K. & Fujii, T. Basic and clinical aspects of non-neuronal acetylcholine: overview of non-neuronal cholinergic systems and their biological significance. *Journal of pharmacological sciences* **106**, 167-173 (2008).

310 Mateos, S. S., Sánchez, C. L., Paredes, S. D., Barriga, C. & Rodríguez, A. B. Circadian Levels of Serotonin in Plasma and Brain after Oral Administration of Tryptophan in Rats. *Basic & Clinical Pharmacology & Toxicology* **104**, 52-59, doi:https://doi.org/10.1111/j.1742-7843.2008.00333.x (2009).

311 Akk, G., Bracamontes, J. & Steinbach, J. H. Pregnenolone sulfate block of GABA(A) receptors: mechanism and involvement of a residue in the M2 region of the alpha subunit. *The Journal of physiology* **532**, 673-684, doi:10.1111/j.1469-7793.2001.0673e.x (2001).

312 Cooper, E. J., Johnston, G. A. & Edwards, F. A. Effects of a naturally occurring neurosteroid on GABAA IPSCs during development in rat hippocampal or cerebellar slices. *The Journal of physiology* **521 Pt 2**, 437-449, doi:10.1111/j.1469-7793.1999.00437.x (1999).

313 Lambert, J. J., Belelli, D., Hill-Venning, C. & Peters, J. A. Neurosteroids and GABAA receptor function. *Trends Pharmacol Sci.* **16**, 295-303. (1995).